THE MEASUREMENT OF WAKE AND SURFACE EFFECTS IN THE SUBCRITICAL FLOW PAST A CIRCULAR CYLINDER AT REST AND IN VORTEX-EXCITED OSCILLATION

by

NELSON FERGUSON
B.Sc., University of Strathclyde, 1963

A THESIS SUBMITTED IN PARTIAL FULFILLMENT OF THE REQUIREMENTS FOR THE DEGREE OF

M.A.Sc.

in the Department of

Mechanical Engineering

We accept this thesis as conforming to the required standard

The University of British Columbia
September, 1965

In presenting this thesis in partial fulfilment of the requirements for an advanced degree at the University of British Columbia, I agree that the Library shall make it freely available for reference and study. I further agree that permission for extensive copying of this thesis for scholarly purposes may be granted by the Head of my Department or by his representatives. It is understood that copying or publication of this thesis for financial gain shall not be allowed without my written permission.

Department of Mechanical Engineering

The University of British Columbia
Vancouver 8, Canada

Date March 11, 1966

ABSTRACT

A pressure transducer, sensitive to acoustic level pressures, was designed and used to measure amplitude, frequency and phase of fluctuating pressure on the surface of a three inch diameter circular cylinder at rest and exhibiting large-amplitude vortex-excited oscillation in a uniform incident wind flow. The phase of the fluctuating pressure relative to the cylinder motion and the cylinder amplitude and frequency were recorded. A disc probe connected to the pressure transducer was used in wake surveys for the stationary and oscillating cylinder. Measurements, made in the Reynolds number range $1.5(10^4) < N_R < 4.1(10^4)$, indicated the following:

Fluctuating pressures on the surface of both a stationary and a vortex-excited circular cylinder experience amplitude modulation, being random for the stationary cylinder and critically dependent on wind speed for the vortex-excited cylinder. Fluctuating pressures for both a stationary and an oscillating cylinder are in phase over one side of the cylinder and 180° out of phase with the opposite side.

For a vortex-excited cylinder, the vortex frequency is 'captured' by the cylinder frequency over a discrete range of wind speed. The amplitude of fluctuating pressure on the surface of a vortex-excited cylinder increases as the resonant wind speed (wind speed corresponding to maximum cylinder amplitude) is approached, but before that actual wind speed is reached, an abrupt decrease occurs, and the amplitude modulation nearly disappears. A sudden change of phase between cylinder motion and fluctuating pressure occurs near the resonant wind speed and the pressure wave form becomes asymmetrical.

The longitudinal spacing of vortices in the wake of a stationary and a vortex-excited cylinder initially increases as the vortices are

swept downstream from the formation zone. Vortex-excited oscillation of a cylinder, as the resonant wind speed is approached, produces an increase in longitudinal vortex spacing and a corresponding abrupt decrease in lateral spacing. At the resonant wind speed, the wake loses its coherent periodicity.

CONTENTS

ILLUSTRATIONS

ILLUSTRATIONS (continued)

ILLUSTRATIONS (continued)

ACKNOWLEDGEMENTS

Sincere appreciation is expressed for the guidance and encouragement given by Dr. G. V. Parkinson during his supervision of this investigation. To the entire technical staff of the Department of Mechanical Engineering, the author expresses sincere thanks. Although the personal interest taken by the technicians in the many problems which arose during the building of equipment is, alone, reason enough for gratitude, such interest was merely representative of their cooperation throughout this programme. The processing of the seemingly endless number of oscilloscope photographs was performed by my wife and for the many hours she spent in the photographic darkroom and in subsequent identification of prints, I am sincerely grateful. The use of the facilities of the Department of Mechanical Engineering is gratefully acknowledged.

Financial assistance was received from the National Research Council of Canada.

SYMBOLS

V = air velocity

ρ = air density

h = lateral dimension of cylinder section

L = length of cylinder

x = longitudinal coordinate for wake survey

y = lateral displacement of oscillating cylinder or lateral coordinate for wake survey

z = spanwise coordinate for wake survey

$\bar{Y}$ = $\bar{y}/h$ = dimensionless amplitude

k = spring constant of oscillating system

m = mass of oscillating system

ω_n = $(k/m)^{1/2} = 2\pi f_n$ = circular frequency of free undamped oscillation of system

U = $V/\omega h$ = dimensionless flow velocity

ν = kinematic viscosity

N_R = $\frac{Vh}{\nu}$ = Reynolds number

C'_L = fluctuating lift coefficient

f = frequency of vortex formation from one shear layer

f_c = frequency of cylinder oscillation

S = fh/V = Strouhal number

p = static pressure

$\bar{p}'$ = mean amplitude of fluctuating pressure about a mean static pressure

p' = fluctuating pressure

C'_{p_s} = $\bar{p}'/1/2\rho V^2$ = fluctuating pressure coefficient amplitude (stationary cylinder)

C'_{p_o} = $\bar{p}'/1/2\rho V^2$ = fluctuating pressure coefficient amplitude (cylinder exhibiting vortex-excited oscillation)

a = longitudinal spacing of vortices in the wake

b = lateral spacing of vortices in the wake

V_3 = fa = speed of vortices in the wake

θ = angular position on cylinder surface

α = speed of sound

δ = calibration piston amplitude

Ω = circular frequency of piston

t = time

Subscripts

D = recorded from disc probe

I. INTRODUCTION

Flow past a circular cylinder, for many years, has been a subject of discussion and investigation for theoreticians and practical engineers alike. The former accept the phenomena as a challenging problem for which, as yet, no satisfactory theory exists, while the latter are faced with the very real and insistent problems of the effects on structures such as smoke-stacks, aerial pipelines, etc. It is not the purpose of this section to give an historical background of the many investigations which have been undertaken since Leonardo da Vinci, in the fifteenth century, sketched vortex formation in the wake of bluff bodies (1); such an account is given by Brooks (2), while a concise summary of available data up to 1962, including recent theoretical and experimental results (2), (3) for a variety of bluff body shapes is given by Parkinson (4).

Although numerous investigators have turned their attention to the measurement and observation of flow around a stationary circular cylinder, it must be pointed out that their work is spread over a large range of Reynolds number ($0.1 < N_R < 10^7$) and due to the dependence of flow characteristics on N_R, reliable date are still in demand. Enough data are available, however, to enable the major flow regimes to be identified. A summary of these regimes with relevant references is given by Morkovin (5) and a more recent report by Kuchemann (6) summarizes past and present work in the more general field of concentrated vortex motion in fluids. For completeness, a brief description of each flow regime follows.

a) $N_R < 1$

No periodicity occurs in the laminar wake and the flow pattern resembles that obtained by an ideal inviscid flow solution.

b) "Twin-Vortex Stage", $3 < N_R < 40$

No periodicity occurs in the laminar wake, but two large stationary

vortices form directly behind the cylinder, one on each side of the stream axis.

c) "Incipient Karman Range", $40 < N_R < 90$

Immediate wake forms as in the "Twin-Vortex Stage", but downstream of the stationary vortices, the laminar wake is unstable.

d) "Pure Karman Range", $90 < N_R < 300$

A well defined, stable, vortex street forms in the laminar wake and persists for a long distance downstream until the vortices are dissipated by viscosity. The vortices form an unsymmetrical double row, each vortex being opposite the mid-point of the longitudinal space between consecutive vortices in the other row.

e) "Subcritical Range", $300 < N_R < 13(10^4)$

Flow around the cylinder separates from the surface in two laminar shear layers (the separation occurring near the transverse diameter). The two shear layers, whose transition to turbulence approaches the cylinder with increasing N_R, roll up alternately into discrete vortices. A periodicity is observed in the turbulent wake, but it is subsequently dissipated by viscous diffusion. The formation frequency occurs at a nearly constant Strouhal number, $S = fh/V$. This is the N_R range of the present investigation.

f) "Critical and Post-Critical", $13(10^4) < N_R < 35(10^5)$

Flow reattachment to the cylinder surface and subsequent turbulent reseparation occurs, resulting in a narrowing of the wake. No discrete vortices are observed, the dominant periodicity of the wake being lost.

g) "Transcritical", $N_R > 35(10^5)$

The point of flow separation moves towards the front of the cylinder resulting in a wake which is wider than that of the preceding range. A dominant periodicity of the wake is recovered.

Flow past a circular cylinder is not strictly two-dimensional, spanwise effects exist and have been observed by Humphreys (7) and Mattingly (8) in the subcritical and critical range. Other investigators (1), (9) have noted the three-dimensionality of the flow.

The measurement of fluctuating effects on the surface and in the wake of a stationary circular cylinder in a uniform flow has been undertaken by several investigators; a brief account of their work follows.

McGregor (10) investigated fluctuating pressures on a cylinder surface $\left[N_R \simeq 5(10^4) \text{ and } 12(10^4)\right]$ by means of a condenser microphone. The microphone was mounted inside the cylinder and the fluctuating pressures were transmitted via a hole in the cylinder surface to the microphone cavity. An estimate of the oscillating lift and drag forces was obtained by integration of the surface pressure coefficients. A mathematical model of the flow was developed by assuming an alternating vortex to be positioned at the rear of the cylinder. A similar investigation was undertaken by Gerrard (11), $4(10^3) < N_R < (10^5)$, the pressure pick-up being essentially a condenser microphone type, but with the pressure sensitive area forming part of the cylinder surface. A different method of investigation was employed by Heine (12) who mounted a pressure transducer remote from the cylinder. The fluctuating pressure was conveyed from the model surface to the transducer via a small bore tube. The pressure transducer relied upon the voltage response of a piezoelectric crystal to small displacements. Heine's investigation included, besides a circular cylinder, other body shapes of both bluff and streamline form.

While the work described above produced estimates of the fluctuating forces on a cylinder by the indirect means of integration of the fluctuating pressures, direct measurement of forces has been made. Bishop and Hassan (13)

measured fluctuating lift and drag forces on a stationary circular cylinder placed in a water channel $\left[3.6(10^3) < N_R < 11(10^3)\right]$. Strain gauge transducers, built into the cylinder supports, provided a means of fluctuating force measurement. The fluctuating forces on a short segment of a stationary circular cylinder were measured by Keefe (9). Measurements were made in a wind tunnel in the range $5(10^3) < N_R < (10^5)$. The effect of two circular discs mounted on the cylinder near the force transducer was examined. End effects were considered and experiments performed to establish the limits of their influence. In a higher range of Reynolds number, $4(10^4) < N_R < 6(10^5)$, Humphreys (7) investigated fluctuating lift and drag, the force transducers being incorporated in the cylinder support. Further observations on spanwise effects are included in his report.

Measurements in the wake of a stationary circular cylinder were first made by Fage and Johansen (14) who employed a hot-wire technique to determine the velocity and frequency of individual vortices passing downstream, $N_R = 2.76(10^4)$. Cylinder shapes other than circular were investigated in the above reference and, in an earlier paper by the same authors, measurements in the wake of an inclined flat plate are reported. A photographic study of streamlines in the wake of a stationary circular cylinder was made by Thom (15). Dye techniques were used in a water channel at low Reynolds numbers $(20 < N_R < 80)$. A similar investigation in air flow was carried out by Kovasznay (16). Hot wire measurements of velocity distribution and frequency were made in the range $40 < N_R < 160$. The effect of channel breadth on wake structure was investigated by Rosenhead (17). A water channel having a variable breadth was used, the cylinder being pushed through the water at various velocities $(40 < N_R < 800)$. Wake structure was observed by means of the presence of aluminum powder on the water surface. In a more recent report by

Shair, et al. (18), the effect of confining walls on the wake stability is discussed. Frequency and velocity measurements in the wake of stationary circular cylinders made by Roshko (1), (19) encompass the entire range of major flow regimes. Hot-wire measurements locating the position of the region of transition to turbulence and the manner in which turbulence develops have been made by Bloor (20), in the range $100 < N_R < 52(10^3)$.

The foregoing summary of investigations of surface and wake effects of flow past a stationary circular cylinder is far from complete, yet its volume is in sharp contrast to that of published data for similar measurements on an oscillating cylinder. In particular, such data pertaining to vortex-excited cylinders are almost non-existent, a fact which might be related to the complications in instrumentation which arise from the cylinder motion.

Vortex excitation of an elastically-mounted cylinder occurs when the frequency of the vortex formation (proportional to the wind speed in the subcritical range, i.e., S = constant), approaches a natural frequency of the elastic system. The periodic characteristic of the flow field causes a periodic pressure distribution on the cylinder surface and the resulting periodic forces excite cylinder oscillations over a discrete range of wind speeds. Typically, a graph of cylinder amplitude versus wind speed has a form not unlike that of a forced vibration with damping, while a graph of vortex frequency versus wind speed portrays a 'capture' phenomenon, i.e., when a particular wind speed in the cylinder oscillation range is reached, the vortex frequency ceases to be proportional to wind speed, remaining at the natural frequency of the elastic system. At a wind speed greater than that for maximum cylinder amplitude, the vortex frequency reverts to the stationary cylinder value (S = constant). Measurements of vortex frequency, cylinder frequency and amplitude made by Brooks (2) verify the above

phenomenon. Reference (2) includes data obtained from a variety of cylinder shapes (circular cylinder, D-section and rectangles of various aspect ratios); 'capture' is seen to occur both in plunging and torsional modes of vibration for a D-section and a circular cylinder. Further evidence of 'capture' is reported by Eagleson, et al. (21) in a study of the torsional vibrations of flat plates when placed parallel to a uniform stream.

When a cylinder is forced to vibrate at a variable frequency in a uniform flow, frequency measurements in the wake show 'capture' behaviour. In investigations by Smirnov and Pavlihina (22) and Bishop and Hassan (23), the vortex frequency, over a range of cylinder frequencies, was found to be controlled. The adjustment of the vortex frequency to the cylinder oscillation frequency, as for the case of vortex excited cylinders, was found to be a sudden occurrence.

With the exception of Bishop and Hassan's measurements of fluctuating lift and drag on a circular cylinder forced to vibrate at a variable frequency in a uniform flow, published technical literature is devoid of surface effect measurements on oscillating cylinders. A similar exception for the case of wake effects for oscillating cylinders is a report by Wehrmann (24) in which the cylinder is described to oscillate transversely to the flow at a frequency determined by a feedback circuit from a hot-wire in the wake.

The following investigation is an attempt to examine the amplitude, modulation, frequency, and phase of fluctuating pressures on the surface of both a stationary and vortex excited circular cylinder and to establish the geometry and behaviour of the wake.

II. INSTRUMENTATION

2.1 Wind Tunnel

The wind tunnel used in this programme is a low speed, low turbulence, return type. Velocities can be varied through the range 4 feet per second to 150 feet per second with turbulence level of less than 0.1%. The pressure differential across the contraction section of 7:1 ratio is measured on a Betz micromanometer which can be read to 0.2 millimeter of water; the test section velocity is calibrated against the above pressure differential. The test section is rectangular in cross-section (36 inches by 27 inches) with 45° corner fillets. Variation of the corner fillets from 6 inches by 6 inches to 4 3/4 by 4 3/4 inches compensates for boundary layer growth. The spatial variation of velocity is less than 0.25%. Tunnel power is supplied by a 15 horsepower direct current motor driving a commercial axiflow fan with a Ward-Leonard system of speed control. An aerodynamic outline of the tunnel is shown in fig. 1.

2.2 Models

Two models were constructed, a 3 inch diameter circular cylinder and a 3 inch D-section (fig. 2). Since it was intended to oscillate both models under vortex excitation, weight was the dominant consideration in the design. Pressure taps on the surface of the models with internal tube connections leading to the ends of the models complicated the effort to minimize weight. Combined with surface finish and strength considerations, the above complication suggested that a thin aluminum skin with plastic fittings be adopted as a construction technique. Polyethylene tubing used to convey the pressure from the surface taps was 0.066 inch inside diameter, 0.095 inch outside diameter, and 4 feet in length. The above choice resulted from an

investigation of various tube diameters (see par. 3.2.1).

Circular Cylinder

A 3 inch outside diameter, 0.022 inch wall thickness aluminum tube provided the body of the model. Plastic end fittings which allowed the model to be rotated about its own axis, yet remain attached to the air bearing shaft brackets, were secured by an epoxy adhesive to the aluminum tube. A typical end fitting is shown in fig. 3. Due to the advantages of the symmetry of the section and the ability to rotate the model, the distribution of pressure taps on the model surface was kept to a minimum. Four taps were equally spaced (30°) over one quadrant of the model surface at mid-span. Two spanwise taps, 3 inches and 6 inches above mid-span, were positioned in line with one extremity of the above quadrant. Pressure tap holes in the model surface were 0.025 inch in diameter. To maintain the unmarred surface finish which resulted from lathe-polishing of the aluminum tube, it was decided to insert pressure tube connections from the ends without resorting to splitting the aluminum tube longitudinally and partially spreading to allow access. Plastic blocks, which were radiused to fit the model inside diameter, were drilled to effect a 90° bend. An epoxy adhesive served to bond the plastic block to the aluminum and to the polyethlene tubing. The polyethylene tubing was first bonded to the plastic block; the block was then fitted on an insertion device which allowed alignment with the .025 inch tap in the aluminum skin and contact pressure to be applied to the model interior. For the four equally spaced taps at mid-span, a quadrant-shaped plastic block was made to accommodate the four tube connections and was inserted as a unit.

D-Section

Construction of the D-section model (fig. 2) was similar to that of the circular cylinder. The radiused surface was cut from a length of 3 inch outside diameter, 0.022 inch wall thickness aluminum tube while the flat face was of 3/32 inch thick clear plastic. Plastic end fittings were similar to those of the circular cylinder and allowed rotation of the model about a longitudinal axis. Plastic stiffening bulkheads were fitted at the quarter span positions. Due to the asymmetry of the section at non-zero angles of attack it was necessary to distribute 32 pressure taps around the model surface at mid-span. Two pressure taps were located at one extremity of the radiused surface, 3 inches and 6 inches from mid-span. Tube connections to the 0.025 inch holes in the model surface were made by the same method used with the circular cylinder. A mid-span bulkhead was drilled to accommodate the tube connections, but where space did not allow such a connection, a small plastic block was fitted as close as possible to the mid-span position. Fig. 4 shows the mid-span bulkhead and individual plastic blocks before the radiused aluminum skin was attached. The distribution of the pressure taps on the model surface is given in fig. 5.

2.3 Model Mounting System

An air bearing system designed by Smith (3), had been found satisfactory during his tests and during subsequent experiments (12). This arrangement of model mounting was adopted. The models were constrained to one degree of freedom (plunging) with a minimum of damping from the mounting system. Slots in the top and bottom panels of the test section allowed the model to be attached to the air bearing shafts. Fig. 6 shows typical bearings, shaft and model bracket: In the photograph, the model is not mounted and the

tunnel access panel has been removed. Air supply for the bearings was produced by an Ingersoll-Rand 2-stage compressor, model 11 3/4 x 7 x 8 VHB-2, via a 250 cubic foot storage tank. A flexible hose conducted the air to a throttling valve at the tunnel test section. To provide the elastic system for the model four helical, tension springs were attached to the shaft brackets and to the air bearing frame. An arrangement of the model, bearings, shafts, and springs is shown in fig. 7. The springs were designed so that the natural frequency of the spring-mass system allowed the aerodynamic investigations to be carried out at wind speeds greater than 10 feet per second. A streamline model (25) was used to determine the damping due to the spring-bearing system. These data are given in Appendix A along with spring dimensions.

2.4 Wake Traversing Gear

To enable a wake probe to be positioned with control of movement in a lateral, vertical and longitudinal sense, a traversing gear was designed. While accuracy of probe placement was the basic requirement, tunnel blockage and convenience of control had to be considered. Tunnel blockage was kept to a minimum as can be seen in fig. 8. To provide accurate placement in the lateral direction, a 5/8 inch 10 acme, double start lead screw spanned the test section. Two followers mounted on the lateral lead screw carried vertical, 1/4 inch - 20 NC lead screws enclosed in guide tubes. The probe mounting brackets were carried by follower nuts on the vertical lead screws. The entire assembly was mounted on a horizontal, rigid frame which, having grooved wheels to match rails on the exterior of the tunnel side panels, could be positioned longitudinally. To allow the longitudinal motion of the frame, new side panels (fig. 9) having 3/4 inch longitudinal slots were designed and fitted to the test section. The upstream end of the slots could be extended

to the removeable window section, thus the entire traversing gear could be removed from the tunnel with a minimum of dismantling. Hand wheels controlling both lateral and vertical motion of the probe were conveniently mounted on the working area side of the frame (fig. 9). Rotation of the vertical lead screws was achieved by flexible shafts. A scale attached to the rail on the tunnel side panel gave a direct reading of longitudinal position. The error in positioning the probe was estimated to be approximately 1/32 inch, or about 1% of cylinder diameter. This accounted for clearance play in the lead screws and guides.

2.5 Pressure Transducer

The type of measurements, i.e., fluctuating acoustic level pressures, which were to be made in this programme suggested that use be made of a transducer developed by Heine (12). Heine's design incorporates a rubber diaphragm and a standard ceramic crystal commonly used in phonographs. Diaphragm deflections due to the fluctuating pressures are transmitted by means of a link to the crystal which, in turn, produces a voltage output. During initial work with the above transducer, however, doubts arose as to the nature of its response, and the following investigation was carried out.

To examine the response of the crystal independent of tubing, cavity and diaphragm, a link connection was made from the crystal direct to a cantilever steel beam. (section 2.6). Amplitude and frequency of the beam deflection were controlled by a Goodmans Model V47 Vibration Generator attached to the free end of the beam. Strain gauges mounted on the beam gave a signal proportional to beam deflection, thus crystal displacement. A diagrammatic layout of apparatus is shown in fig. 10 and the cantilever beam, vibration generator and frame are shown in fig. 11. Observation of signal

amplitudes and phase relation over a frequency range of 10 cycles/sec. to 80 cycles/sec. for both sinusoidal and non-sinusoidal displacement wave forms showed that the crystal output depended upon the rate of displacement rather than pure displacement only. Typical oscilloscope traces of strain gauge and crystal output are shown in fig. 12. Data for this particular investigation are given in Appendix B. It will be noted that although the strain gauge signal amplitude was kept constant, the crystal output increased when a non-sinusoidal displacement wave form was introduced. Above 50 cycles/sec. the beam displacement signal tends to a sinusoidal wave form and the crystal output returns to that of the sinusoidal displacement case. Non-sinusoidal displacement of the cantilever beam was achieved by emitting a triangular wave form from the low frequency function generator and accepting the response of the vibration generator-beam system. The apparent sensitivity of the crystal to wave shape, rather than wave amplitude, the necessity to rely upon a sinusoidal wave shape calibration (12), and the inadequate sensitivity at the low wind speeds used in this programme suggested that a different means of determining fluctuating pressure be found. Due to the fact that part of this investigation was to measure fluctuating pressures on the surface of oscillating models, it was necessary to design a transducer which was either both light and small, (this would enable it to be incorporated inside the model), and insensitive to acceleration or, alternatively, the pressure could be conveyed via a tube to an externally mounted transducer. The latter method, employed by Heine (12), was chosen to avoid the practical problems of miniaturization and inertia. The effect of the tubing on the signal amplitude and phase was subsequently investigated (section 3.2.1). Following the work of Heine, i.e., utilizing the response of a rubber diaphragm to the fluctuating pressures, a means of converting this deflection

into an electrical signal was sought. A crude, first attempt to employ an electrical resistance which varied with light intensity (Phillips type no. B 8 731 03) showed that a shutter placed in a light beam from an ordinary flashlight bulb required a minute displacement to give a substantial resistance change, the relationship between resistance change and shutter displacement being a function of the light intensity. By mounting the shutter on the rubber diaphragm and subjecting the latter to fluctuating pressures of the order of magnitude of those expected on the models, a suitable resistance change was observed. In order to convert this change in resistance to a voltage signal, the light dependent resistance was included in one arm of a two arm bridge circuit and connected to a bridge amplifier and meter (Ellis Associates BAM-1). The output from the above instrument was displayed on a cathode ray oscilloscope. Since the upper limit of arm resistance which could be used with the bridge amplifier and meter was 2000 ohm and since the light dependent resistance at a light intensity available from a simple 6 volt bulb-battery circuit was of the order of 30,000 ohm, it was necessary to connect a shunt resistance across the arm. Initially, a 0-2000 ohm potentiometer was used as a shunt, thus the arm resistance could be varied. The second 0-2000 ohm potentiometer was used as the dummy arm of the bridge circuit. The above arrangement, although producing a clean signal, proved to be extremely susceptible to temperature changes thus making it impossible to maintain a bridge balance. The dummy arm was modified to include a light dependent resistance and shunt similar to that in the active arm, but in this case, the light beam was interrupted by a stationary shutter which could be adjusted to bring the light dependent resistance value equal to that in the active arm. This proved to eliminate, to a large extent, the thermal drift problem. Once optimum shunt resistance values were chosen, the

potentiometers were replaced by first, standard carbon resistances (10% tolerance) and secondly, deposited carbon film precision resistances (1% tolerance). Thermal drift continued to cause a small, but awkward unbalancing effect on the circuit. The source of this thermal drift was found to be the thermal instability of shunt resistances: it was eliminated by the use of strain gauges as shunt resistances. The gauges were steel compensated and mounted on a mild steel flat bar in a temperature compensating circuit.

A secondary problem arose with the vibration of light bulb filaments. Various commercially available bulbs were tested, but even with the most suitable, it was found necessary to insert ground glass between the light source and the light dependent resistance. This diffusion of the light beam reduced the filament vibration effect, and made the bulb alignment relative to the light dependent resistance less critical. The latter problem arose only when it was necessary to replace bulbs. Other parameters of the design were investigated. Diaphragm stiffness and shutter widths were varied. It was found that a more flexible diaphragm than that used by Heine was necessary to give the required sensitivity. Fig. 13 and fig. 14 show details of the final design. The entire transducer casing and shunt resistances were enclosed in a cabinet (fig. 15). Meters on the cabinet face were included to serve as a rough guide when setting light intensity. During tests, final adjustment to light intensity was made as described in section 3.1.3. A schematic wiring diagram for the transducer is given in fig. 16. A detailed list of transducer components is given in Appendix C.

Later work with oscillating tubing (section 3.1.3) led to the following modification of the transducer casing. In order to admit a pressure fluctuation to the side of the diaphragm opposite to that inside the cavity, a hole was drilled through the casing side to intercept the central hole

above the shutter. The ground glass effected a pressure seal at the light dependent resistance; a similar translucent seal was inserted in the bulb holder socket. A set screw isolated the volume surrounding the shutter and diaphragm from the dummy arm components.

Correlation of two pressure signals on the model surface, or a model surface pressure with a wake signal, required that two pressure transducers be used. The transducers were built identical in all respects and the calibration data (section 3.1.3) given in fig. 25 applies to both.

2.6 Transducer Calibration Apparatus

In previous work (12) a calibration technique included the use of a horn driver, cavity and a sound level meter (sections 3.1.4 and 3.1.5). Due to distortions arising from the amplifier and the response of the horn driver, the lower frequency limit for such an arrangement proved to be 15 to 20 cycles/sec. Heine (12) extended the calibration below this limit by utilizing the linear nature of the signal amplitude versus frequency curves. Due to the fact that the frequency of pressure fluctuations anticipated in this experimental programme fell almost entirely within the range 7-20 cycles/sec., it was felt that a more positive means of calibration should be adopted. Since it had been decided to mount the transducer outside the tunnel test section, thus employing tubing to convey the pressures from the model surface (or from a wake probe) to the transducer, an investigation of the effects of the tubing on the signal phase relation was necessary (section 3.2.1). This aspect of the programme further pointed out the need for a calibration procedure which would give a reference signal which was in a known phase relation with the generated pressure at the pressure source.

A piston-cylinder type calibration had been attempted by Heine (12),

employing a piston of a much smaller diameter than that of the cylinder: a refinement of this technique was adopted. A piston was introduced directly into the polyethylene tube; the piston diameter was matched to the tube inside diameter and the necessary clearance was sealed by vaseline. Fluctuating pressures were obtained from the piston oscillations. Quantitative pressure fluctuations were calculated following the theory given in Appendix D. Since the pressure produced by the piston was a function of both piston amplitude and frequency, a control of both these parameters was necessary. The cantilever beam and calibration frame already used to investigate the response of Heine's transducer crystal (12) provided a ready means by which to achieve this control.

The mild steel beam had a cross section of 1.032 inches by 0.108 inches. From the top of the clamp to the centre of the vibration generator attachment was 6 3/4 inches. Four Budd Metalfilm strain gauges (type C6-121, 120 ohms) were mounted in a four arm bridge circuit on the beam just above the clamp.

The calibration frame was rigidly constructed of 3/8" thick mild, steel plate. A clamp on the base provided a means of holding the beam in a vertical position and slotted holes allowed adjustment of both the clamp horizontal position and the vibration generator vertical position. Calibration frame and beam are shown in fig. 11.

By mounting the piston opposite the vibration generator at the upper end of the cantilever beam the required control was achieved. A simple bracket and clamp which was rigidly attached to the frame held the polyethylene tube. The upper end of the cantilever beam with piston attached and tube clamp is shown in fig. 17.

The strain gauges on the beam provided a means of determining

piston displacement as well as a signal which was in phase with piston displacement and thus 90° out of phase with the pressure generated by the piston. The frequency of the piston oscillations depended upon the chosen setting of the function generator. To accommodate the various inside diameters of tubing which were investigated, it was necessary only to substitute the corresponding diameter piston. A diagramatic layout of the calibration apparatus is shown in fig. 23.

2.7 Wake Probe

On the assumption that the air flow in the wake was mainly in the plane of the model cross-section, i.e., spanwise components were of a lower order of magnitude, a disc probe was constructed (fig. 18). A similar probe had been investigated (27) as a means of static-pressure determination and for that particular purpose was found to be insensitive to changes of flow direction in the plane of the disc and not subject to scale effect. Appendix E includes data taken from ref. (27). It will be noted from the data that a yaw of $\pm 3^{\circ}$ out of the plane of the disc produced only a slight effect on the C_p value.

The use of such a probe for the determination of fluctuating pressures raised a question as to the interpretation of the transducer signal and to that end, a calibration test was performed (section 3.1.5).

2.8 Displacement Transducer

A signal corresponding to model amplitude was obtained from an air core transformer designed and used by Smith (3) and in subsequent experiments (12). The coaxial cylindrical construction allowed the air bearing shaft to be inserted between the primary and secondary windings, thus varying the

magnetic coupling. A 10 kc frequency signal supplied by a Hewlett-Packard 200 CD oscillator was modulated by the shaft oscillations and this signal was rectified by means of a full wave rectifier (3). The resulting signal was displayed on one channel of a Tektronix Type 564 Storage Oscilloscope. The linear nature of the displacement transducer response was established and a calibration was performed during each series of tests.

2.9 Photography

The storage capabilities of a Tektronix Type 564 Storage Oscilloscope enabled the experimental data to be displayed for qualitative observation and to be recorded on film for later detailed analysis. Satisfactory results were obtained by the use of an Asahi Pentax 6N14, single lens reflex, 35 mm camera with a no. 3, 49 mm close up lens attachment. The camera was mounted on the oscilloscope by means of a specially designed mounting bracket. Film used was Kodak Plus-X Panchromatic and best exposure values were found to be f2.8 at 1/30 sec. Enlargements (4 inches by 5 inches) were printed. Over two thousand data shots were taken and the majority of the processing was performed in the dark-room of the Department of Mechanical Engineering.

III. EXPERIMENTAL PROCEDURES

3.1 Calibration Procedures

3.1.1 Transducer total head, steady pressure calibration

Calibration of the transducer for fluctuating pressures was performed at a mean tube-cavity pressure close to atmospheric pressure. During tunnel tests, however, the mean pressure level depended upon the distribution of the static pressure around the model surface. It was necessary, therefore, to ensure that the response of the transducer to steady pressures was sufficiently linear to allow the calibration data to be used for model tests. A total head tube placed in the wind tunnel test section was connected to first, a Lambrecht micromanometer and second, the pressure transducer. A diagrammatic outline of the apparatus is given in fig. 19. The oscilloscope amplifier was set to give a read-out of the d.c. signal and the transducer output was recorded at increasing increments of total head. The results, plotted in fig. 20, show that the linear portion of the curve extends to approximately 20 mmwg, well above the required range of investigation. A further check on the effect of the static pressure level in the transducer cavity was made. A fluctuating pressure at a frequency of 30 cps was subjected to various increasing cavity static pressures. The amplitude of the fluctuating pressure signal remained constant over the established linear response range of static pressure levels (fig. 21). If desired, the transducer calibration data could be applied at cavity static pressures above the linear range by applying correction obtainable from fig. 20, i.e. the ratio, slope of curve at required cavity pressure: slope of curve in linear range. This procedure was investigated and found to give reasonable results.

3.1.2 Cantilever Beam Calibration

The mild steel cantilever beam used to indicate piston amplitude and phase relation in the transducer calibration and subsequent tube investigations is described in section 2.6. Beam deflection was interpreted from a voltage signal given by a bridge amplifier and meter (Ellis Associates, BAM-1). The entire transducer calibration was dependent upon a consistent method of determining piston amplitude and since the gain control on the bridge amplifier meter varied the amplitude of the beam deflection signal, a means of calibrating the BAM-1 gain control was established.

Two strain gauges (Budd Metalfilm, 120 ohm) were mounted on a short section of aluminum, in a temperature compensating two arm bridge circuit. After connections had been made to the bridge amplifier and meter, and bridge balance obtained, an internal resistance (1 M ohm) in the above instrument was shunted across one arm of the strain gauge circuit. The unbalance caused a current to flow in the bridge and a meter reading was registered. Adjustment of the gain control varied this reading and for convenience, it was set at 100 on the upper scale of the meter face. Thus, as long as the same bridge amplifier and meter was used, the gain control setting, determining the signal proportional to a given deflection could be duplicated. The gain calibration circuit was incorporated in the pressure transducer cabinet. A depth micrometer rigidly mounted in a manner such that its shaft was opposite the piston at the upper end of the beam, applied the deflecting force and gave a measure of deflection. Since the required piston displacements were small, the change of slope at the beam end could be neglected and caused no problems in regard to piston misalignment or pressure sealing. Calibration results are plotted in fig. 22.

Although beam design calculations showed that the vibration mode

change occurred outside the frequency range of interest, experimental evidence was obtained which confirmed the calculations. Two strain gauges in a two arm bridge circuit were mounted approximately at the mid-span of the beam. The phase relationship between signals from these gauges and those mounted near the clamped end showed that the change of mode occurred between 125 cycles per second and 140 cycles per second.

3.1.3 Transducer Calibration

A diagrammatic outline of the transducer apparatus is shown in fig. 23 and the actual apparatus is shown in fig. 24. From the theory given in Appendix D, piston amplitudes were calculated for several pressure amplitudes (0.0005 psi to 0.050 psi) through a frequency range of 5 cycles/second to 100 cycles/second. The low frequency function generator provided control over the frequency and amplitude of the piston; the amplitude was interpreted from the beam strain gauge signal. Beam deflection and bridge amplifier gain calibration were established as described in section 3.1.2. The dual input to a Tektronix Type 502A Oscilloscope enabled the phase relation between the piston motion and the transducer response to be investigated. For a constant value of fluctuating pressure amplitude at a given frequency and a tube of given length and diameter, the amplitude and phase of the transducer signal was governed by two factors: bridge amplifier gain setting and light intensity. Calibration of the amplifier gain was achieved by means of the calibration circuit described in section 3.1.2. A 0.5 M ohm internal shunt resistance was used and the meter set to read 70 on the top scale. The 0-10 ohm potentiometer in the transducer light circuit (fig. 16) allowed the power input to the bulbs to be varied. The extreme sensitivity of the transducer output to light intensity suggested

that for calibration, no reliance be put on the light circuit meter readings. The following calibration procedure was adopted and used throughout the test programme.

Bridge amplifier gains for both the strain gauge and transducer circuits were calibrated as previously discussed. A known pressure, generated at 10 cycle/second, was introduced to the transducer cavity by means of a 4 foot, 0.066 inside diameter, polyethylene tube. Adjustment of the light circuit potentiometer controlled the transducer output and allowed a standard signal to be established. The above procedure was repeated at the beginning of each series of tests and proved to be satisfactory in producing consistent results. Calibration curves (fig. 25) based on the above 10 cycles/second standard signal were then applicable to all model surface pressure data. The effect of the model tap constriction on the above calibration is discussed in section 3.1.4.

Tube connection to the transducer was a simple press fit of the tube outside diameter into the transducer casing. Since, when connected the tube, cavity and piston formed a closed volume, the static pressure level was dependent upon the depth of the tube insertion. To ensure that calibration was performed at, or near, atmospheric pressure, a plastic connection block was fitted at the transducer casing. A 0.030 inch diameter hole drilled from the surface of the block to intercept the pressure tube bore at 90°, allowed the tube to be inserted with no increase of the static pressure level. After insertion, adhesive tape on the block surface effected a pressure seal. Since it was required to record surface pressure data from an oscillating model, it was unavoidable that the tube connection to the transducer be subjected to oscillations of the model frequency. Initial bench testing showed that the fluctuating pressures arising from tube

flexure were of the same order of magnitude as those on the model surface. In order to eliminate this signal, the transducer was modified (see section 2.5), and a dummy tube, similar to that leading from the model surface pressure connection, was fitted. Both tubes led from the transducer casing to the lower end of the model and, since they were bound together, experienced similar oscillations. At the model, the dummy tube was led along the underside of the test section and the open end located in an area free of induced air flow. The length of the dummy tube was approximately 4 feet. Since the tube motion was common to both and the tubes reported to opposite sides of the transducer diaphragm, the signal resulting from the tube motion was cancelled. Before using this arrangement in the actual tunnel tests, a bench investigation was carried out. Fig. 26 shows typical CRO traces with and without the dummy tube attached: tubes were oscillated by hand to amplitudes far exceeding those experienced during model tests.

3.1.4 Model Tap Constriction Calibration

The transducer calibration procedure described in section 3.1.3 was performed on tubing which did not duplicate the geometrical end conditions of the model tap. In order to determine the effect of the model surface tap constriction, the following investigation was undertaken. Using the calibration apparatus employed by Heine (12), i.e. a horn driven cavity pressure source, fluctuating pressures were produced. Calibration apparatus is shown in fig. 24. Comparison of signals from an open-end tube and an identical tube with a simulated model tap connected showed that the model tap had a negligible effect on the signal amplitude and phase. Due to amplifier distortion and horn driver response at low frequencies, quantitative pressures could not be measured. Signal amplitude ratios and relative phase angles for

a range of frequencies 0 - 80 cycles/second were recorded and are shown in fig. 27. To ensure that no effects due to the cavity geometry or tube position in the cavity were included, two identical open-ended tubes were investigated; the signals from the tubes remained in phase and equal in amplitude throughout the frequency range.

3.1.5 Wake Probe Calibration

Calibration of the wake probe (fig. 18) was carried out by means of the horn driver and cavity shown in fig. 24. As discussed in section 3.1.4, quantitative pressure measurements could not be made. Fig. 28 shows the effect of the probe on signal amplitude and phase angle relative to a tube connected to a simulated model tap. During investigations into the effect of tube lengths and diameters on signal attenuation and phase lag (section 3.2.1), it was noted that the phase relation was independent of pressure amplitude. Thus, the phase relation given in fig. 28 could be accepted with some degree of confidence. Typical oscilloscope traces of a fluctuating pressure signal from the wake probe and a simulated model tap are shown in fig. 29.

3.2 Test Procedures

3.2.1 Tubing

The pressure transducer calibration apparatus discussed in section 2.6 and section 3.1.3 was used to investigate the effect of tube length and diameter on the attenuation and phase shift of the pressure signal. Tube diameters of 0.070, 0.066, 0.055 and 0.045 inches were used and each tube was tested for lengths of 5.0, 4.0, 3.0, 2.0, 1.0 feet. Fluctuating pressure amplitudes of 0.0005, 0.00075, 0.001, 0.002, 0.003, 0.004 and 0.005 psi

were generated by the piston at frequencies ranging from 5 cycles/second to 100 cycles/second. Amplifier distortion occurred at low frequencies and proved to be a problem when determining phase angle relationships from the oscilloscope traces.

3.2.2 Surface Pressures on Model

(a) Stationary Model

Two pressure transducers (section 2.5) were connected to the pressure taps on the model surface. A reference pressure signal (90°) was displayed simultaneously with a signal from the other tap positions. Signal amplitude modulations were recorded by utilizing the storage capabilities of the Tektronix Type 564 Storage Oscilloscope on slow sweep speeds. Faster sweep speeds, portraying fewer cycles, provided data on frequency and phase relation. Pressure readings were taken at several wind speeds in the range 10 feet/second to 30 feet/second.

(b) Oscillating Model

Pressure data were obtained as described above, but due to tube oscillations, a dummy tube (section 3.1.3) connection to each pressure transducer was necessary.

3.2.3 Model Amplitude and Surface Pressure

A signal from the model displacement transducer (section 2.8) and a pressure signal from the model surface were displayed simultaneously on the oscilloscope screen. As in the surface pressure investigation, a slow sweep speed provided a record of amplitude modulation, while faster sweep speeds enabled the frequency and phase relation to be observed. Data were taken at several wind speeds through the model oscillating range. Correlation

of surface pressure and model amplitude was obtained for both the transient model amplitude build-up region and at steady state amplitude. The build-up region was investigated by triggering the CRO sweep while the model was stationary, i.e., no air being supplied to the air bearings; on opening the air bearing throttling valve, model oscillations were allowed to build-up.

3.2.4 Wake Survey

In order to correlate pressure signals from the model surface with those in the wake, one pressure transducer was connected to the 90° tap on the model and the other connected to the disc wake probe (section 2.7). Tube connections to the transducers were identical (5.0 feet long by 0.066 inch inside diameter). Calibration of the probe is discussed in section 3.1.5. The control offered by the traversing gear (section 2.4) enabled the probe to be positioned in the model wake. Lateral traversing determined the position of probe signal maximum amplitude. Longitudinal traversing at the above lateral position provided a phase relation of the probe signal relative to the surface pressure signal. A diagrammatic outline of the apparatus is given in fig. 30. The signals from both transducers were allowed to build up on the screen of the Tektronix Type 564 Storage Oscilloscope until a coherent relation of the fundamental was detectable. In order to obtain a coherent build up, it was necessary to trigger the CRO externally from the model surface pressure signal. Since stable triggering required approximately a 3 volt signal (peak to peak), the model signal was fed into a voltage amplifier before entering the trigger circuit of the oscilloscope. A Bogen 60 watt/ amplifier provided a power supply for the voltage amplifier. Adjustment of the triggering level of the oscilloscope selected a signal amplitude which led to a coherent build-up. The procedure for wake survey was identical for both stationary and oscillating models.

IV. EXPERIMENTAL RESULTS

4.1 Fluctuating Pressures on the Surface of a Stationary Circular Cylinder

A three inch diameter circular cylinder, mounted as described in section 2.3, spanned the test section of the wind tunnel. Air was not admitted to the air bearings, thus cylinder oscillation was prevented. Measurements of fluctuating pressures on the cylinder were made as described in section 3.2.4, $\left[1.5\ (10^4) < N_R < 4.1\ (10^4)\right]$.

Typical oscilloscope traces of a fluctuating pressure signal are shown in fig. 31. It is seen that the signal experiences a random amplitude modulation which is in phase around the cylinder. The fast sweep traces in fig. 31 show that the fluctuating pressures at the fundamental frequency are in phase over one side of the model and 180° out of phase with the opposite side. Fig. 31 (f) shows the appearance of the second harmonic at the 180° tap position. Pressure fluctuations were not detectable at the 0° tap position. The observation that the pressure amplitude modulation was in phase at all points on the cylinder enabled the pressure distribution to be plotted in terms of a ratio, the amplitude of the fluctuating pressure at 90° being the common reference. A planimeter was used to determine the area of the envelope on the slow sweep traces and from this, both a mean signal amplitude and the ratio of mean signal amplitudes were obtained. The distribution of fluctuating pressures on the model surface at several Reynolds numbers is shown in fig. 32 together with earlier measurements by Gerrard (11) and McGregor (10). Fig. 33 shows the variation of C'_{p_s} with N_R at the 30°, 60°, 90°, 120° and 150° pressure tap locations. Since each data photograph included a signal from the 90° tap, several C'_{p_s} values were available for that particular position. Strouhal numbers calculated from frequencies measured on the cylinder surface and in the wake (section 4.2) agree with

published data ($0.191 < S < 0.202$).

4.2 Wake Survey-Stationary Cylinder

The survey was performed at a wind speed of 13.80 feet per second, approximately the resonant wind speed for the oscillating cylinder (section 4.4). The coordinate axes referred to in the following text and figures are defined in fig. 34. Wake survey procedure is outlined in section 3.2.4. Phase and amplitude of the probe signal (fundamental frequency signal only) for longitudinal and lateral traverses made in the wake are shown in fig. 35; the phase shown is corrected for the relative probe signal lag discussed in section 3.1.5. A second harmonic signal, arising from the interaction of vortices being shed from opposite sides of the cylinder, was observed when the probe was positioned close to the stream axis ($y = 0$). Fig. 36 shows typical oscilloscope traces of the model surface pressure (90°) and probe signals. Signal amplitude date were taken from the oscilloscope traces after a coherent build up of signal had been attained, and phase data were taken from single sweep traces. The cylinder surface pressure reference signal was taken from the same side of the stream axis as the probe signal. For $x/h > 5$ (fig. 35) the decrease in signal amplitude and the lack of a clearly defined fundamental, prevented further collection of phase data. The downstream position of the first 'in phase' signal ($x/h \simeq 1.0$) correlates with the position of the maximum amplitude of the probe signal. Phase data from both sides of the stream axis ($y = 0$) are in agreement and plot as a line having a slope which, close to the cylinder, decreases downstream and farther downstream reaches a constant value. Thus in the region $x/h < 3.0$, the longitudinal spacing of the vortices increases as they are carried downstream. From the lateral traverse at $x/h = 1.33$ and $x/h = 2.67$ it is seen that the

lateral vortex spacing, assumed to correspond to maximum amplitude of the probe signal is quite clearly defined. Lateral traversing at $x/h = 1.33$ was taken as a standard procedure; this gave the more clearly defined lateral spacing of the vortices, particularly in the case of an oscillating cylinder (section 4.4).

4.3 Fluctuating Pressures on the Surface of an Oscillating Circular Cylinder

When free to oscillate in the air bearing system (section 2.3), the cylinder was found to develop appreciable amplitudes from rest over a discrete range of wind speeds.

(a) Frequency of fluctuating pressures and cylinder oscillations

Typical oscilloscope traces of cylinder oscillation and fluctuating pressures (90°), obtained as described in section 3.2.3, are shown in fig. 37. It is seen in (figs. 37 (a) and (b)) that an amplitude modulation is experienced by the cylinder at wind speeds initiating cylinder oscillation. The modulation shows a beat phenomenon, its frequency being approximately the difference between the fluctuating pressure frequency and the cylinder oscillation frequency. At higher wind speeds in the cylinder oscillating range, the amplitude modulation disappeared (fig. 37 (c) to (e)). Frequency of the fluctuating pressure together with cylinder oscillation amplitude and frequency are plotted on a base of wind speed in fig. 38. The frequency of the fluctuating pressure follows the familiar pattern of the 'capture' phenomenon. While the transition from the 'stationary' Strouhal frequency line to the 'lock-in' region (at approximately the natural frequency of the model-spring system) is clearly defined, the departure from this region proves to be less organized and considerable scatter of data is present. The natural frequency of the system was determined by means of a

streamline model (section 2.3 and Appendix A). The dynamic response of the model is seen to be typical of a resonance phenomenon. Model amplitude-wind speed data from several tests showed reasonable agreement, the slight scatter of data following maximum model amplitude being credited to the sensitivity of air bearing alignment and a possible change in damping resulting from small changes in configuration of the pressure transducer tube connection.

Frequency measurements from this investigation along with previous measurements (22) are plotted in fig. 43; correlation is discussed in section 5.

(b) Phase relation of fluctuating pressure and cylinder oscillation

Phase relation data taken from fast sweep oscilloscope traces (as shown in fig. 37) are plotted in fig. 38. The phase shown is between the maximum negative pressure at the 90° tap and the maximum cylinder displacement in the 90° tap direction. Phase lag due to the transducer tube connection to the 90° tap was accounted for as described in sections 3.1.3 and 3.1.4 and the appropriate correction applied. Considerable scatter of data is evident in fig. 38, but the change of phase which occurs in the wind speed range giving maximum cylinder amplitude is clearly defined. Reasonable agreement from several runs was obtained and it was noted that the phase change was a sudden occurrence, extremely sensitive to wind speed.

Phase data from this investigation along with previous phase measurements (23) are plotted in fig. 44; correlation is discussed in section 5.

(c) Fluctuating pressures on oscillating cylinder

As in the case of the stationary cylinder, pressure signal amplitude modulation was evident (fig. 39); it was observed that the

behaviour of the modulation was dependent upon wind speed. Fig. 39 (a) shows a fluctuating pressure signal for the 90° and 180° positions on the model as the wind speed was increased through the resonant range. It is seen that in a particular range of wind speed, both the signal amplitude and amplitude modulation are affected; a similar effect was produced by a decrease of wind speed through this range. Fig. 39 (b) and (d) show that the amplitude modulation is in phase around the cylinder and that the phase of the fundamental is as for the stationary cylinder. Fig. 39 (c) shows less modulation of the pressure signal and a slight asymmetry of the wave form is apparent. Pressure signal asymmetry was observed in the region of maximum cylinder amplitude, its occurrence having a critical dependence on wind speed. In fig. 39 (d) the asymmetry of the 90° pressure signal is clearly shown. Mean signal amplitudes and their ratios were obtained as described in section 4.1. Fluctuating pressure signals from the 180° position showed the second harmonic effect. Fluctuating pressures were observed at 0°, but neither the fundamental nor the second harmonic was clearly defined; such pressures were of a lower order of magnitude than those measured at other points on the model. Fluctuating pressures at the fundamental frequency are plotted in fig. 40 (b) in the form of the fluctuating pressure coefficient C'_{p_o}. The critical dependence of pressure amplitude on wind speed in the resonance range is seen in the abrupt decrease of C'_{p_o}. Pressures around the cylinder, shown in fig. 40 (a) in terms of the fluctuating pressure at 90°, are seen to experience a redistribution as the wind speed is varied through the resonance range. The cylinder amplitude and phase data from fig. 38 are repeated in fig. 40 (c) for correlation. Fig. 41 shows model oscillation and 90° pressure fluctuation as the model amplitude is allowed to build-up from rest to a steady-state condition, wind speed being kept constant. A similar effect on fluctuating pressures was exhibited

at all pressure tap positions. C'_{p_s} and C'_{p_o} are plotted on a base of wind speed in fig. 42; relevant discussion is included in section 5.

4.4 Wake Survey - Oscillating Cylinder

The survey was performed at several wind speeds in the range of cylinder oscillation. The coordinate axes referred to in the following text and figures are defined in fig. 34. Wake survey procedure is outlined in section 3.2.4. Phase and signal amplitude data plotted in the following figures refer to signals at the fundamental frequency only; a correction for relative probe lag, as discussed in section 3.1.5, has been applied. Signal amplitude data were taken from oscilloscope traces after a coherent build up had been attained, phase data were taken from single sweep traces. Longitudinal traversing at $y/h = 0.47$ gave phase and probe signal amplitudes shown in fig. 45. The lack of a clearly defined fundamental and a reduction of signal amplitude prevented phase observation for $x/h > 5.0$. The absence of phase data at wind speeds of 13.88 and 14.79 feet per second is due to the lack of a coherent signal in the wake; no fundamental signal was detectable from either single sweep traces or after long build-up periods. Results of lateral traversing at $x/h = 1.33$ and $x/h = 2.67$ are plotted in fig. 46. Lateral traversing at wind speeds of 13.88 and 14.79 feet per second provided an indication of lateral vortex spacing immediately behind the cylinder. From fig. 46, it is seen that the probe signal amplitude at $x/h = 1.33$ increases with wind speed (and cylinder oscillation amplitude) up to 13.28 feet per second, after which a decrease occurs: this may be correlated with C'_{p_o} (fig. 40). The position of the first 'in phase' signal (fig. 45) is seen not to vary significantly with wind speed and correlates with the amplitude of the probe signal. Longitudinal spacing of

the vortices, as indicated by the constant slope portion of the phase curves in fig. 45, is plotted on a base of wind speed in fig. 47; lateral vortex spacing at $x/h = 1.33$ and cylinder amplitude ($\bar{Y}$) are also shown.

Up to the limit of available data, it is seen that as the resonant wind speed, i.e., the wind speed corresponding to maximum cylinder amplitude, is approached, the longitudinal spacing of the vortices increases while no significant change occurs in the lateral spacing. In the immediate vicinity of resonance, however, a sharp decrease of lateral spacing is evident. Accurate determination of the wind speed corresponding to the above occurrence was prevented by its abruptness, the extreme sensitivity to wind speed being similar to that found during investigation of fluctuating pressures. The velocity of vortices, given by $V_3 = (fa)$, (fig. 47) appears to increase as resonance is approached. Velocity V_3 is calculated for two longitudinal positions, $x/h = 1.0$ and $x/h = 3.0$, the latter position corresponding to the region of linear phase relation (fig. 45).

V. DISCUSSION OF RESULTS

Fluctuating Pressure - Stationary Cylinder

The random amplitude modulation of the fluctuating pressures shown in fig. 31 has been observed in earlier investigations (10) (11) (12). Direct measurements of lift and drag forces in the Reynolds number range $3.6(10^3)$ to $11\ (10^3)$ made by Bishop and Hassan (13) and Humphreys (7) at Reynolds number $4(10^4)$, show similar amplitude modulations. While frequent mention is made of such amplitude modulation, no reference to its phase round the cylinder could be found. During the investigation, however, the 'in-phase' characteristic of this modulation was observed on numerous oscilloscope traces. At higher wind speeds than those for which data are included in this report, the amplitude modulation persisted, but a random, low frequency effect on the mean pressure was observed. Quantitative measurements were not made since this would have entailed further work on the transducer calibration; a typical qualitative pressure signal is shown in fig. 31(h). Both Gerrard and McGregor employed a wave analyser, thus permitting separation of the fundamental and second harmonic signals. It is reported, however, that the signal at $\theta < 120^\circ$ was a well defined fundamental; this is substantiated by the results of this investigation. The second harmonic showed clearly at $\theta = 180^\circ$. While others (10) (11) report the presence of a relatively small signal at 0°, no significant signal could be interpreted from this investigation. The phase of the fundamental was found to be as assumed by McGregor and as found experimentally by Heine. The inclusion of a wave analyser in the circuitry would permit a more refined investigation of both the fundamental and the second harmonic at the 0° and 180° positions. It is seen from fig. 32 that over the Reynolds number range investigated, there is no appreciable change in the fluctuating pressure distribution. Pressure

distributions at 30° and 60° agree with Gerrard, indicating the fluctuating pressure amplitude at these positions to be greater than that found by McGregor. At 120° and 150°, the pressure distribution is more in agreement with McGregor's findings. No fundamental signal was detectable at 180° and data plotted in fig. 32 for that position are second harmonic values.

Fig. 33 shows agreement of C'_{p_s} with Gerrard, both in the amount of scatter of the data, as shown by the shaded bands, and in a consistent trend of C'_{p_s} increasing with Reynolds number. An estimate of C'_L was obtained from integration of C'_{p_s} around the cylinder. Although these data are not presented in this report, rough calculations indicate $C'_L \simeq 0.42$ at $N_R = 1.5(10^4)$ McGregor (10) finds $C'_L \simeq 0.58$ at $N_R = 5(10^4)$, the higher value being consistent with the upward trend of C'_{p_s} with increasing N_R.

Frequency of fluctuating pressures and cylinder oscillations

From fig. 38, it is seen that 'capture' of the surface pressure frequency occurs at an amplitude $\bar{Y} \simeq 0.03$. Brooks (2) finds this phenomenon occurring later in the resonance region ($\bar{Y} \simeq 0.15$). Eagleson et al. (21), find similar characteristics in the behaviour of flat plates placed parallel to a uniform water stream and allowed one degree of freedom torsional oscillation around a vertical axis along their leading edge. Their measurements of frequency and vibration amplitude show that over the 'capture' range of flow speed, the vibrational frequency increased slightly but remained below the 'stationary' Strouhal value. An investigation by Smirnov and Pavlihina (22) shows further evidence of the capture phenomenon. Circular cylinders of 41 mm and 65 mm diameter were immersed in a water channel and forced to vibrate at a variable frequency with a constant amplitude of 15 mm. Water velocities were 12 cm/sec and 16 cm/sec. Their results are shown in

fig. 43 along with data from the current investigation. Valid comparison can be made for the 'capture' region only, as the cylinders used in the investigation were not allowed to exhibit self-induced oscillations. It is interesting to note, however, that the limits of the 'capture' region agree favourably. Bishop and Hassan (23), using apparatus similar to that of Smirnov and Pavlihina, observed 'capture' in measurements of lift force frequency (Reynolds Number $3.6(10^3)$). When the oscillation frequency of the cylinder approached the frequency of the lift force, the latter suddenly changed to that of the cylinder oscillation.

Phase relation of fluctuating pressure and cylinder oscillation

The sensitivity of the relative phase of cylinder surface pressure and displacement to wind speed is clearly seen in fig. 38; a similar sensitivity of relative phase of lift force and cylinder displacement to cylinder oscillation frequency is reported by Bishop and Hassan (23). Measurements of phase made during this investigation along with data on phase of lift force with respect to cylinder motion from (23) are shown in fig. 44 on a base of 'cylinder Strouhal number', $f_c h/v$. For reasons explained in the preceding paragraph, detailed comparison is not valid, but it is interesting to note that the sudden phase change experienced by the lift force is of the same sense as that experienced by the fluctuating pressures.

Further comparison of these results can be made in the form of the 'critical non-dimensional frequency', i.e., the frequency at which the phase and lift undergo a sudden change. From the current investigation, the phase changes at $\bar{Y} \simeq 0.29$, frequency $\simeq 8.98$ c.p.s. Dividing by the 'stationary' Strouhal frequency (approx. 10. 7 c.p.s.) for that particular wind speed (approximately 13.8. f.p.s.) gives a non-dimensional frequency of

approximately 0.84; this value compares favourably with that of ref. (23), (approximately 0.83). The above comparison is made with regard to phase shift only as it is seen from fig. 40 that the decrease in pressure amplitude occurs at a wind speed lower than the resonant wind speed.

Fluctuating pressures on an oscillating cylinder

The increase and subsequent abrupt decrease of fluctuating pressure amplitude shown in fig. 40 (b) is in keeping with the behaviour of lift force measured by Bishop and Hassan (23). The latter investigators report that in the "range of synchronisation", i.e., 'capture', the wave form of the fluctuating forces becomes fairly constant; a similar effect on the fluctuating pressure wave form is seen in fig. 37 (d). The sensitivity of this phenomenon to wind speed (cylinder oscillation frequency in the case of ref. (23)), cannot be over-emphasised. It is seen from fig. 40 (b) that the decrease in C'_{p_o} occurs before the cylinder reaches its maximum oscillation amplitude and approximately at the mid-point of the 'capture' region. Since C'_{p_o} is the excitation which produces cylinder maximum amplitude, its decrease might be expected to correlate with a reduction of cylinder amplitude. It appears that the subsequent phase change (fig. 38) is an associated factor and more refined measurements of phase and frequency might be the basis of an understanding of the phenomenon. A similar relationship between phase and maximum amplitude is in the case of forced vibrations with viscous damping. The variation of pressure distribution shown in fig. 40 (a) correlates with the C'_{p_o} variation. The region of increasing C'_{p_o} which occurs before maximum cylinder amplitude, includes no significant change in pressure distirbution. Following this region, however, the sudden decrease in C'_{p_o} is accompanied by a distinct pressure redistribution. Although continuous

curves are drawn through the pressure distribution data, there is a possibility that the pressure distribution, like C'_{p_o} and phase, changes suddenly. The sensitivity of the flow characteristics to wind speed pointed out the need for refinements in the apparatus which would permit further investigation of this resonance region. Comparison of C'_{p_s} and C'_{p_o} is made in fig. 42. The shaded bands enclose the scatter of C'_{p_s} data. The increase of C'_{p_o} with increasing wind speed and the subsequent decrease to stationary cylinder values is clearly seen. For correlation, the data from fig. 38 has been included.

D-Section

Although the measurements made on the D-section cylinder were not analysed in detail, to the extent they were analysed they tended to confirm the following phenomena previously discussed for the circular cylinder. For both the stationary and oscillating cylinder, modulation of the fluctuating pressure amplitude was in phase around the cylinder and the fundamental was in phase on one side of the model and 180° out of phase with the opposite side. At the initiation of vortex-excited oscillation, the cylinder experienced a beating amplitude modulation, which at higher wind speeds disappeared. Fluctuating pressures experienced a severe amplitude modulation at wind speeds corresponding to cylinder amplitude modulation, but this was almost completely eliminated with the disappearance of cylinder amplitude modulation.

Wake Survey - stationary and oscillating cylinder

Several investigators (1), (15), (17) have made measurements in the wake of stationary cylinders, but their efforts have been concentrated in the low Reynolds number range (20 to 1000). More relevant are measurements

of velocity, frequency and longitudinal spacing of vortices in the wake of a variety of bluff body shapes made by Fage and Johansen (14). Results of these experiments for a circular cylinder $\left[N_R = 2.76(10^4)\right]$ are, in part, $V_3/V = 0.80(0.796)$, $b/a = 0.234(0.269)$. The numbers in the brackets are from the current investigation $\left[N_R = 2.0(10^4)\right]$. Reference (14) does not provide data regarding the variation of vortex spacing with increasing distance from the cylinder. It is assumed that measurements were made as in a previous investigation (26), i.e., in the region $2.0 < x/h < 12.0$; this being the case, the curvature on a phase - x/h plot, such as shown in fig. 35 could have been overlooked and a straight line relationship accepted. The position of the first in-phase signal ($x/h \simeq 1.0$) shown in fig. 35 correlates with the position of maximum suction pressure on the wake centreline ($x/h \simeq 1.1$) measured by Roshko (19).

No reference to measurements in the wake of vortex excited cylinders could be found in the technical literature. Wehrmann (24) investigated velocity fluctuations in the wake of an obround cylinder which was forced to vibrate at 90° to a constant flow velocity ($N_R = 68$). The frequency of vibration was controlled by a feedback system from a hot-wire anemometer placed in the wake. The phase of vibration was varied by changing the position of the hot-wire in the wake and the amplitude controlled by an amplifier in the feedback circuit. With the right choice of amplitude and phase, it was found that velocity fluctuations in the wake could be reduced by 72%. Smirnov and Pavlihina (22), whose findings on 'capture' were previously discussed in this section, make reference to visual observations of vortex formation behind a cylinder experiencing forced vibrations. At 'low' frequencies of cylinder oscillation, vortex formation was observed to be similar to that of a stationary cylinder, i.e., the first vortex being

formed in line with the separating shear layers. At 'high' frequencies, initial vortex formation occurred immediately behind the cylinder. No definition is given to the terms 'low' and 'high' frequencies, but it might be assumed that the phenomenon correlates with the b/h reduction shown in fig. 47. The corresponding loss of coherent probe signal farther downstream, although at a higher N_R, may be interpreted as a phenomenon similar to that observed in reference (24).

Parkinson (4) has suggested that as the cylinder oscillation amplitude increases, the vortices form a wider street and on the assumption that the stability requirement is unchanged by cylinder motion, a corresponding increase in longitudinal spacing occurs. Comparison of b/h for a stationary and oscillating cylinder shows (fig. 47) a reduction of street width rather than an increase, while the longitudinal spacing of the vortices, up to the measurable limit, increases. It appears that the street width is dependent not only upon cylinder oscillation amplitude, but on the phase relation of the vortex formation and the cylinder oscillation. The sudden decrease of street width which occurs between 13.3 and 13.9 feet per second (fig. 47) is accompanied by a phase change (fig. 38) already discussed in this section.

In an effort to establish the longitudinal spacing of vortices in the particular range of wind speeds (approximately > 13.5 f.p.s.) at which no coherent signal was detectable in the wake, the probe was positioned outside the wake ($y/h > 3$). A fundamental signal was observed, but the phase with respect to a surface pressure signal (90°), remained constant for all downstream positions.

Wake data plotted in this report refer to measurements made in the plane of the cylinder mid-span ($z = 0$). Longitudinal traverses made with

the probe in the planes $z/h = 1.0$ and $z/h = 2.0$ and the surface pressure reference signal at $z/h = 0$ showed no coherent spanwise effect on phase. This result was thought to be influenced by the existence of cylinder end effects. Three dimensional flow was observed by Humphreys (7) in his experiments with fine silk threads fastened to a circular cylinder. Thread motion at $N_R < 10^5$ indicated a random spanwise irregularity, but at $N_R \approx 10^5$, a distinct cellular pattern developed and remained until $N_R \approx 3(10^5)$. Mattingly (8) investigated the three dimensionality of flow around a circular cylinder by means of dye techniques in a water tank. In the range $10^4 < N_R < 10^5$, the flow was found to be strongly three dimensional. It was thought that discs, similar to those used by Keefe (9), would enable spanwise effect on phase to be measured both on the cylinder surface and in the wake. Plastic discs were made, but time did not permit their use in this programme. Spacing ratios b/a shown in fig. 47 are calculated for b measured at $x/h = 1.33$. An increase in b for $x/h > 1.33$ is indicated in fig. 46. The data in fig. 47, therefore, should be interpreted as a trend only, not as the fully developed wake ratios.

VI. SUMMARY OF RESULTS

Results of this investigation are summarized as follows:

1. Fluctuating pressures on the surface of both a stationary and vortex-excited circular cylinder experience amplitude modulation which is in phase around the cylinder. For a stationary cylinder, the modulation is random, but for a vortex-excited cylinder the modulation is critically dependent on wind speed, and at the initiation of cylinder oscillation, displays a beat phenomenon similar to that discussed in 3 below.
2. Fluctuating pressures at the fundamental frequency for both a stationary and a vortex-excited circular cylinder are in phase over one side of the cylinder and 180° out of phase with the opposite side.
3. At the initiation of cylinder oscillation where cylinder and vortex frequencies are slightly different, the cylinder experiences a beat amplitude modulation. Then the phenomenon of 'capture' of vortex by cylinder frequency is well defined, departure from that region of wind speeds being less organized than its initial occurrence. Appreciable cylinder oscillation amplitude exists at the end of the 'capture' range.
4. The amplitude of fluctuating pressure on the surface of a vortex-excited circular cylinder has a critical dependence on wind speed, the initiation of cylinder oscillation producing pressure amplitudes similar to that for a stationary cylinder. As the wind speed approaches the resonant value (that for maximum cylinder amplitude), fluctuating pressure amplitude is approximately doubled, but before the resonant wind speed is actually reached, the pressure amplitude reduces abruptly to approximately its initial value and the modulation, both of surface pressure amplitude and cylinder amplitude, disappears. This is maintained for the remainder of the wind speed range for 'capture'. Similar behaviour is observed during

the transient build-up of cylinder oscillation amplitude when the cylinder is released from rest in a constant wind speed close to the resonant value.

5. Near the resonant wind speed, the phase between cylinder motion and fluctuating pressure changes suddenly and an asymmetry in the pressure wave form is apparent.

6. The longitudinal spacing of vortices in the wake of a stationary circular cylinder increases as the vortices are swept downstream from the formation zone, reaching a constant spacing at $x/h \simeq 3.0$. A similar increase occurs in the wake of a vortex-excited cylinder, the constant spacing value being dependent on wind speed. As the resonant wind speed is approached, the longitudinal spacing increases, but before the speed actually reaches the resonant value, the wake loses its periodicity and further longitudinal spacing data are unobtainable. A narrowing of the wake occurs when the cylinder experiences vortex-excited oscillation. In the range of wind speed preceding the resonant value, the lateral spacing of the vortices does not change significantly. Before the actual resonant wind speed is reached, however, a sudden decrease in lateral spacing occurs, the actual spacing being unobtainable due to the loss of the coherent signal in the wake; this loss corresponds to the loss of wake periodicity discussed above. The lateral spacing indicated at the resonant wind speed for a vortex-excited cylinder is less than half the value for a stationary cylinder at the same wind speed.

APPENDIX A

Tension Spring particulars:

Material	:	oil tempered steel wire
Coil O.D.	:	0.649 inch
Wire diam	:	0.091 inch
Number of coils	:	113
Length of coils	:	12 inch
Length inside hooks	:	13 inch

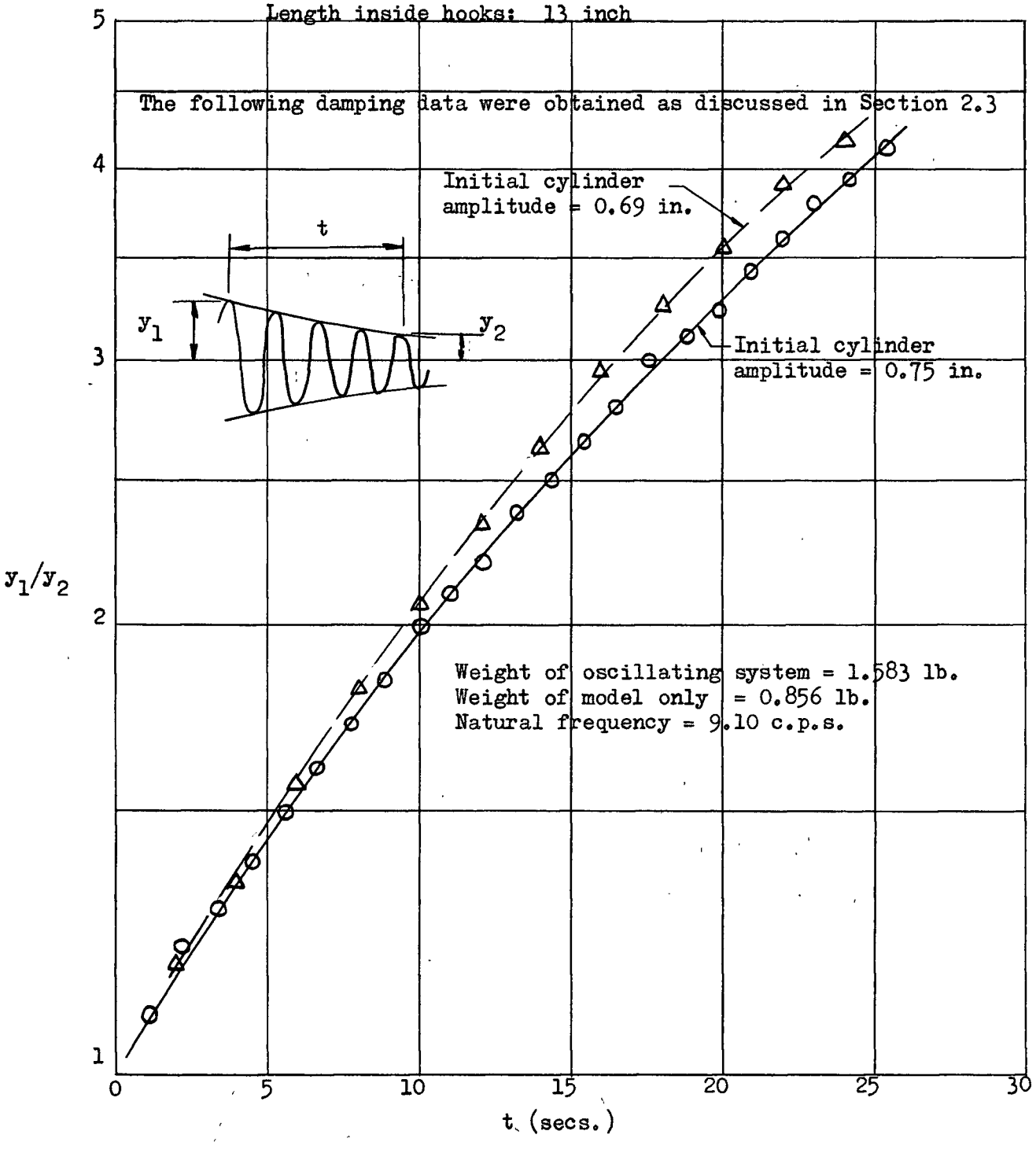

APPENDIX B

PIEZOELECTRIC CRYSTAL RESPONSE DATA
(Astatic No. 445-A)

Link Displacement = $A \sin \omega t$
Link Velocity = $A\omega \cos \omega t$
Max. Link Velocity = $A\omega$

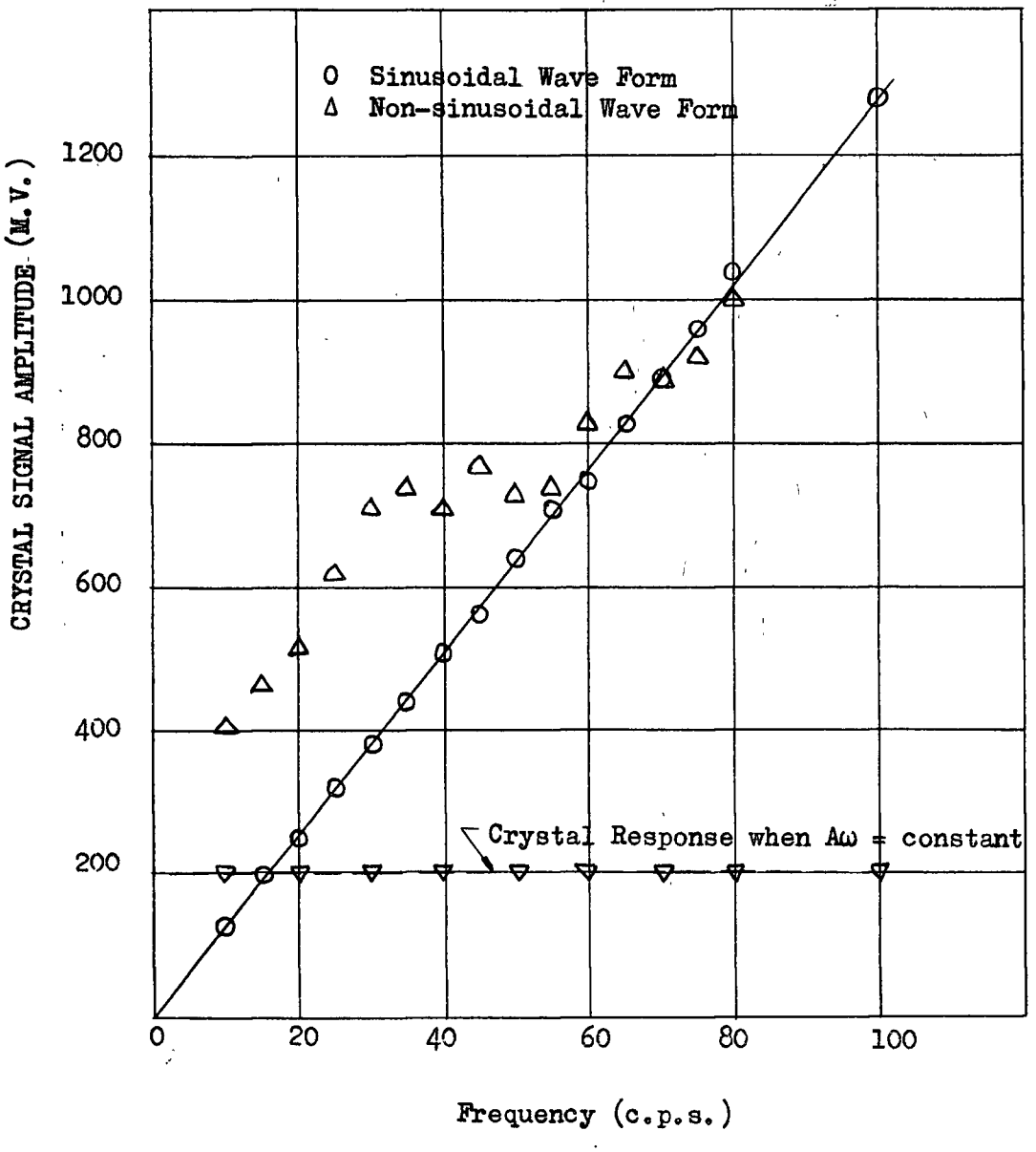

APPENDIX C

TRANSDUCER COMPONENTS

Light dependent resistance:	Phillips type No. B 8 731 03
Shunt resistance	Budd Metalfilm strain gauges Type C6 - 141 - 1000 resistance 1000 ohms
Light bulbs	Westinghouse No. 605 6.15 volt, 0.50 amp
Voltmeter	Triplet, 0-5 volts d.c.
Ammeter	Triplet, 0-400 m.a.
Potentiometer	Wire wound 0-10 ohm linear taper
Diaphragm	Dental Dam, Dark Extra Heavy, Pure Latex (.015 in.)
Shutter	.002 brass shim stock.

APPENDIX D

WAVE PROPAGATION IN A TUBE

The pressure developed by the piston (Section 3.1.3) at the input end of the tube was calculated from elementary one-dimensional acoustic theory (29).

At the piston, $p'(t) = \alpha \rho \Omega \delta \cos \Omega t$

where piston displacement $= \delta \sin \Omega t$

APPENDIX E

DISC STATIC PROBE

The following data are taken from Ref. (27)

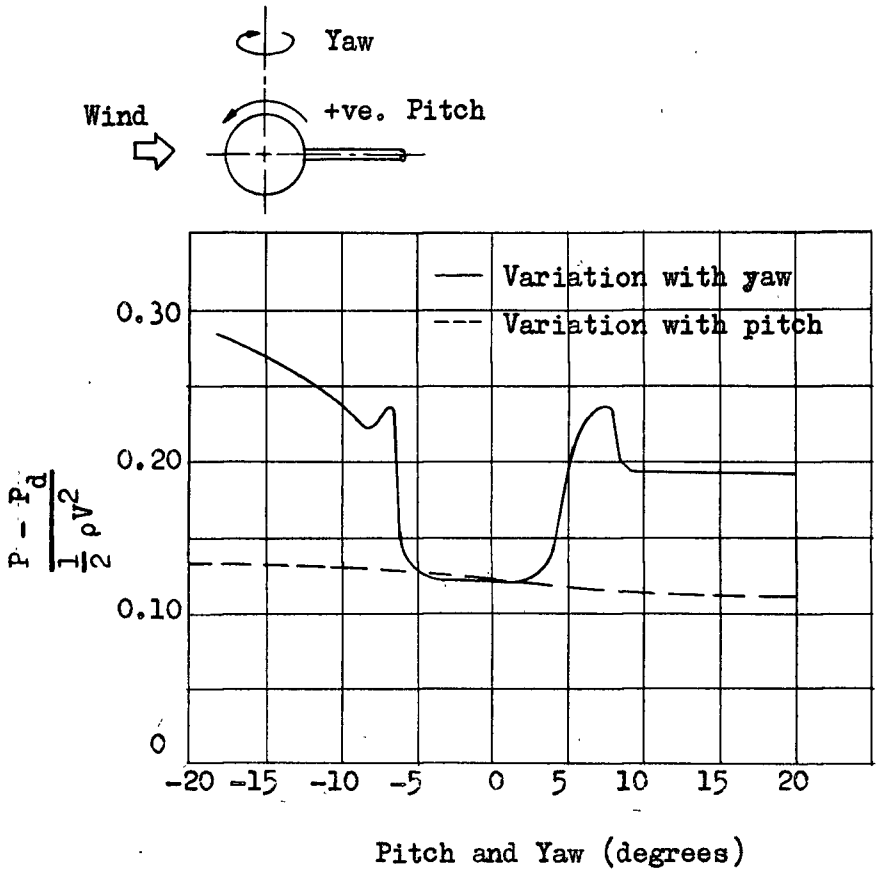

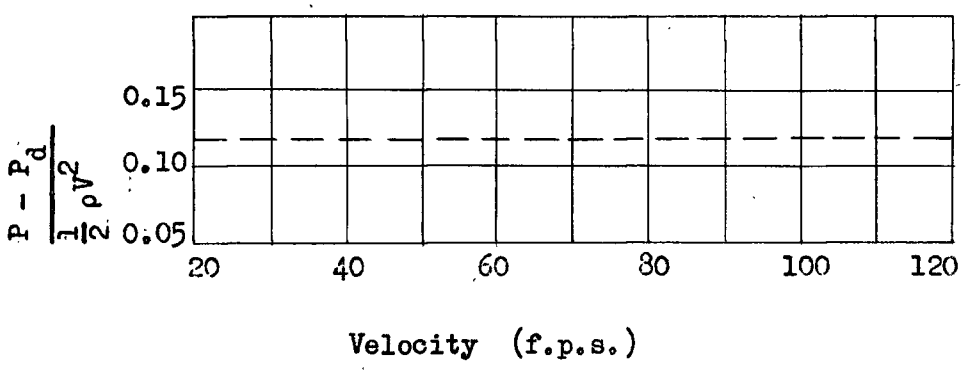

APPENDIX F

TUNNEL CORRECTIONS TO WIND SPEED

Wind speeds were corrected according to Ref. (28). In the absence of better data, corrections to wind speed for the oscillating cylinder were the same as for the stationary cylinder.

Solid Blockage:

$$V = V_{uncorr.} \left[1 + C \lambda \left(\frac{h}{H}\right)^2\right]$$

where $C = 0.822$ for a closed tunnel

$\lambda = 1.0$ (model shape factor)

h = model width

H = tunnel width

Wake Blockage:

$$V = V_{uncorr.} \left[1 + 0.25 \left(\frac{h}{H}\right) C_d\right]$$

where C_d = measured drag coefficient (assumed 1.25)

Therefore $V = V_{uncorr.} \left[1 + 0.82 \left(\frac{3}{36}\right)^2 + 0.25 \ (1.25) \left(\frac{3}{36}\right)\right] = 1.032 \ V_{uncorr.}$

BIBLIOGRAPHY

1. Roshko, A. "On the Development of Turbulent Wakes from Vortex Streets," National Advisory Committee for Aeronautics, Report 1191, 1954.

2. Brooks, N.P.H. "Experimental Investigation of the Aeroelastic Instability of Bluff Two-Dimensional Cylinders," M.A.Sc. Thesis, University of British Columbia, July, 1960.

3. Smith, J.D. "An Experimental Study of the Aeroelastic Instability of Rectangular Cylinders," M.A.Sc. Thesis, University of British Columbia, August, 1962.

4. Parkinson, G.V. "Aspects of the Aeroelastic Behaviour of Bluff Cylinders," Engineering Institute of Canada, Annual General Meeting Paper No. 58, 1962.

5. Morkovin, M.V. "Flow Around Circular Cylinder - A Kaleidoscope of Challenging Fluid Phenomena," Symposium on Fully Separated Flows, The American Society of Mechanical Engineers, May, 1964.

6. Kuchemann, D. "Report on the I.U.T.A.M. Symposium on Concentrated Vortex Motion in Fluids," Journal of Fluid Mechanics. vol. 21, part 1, January, 1965, pp. 1-20.

7. Humphreys, J.S. "On a Circular Cylinder in a Steady Wind at Transition Reynolds Numbers," Journal of Fluid Mechanics, vol. 9, 1960, pp. 603-612.

8. Mattingly, G.E. "An Experimental Study of the Three Dimensionality of the Flow Around a Circular Cylinder," The Institute for Fluid Dynamics and Applied Mathematics, Technical Note BN-295, June, 1962.

9. Keefe, R.T. "An Investigation of the Fluctuating Forces Acting on a Stationary Cylinder in a Subsonic Stream and of the Associated Sound Field," Institute of Aerophysics, University of Toronto, UTIA Report No. 76, September, 1961.

10. McGregor, D.M. "An Experimental Investigation of the Oscillating Pressures on a Circular Cylinder in a Fluid Stream." Institute of Aerophysics, University of Toronto, UTIA Technical Note No. 14, June, 1957.

11. Gerrard, J.H. "An Experimental Investigation of the Oscillating Lift and Drag of a Circular Cylinder Shedding Turbulent Vortices," Journal of Fluid Mechanics, vol. 11, 1961, pp. 244-256.

12. Heine, W. "On the Experimental Investigation of Vortex Excited Pressure Fluctuations," M.A.Sc. Thesis, University of British Columbia, August, 1964.

13. Bishop, R.E.D. Hassan, A.Y. "The Lift and Drag Forces on a Circular Cylinder in a Flowing Fluid," Proceedings of the Royal Society of London. Series A, vol. 277, 1964, pp. 32-50.

14. Fage, A. Johansen, F.C. "The Structure of Vortex Sheets," Philosophical Magazine, Series 7, vol. 5, January-June, 1928. pp. 417-440.

15. Thom, A. "The Flow Past Circular Cylinders at Low Speeds," Proceedings of the Royal Society of London, Series A, vol. 141, 1933, pp. 651-669.

16. Kovasznay, L.S.G. "Hot Wire Investigation of the Wake Behind Cylinders at Low Reynolds Numbers," Proceedings of the Royal Society of London, Series A, vol. 198, 1949, pp. 174-190.

17. Rosenhead, L. "An Experimental Investigation of the Flow Behind Circular Cylinders in Channels of Different Breadths," Proceedings of the Royal Society of London, Series A, vol. 129, 1930, pp. 115-135.

18. Shair, F.H. Grove, A.S. Petersen, E.E. Acrivos, A. "The Effect of Confining Walls on the Stability of the Steady Wake Behind a Circular Cylinder," Journal of Fluid Mechanics, vol. 17, 1963, pp. 546-550.

19. Roshko, A. "On the Drag and Shedding Frequency of Two-Dimensional Bluff Bodies," National Advisory Committee of Aeronautics, Technical Note 3169, July, 1954.

20. Bloor, M.S. "The Transition to Turbulence in the Wake of a Circular Cylinder," Journal of Fluid Mechanics, vol. 19, part 2, June, 1964, pp. 290-304.

21. Eagleson, P.S. Daily, J.W. Noutsopolous, G.K. "Flow Induced Vibration of Flat Plates," Massachusetts Institute of Technology, Department of Civil Engineering, Report No. 58, February, 1963.

22. Smirnov, L.P. Pavlihina, M.A. "Vortical Traces for Flow Around Vibrating Cylinders," Studii si Cercetari Mecan. Appl. v.9, 1958.

23. Bishop, R.E.D. Hassan, A.Y. "The Lift and Drag Forces on a Circular Cylinder Oscillating in a Flowing Fluid," Proceedings of the Royal Society of London, Series A, vol. 277, 1964, pp. 51-75.

24. Wehrmann, O.H. "Reduction of Velocity Fluctuations in a Karman Vortex Street by a Vibrating Cylinder," Boeing Scientific Research Laboratories, Seattle, Washington, August, 1964.

25. Santosham, T.V. "Non-Linear Characteristics of Rectangular Sections and Force Measurements on a D-Section," M.A.Sc. Thesis, University of British Columbia, 1965.

26. Fage, A. Johansen, F.C. "On the Flow of Air Behind an Inclined Flat Plate of Infinite Span," Proceedings of the Royal Society of London, Series A, vol. 116, 1927, pp. 170-197.

27. Bryer, D.W. Walshe, D.E. Garner, H.C. "Pressure Probes Selected for Three-Dimensional Flow Measurement," Aeronautical Research Council Reports and Memoranda, R. and M. No. 3037, 1958.

28. Pankhurst, R.C. Holder, D.W. "Wind Tunnel Technique," Pitman, 1948.

29. Liepmann, H.W. Roshko, A. "Elements of Gas Dynamics," Wiley, 1960, Chapt. 3.

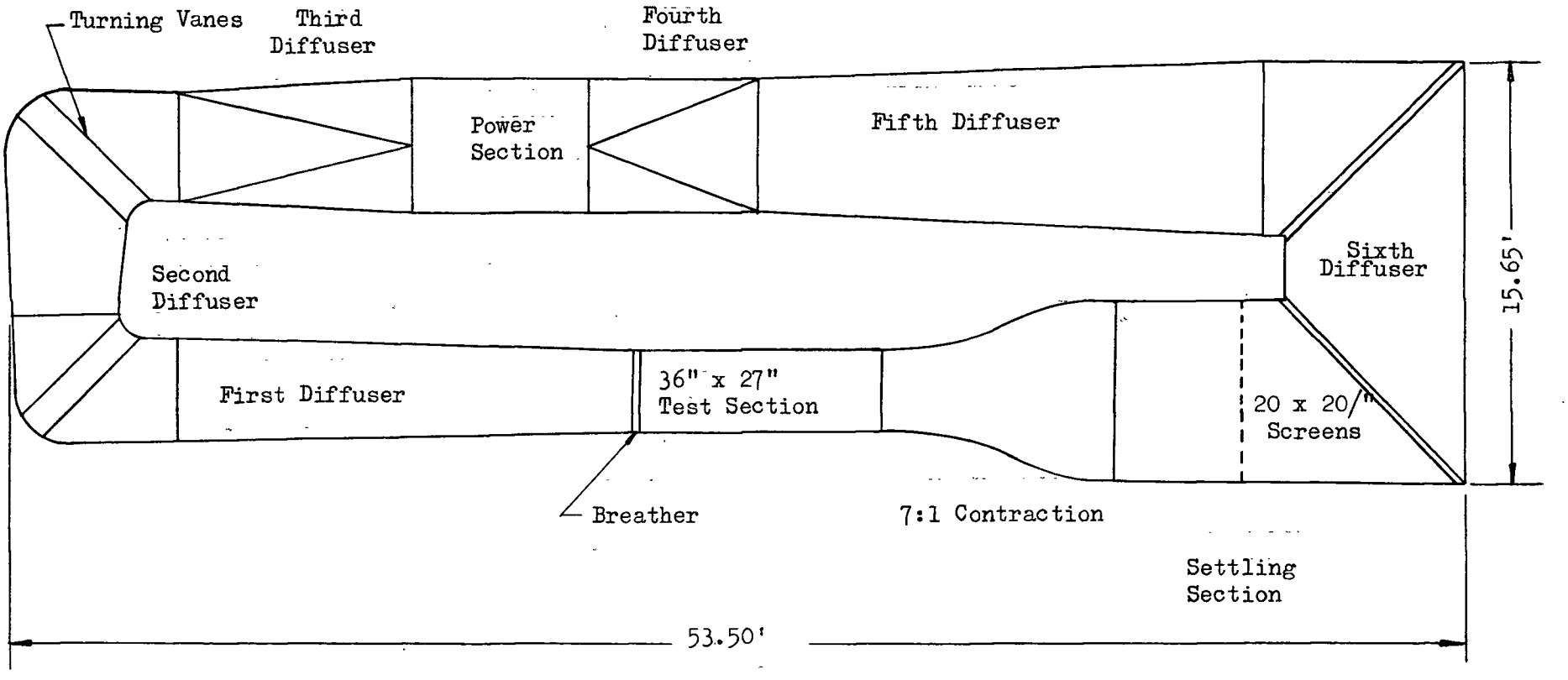

AERODYNAMIC OUTLINE OF WIND TUNNEL

Fig. 1

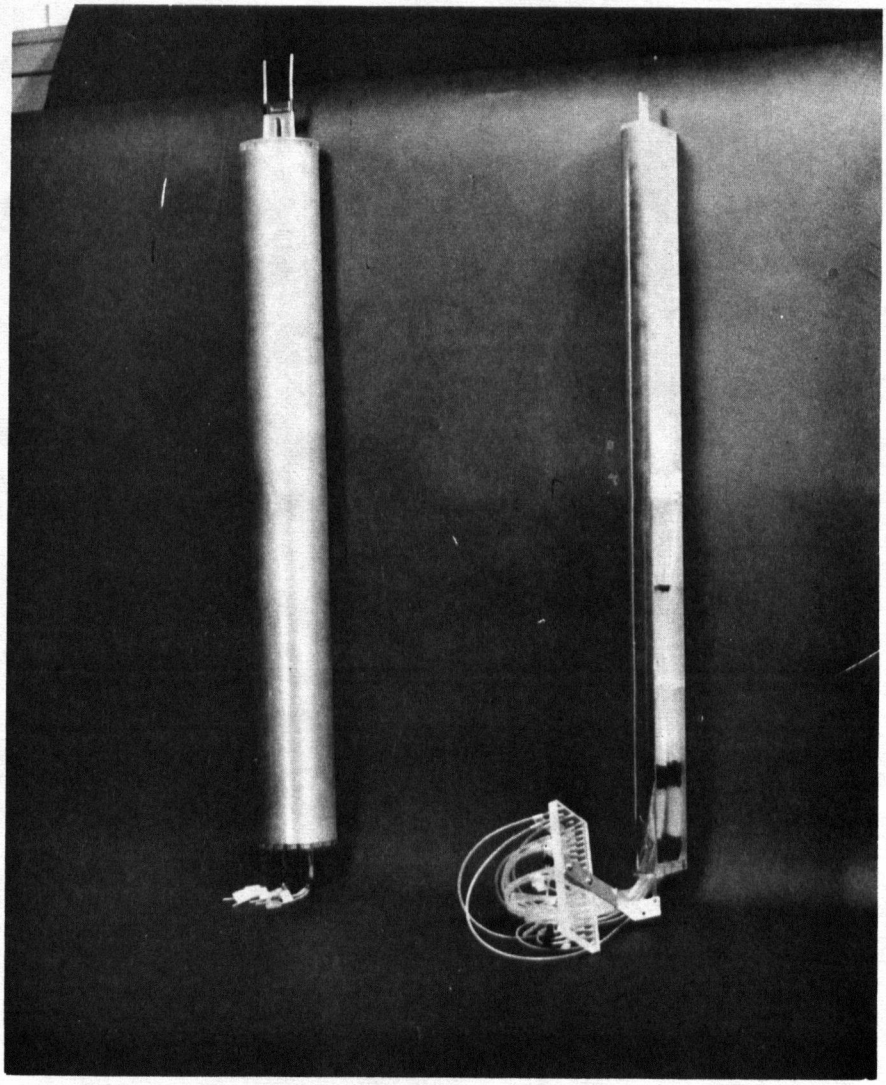

MODELS, 3 INCH DIAMETER CIRCULAR CYLINDER AND
3 INCH D-SECTION

Fig. 2

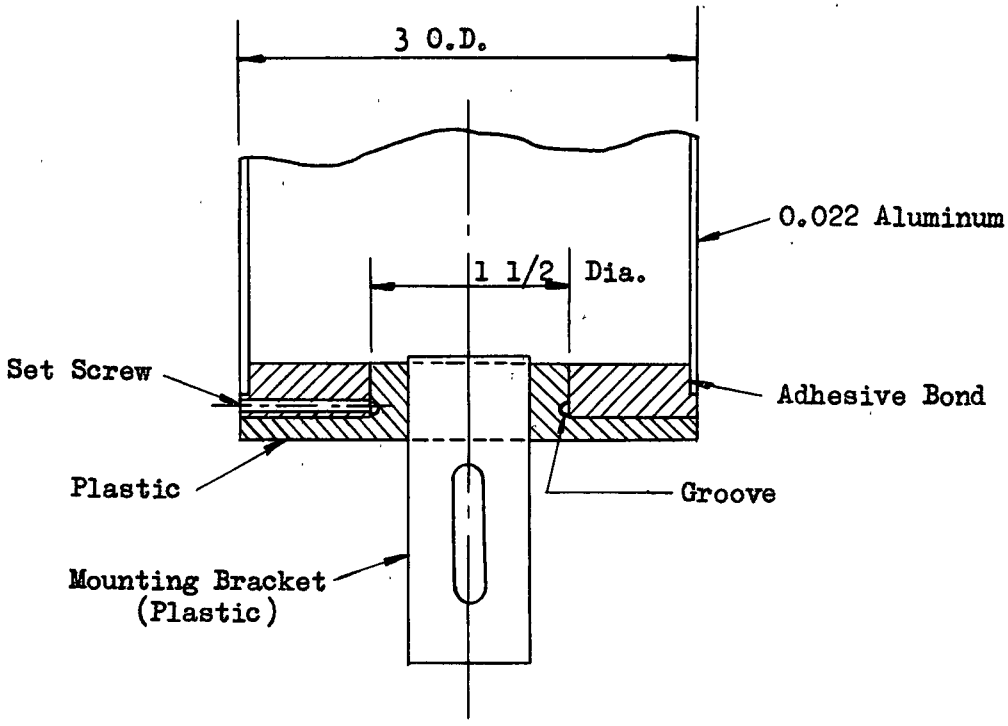

PLASTIC END FITTINGS FOR CIRCULAR CYLINDER

Fig. 3

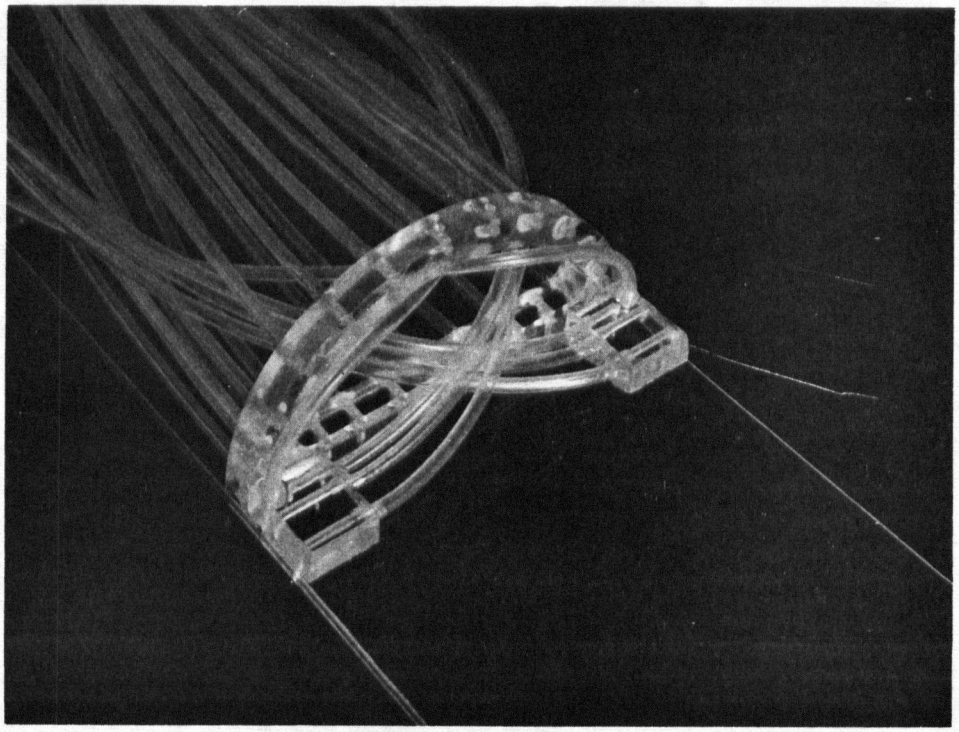

MID-SPAN BULKHEAD OF D-SECTION MODEL BEFORE
ALUMINUM SKIN WAS ATTACHED

Fig. 4

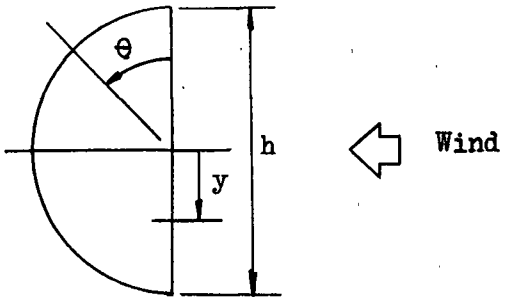

Tap No.	θ Deg.	Tap No.	y/h
1	2 1/2	18	0.490
2	5	19	0.469
3	10	20	0.427
4	20	21	0.375
5	30	22	0.292
6	45	23	0.208
7	60	24	0.104
8	75	25	0
9	90	26	-0.104
10	105	27	-0.208
11	120	28	-0.292
12	135	29	-0.375
13	150	30	-0.427
14	160	31	-0.469
15	170	32	-0.490
16	175		
17	177 1/2		
33	2 1/2, 3 in. below mid-span		
34	2 1/2, 6 in. below mid-span		

PRESSURE TAP POSITIONS FOR D-SECTION MODEL

Fig. 5

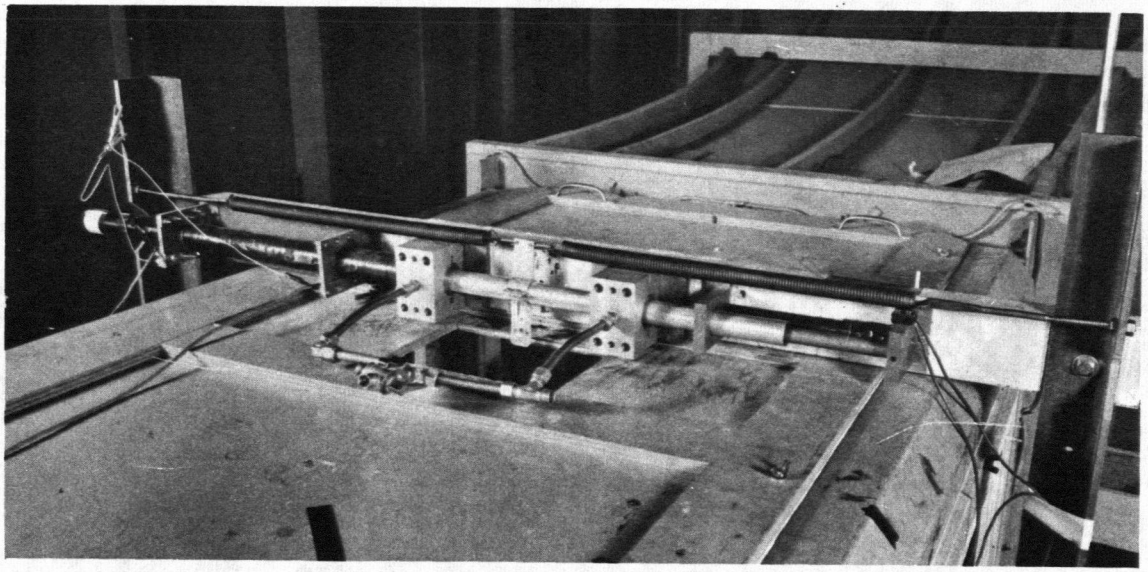

AIR BEARINGS, SHAFT AND SPRINGS

Fig. 6

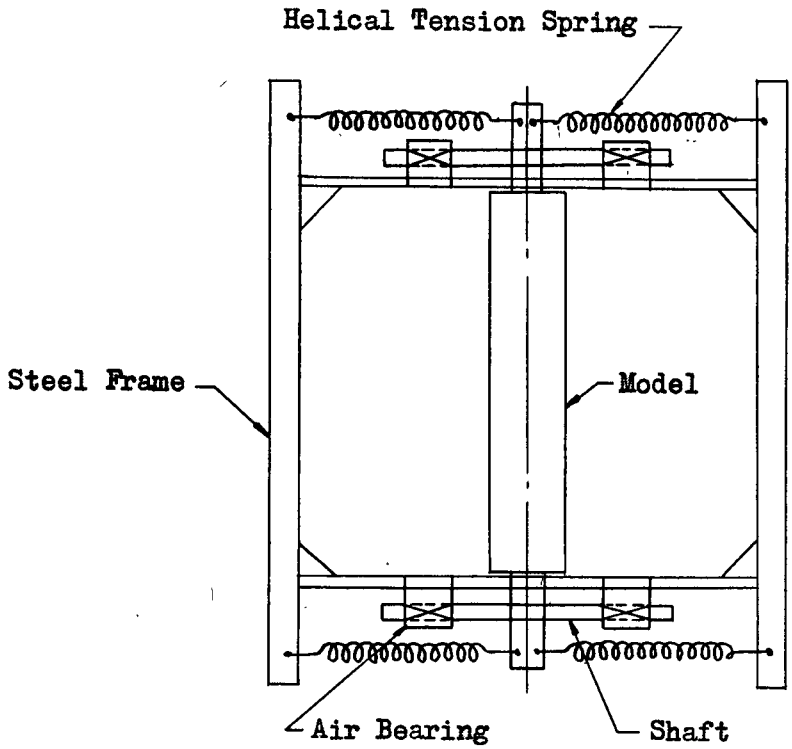

ARRANGEMENT OF MODEL MOUNTING SYSTEM

Fig. 7

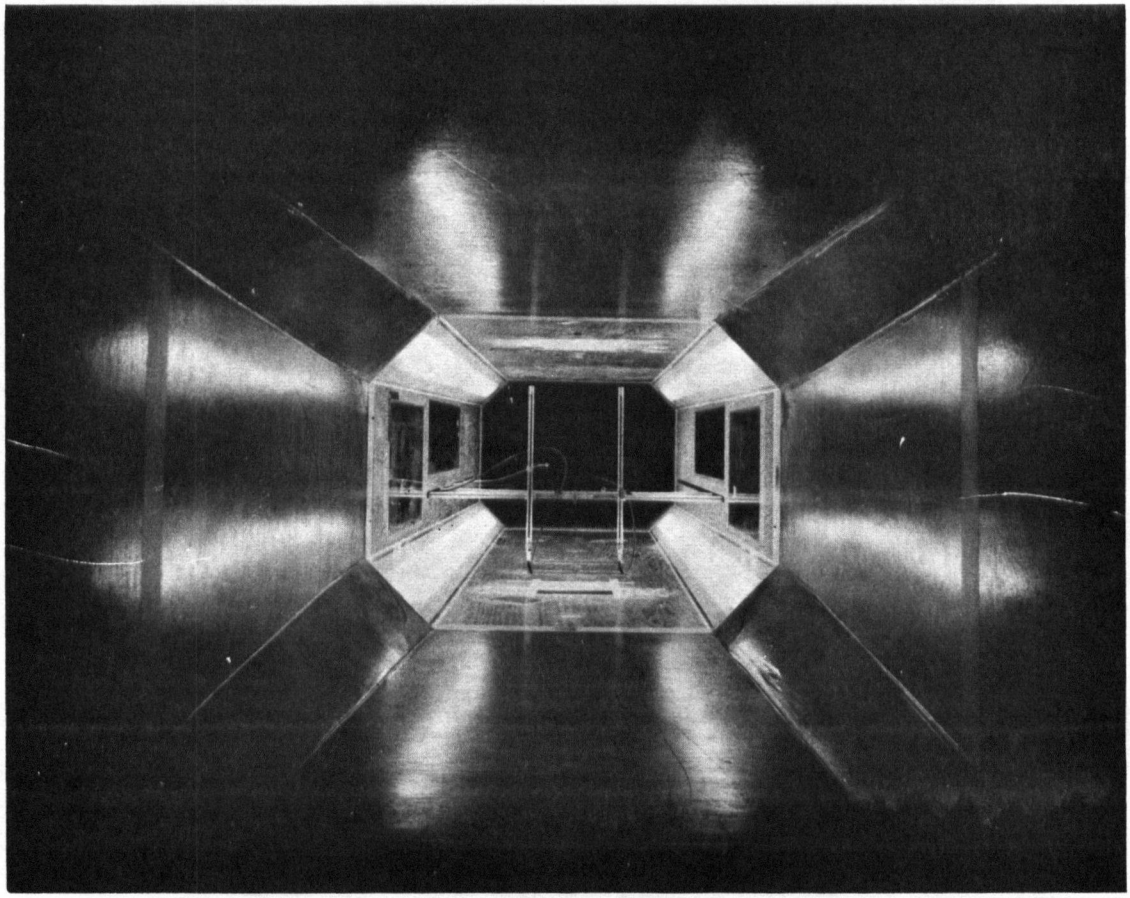

TRAVERSING GEAR - LOOKING DOWNSTREAM INTO
WIND TUNNEL TEST SECTION

Fig. 8

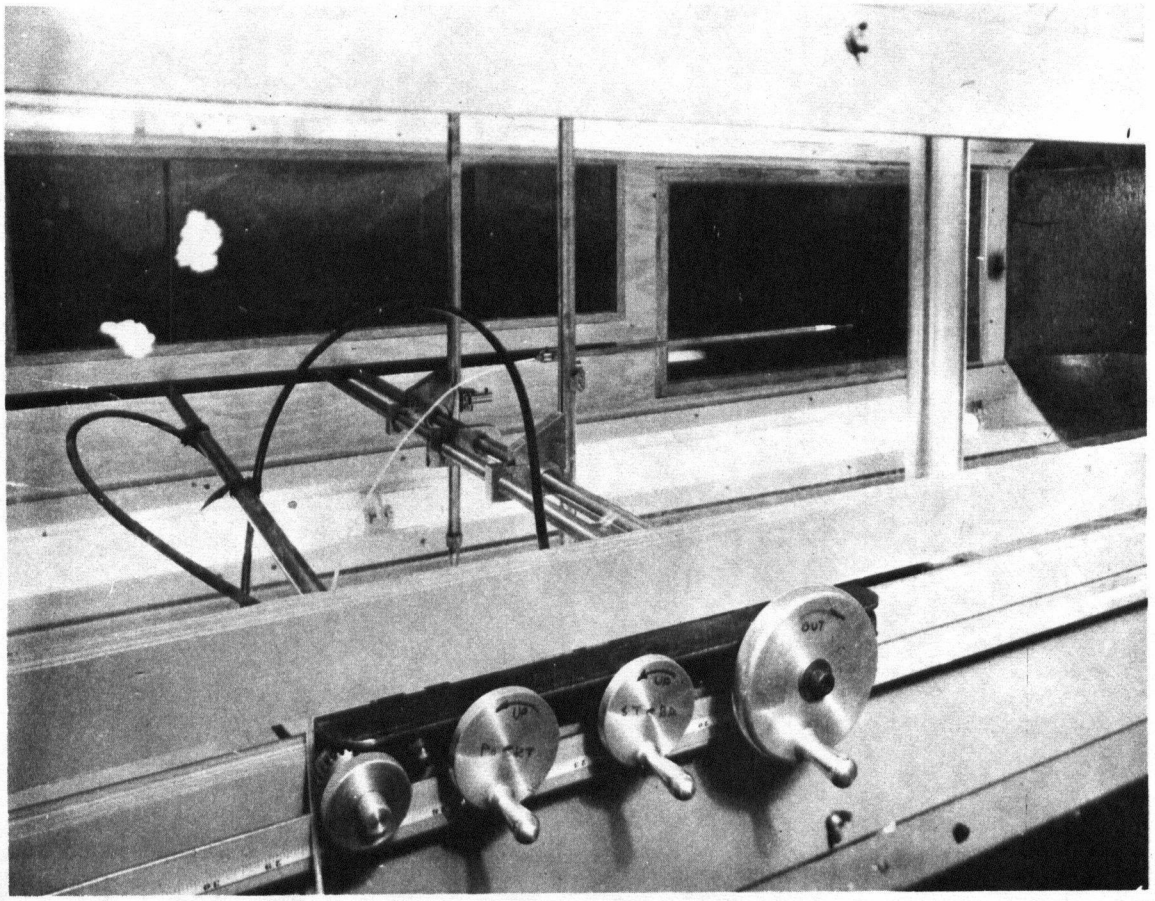

TRAVERSING GEAR IN TEST SECTION SHOWING WORKING AREA SIDE PANEL

Fig. 9

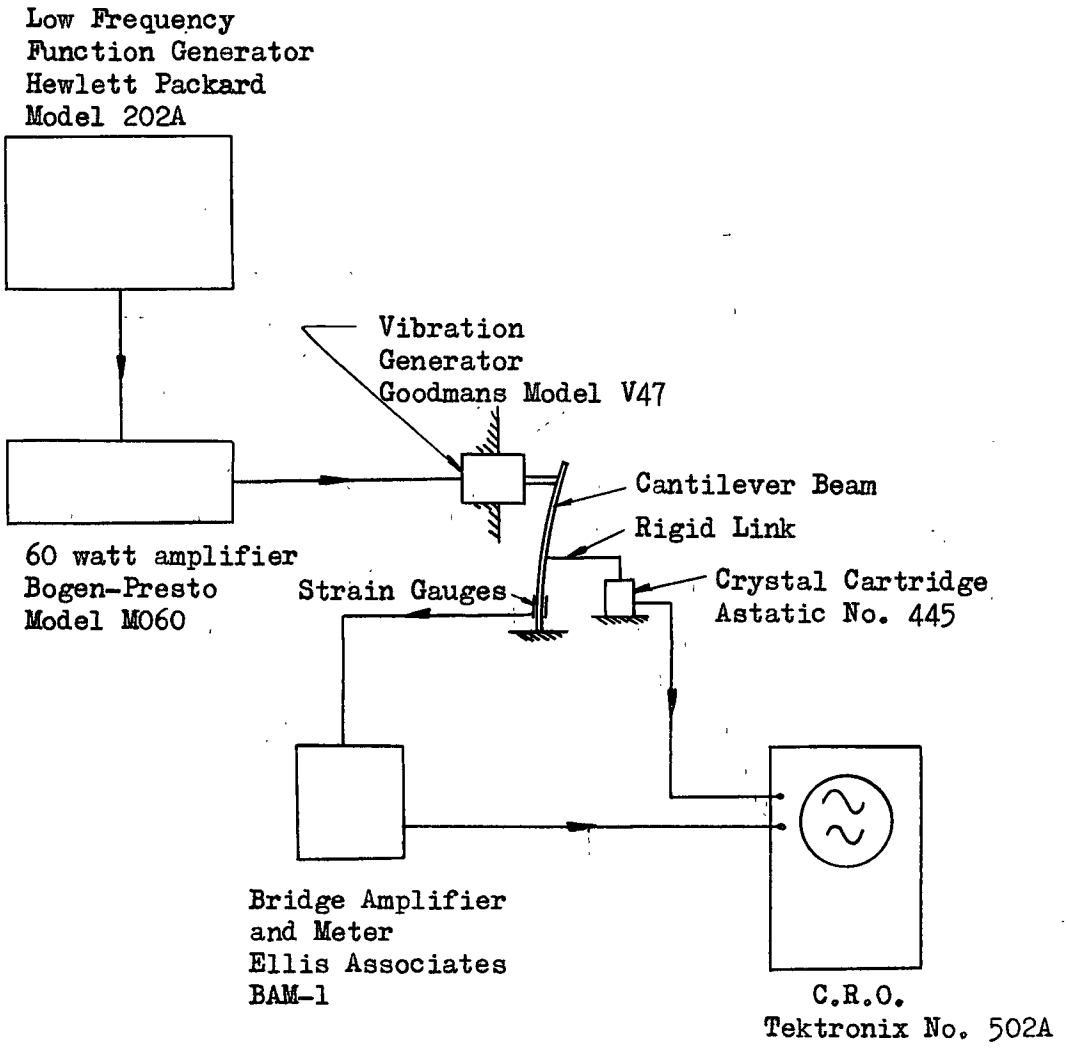

DIAGRAMMATIC LAYOUT OF APPARATUS USED
IN CRYSTAL RESPONSE INVESTIGATION

Fig. 10

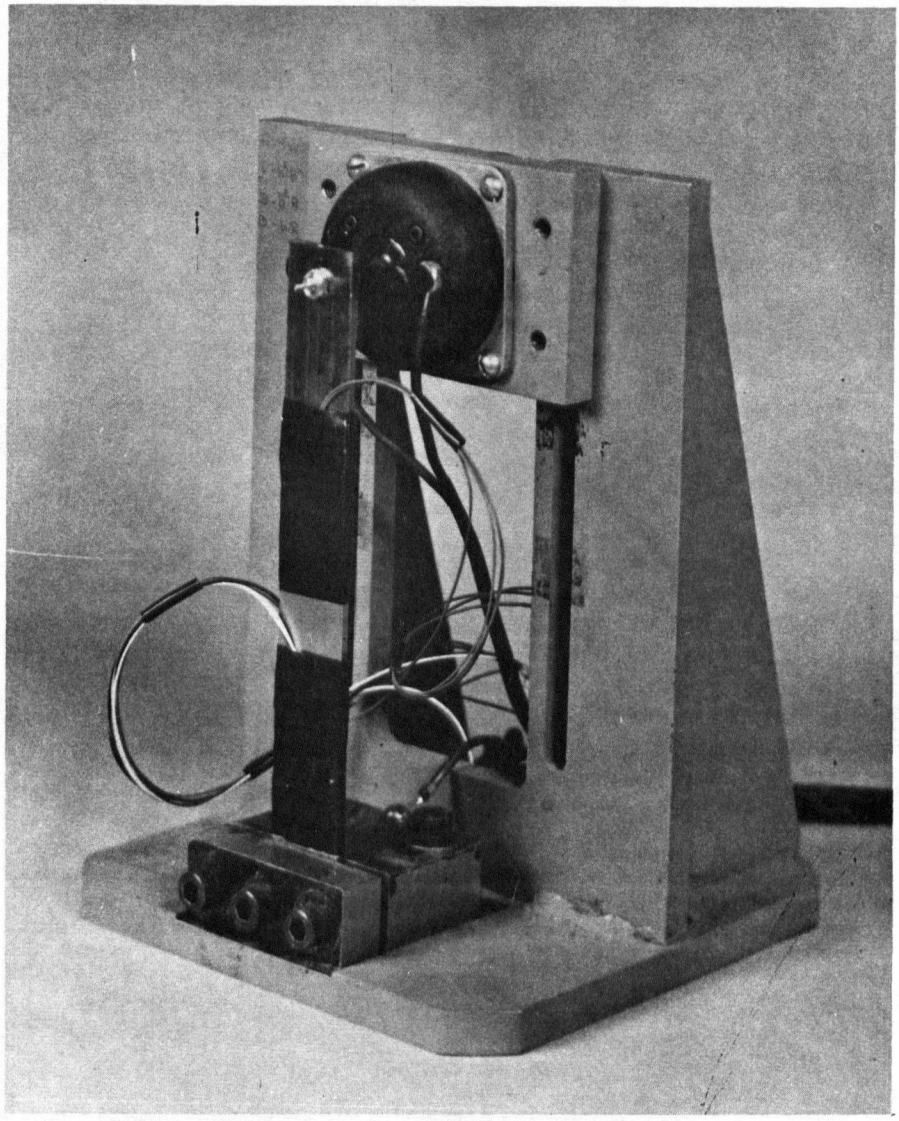

VIBRATION GENERATOR AND CANTILEVER BEAM
MOUNTED IN FRAME

Fig. 11

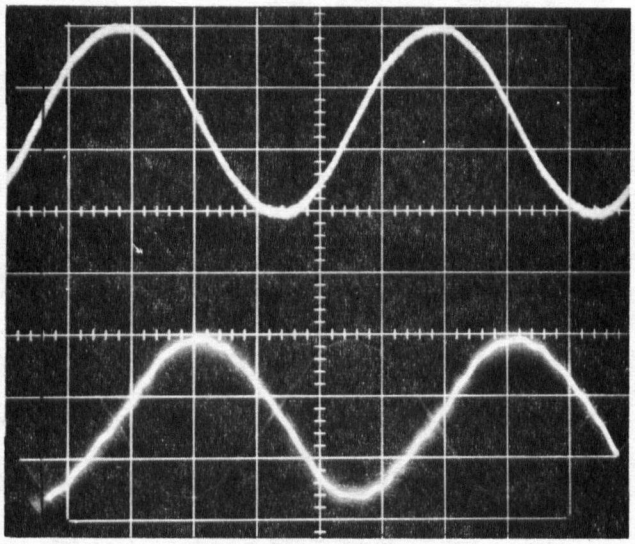

Strain gauge signal

Crystal signal

Sinusoidal Wave Form - 20 cps

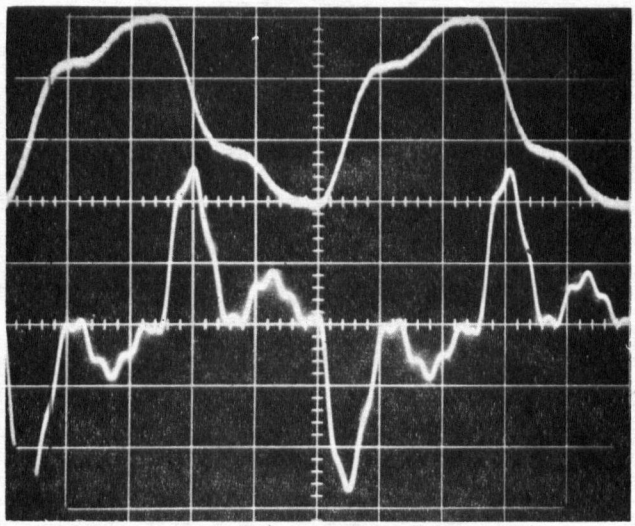

Strain gauge signal

Crystal signal

Non-sinusoidal Wave Form - 20 cps

TYPICAL OSCILLOSCOPE TRACES ... RESPONSE

Fig. 12 (continued)

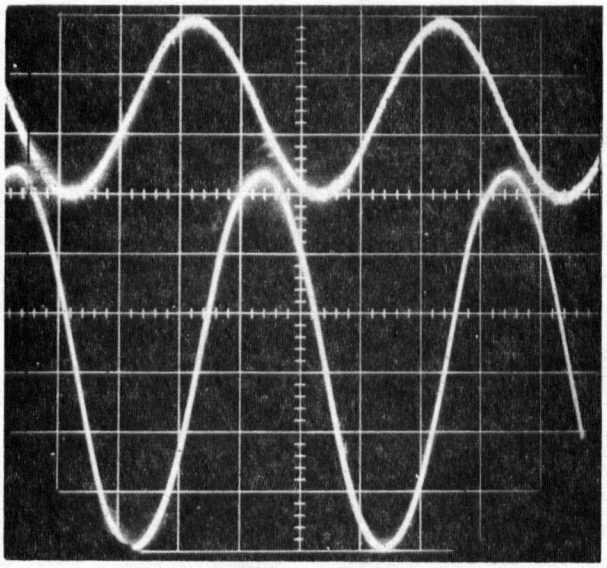

Strain gauge signal

Crystal signal

Sinusoidal Wave Form - 50 cps

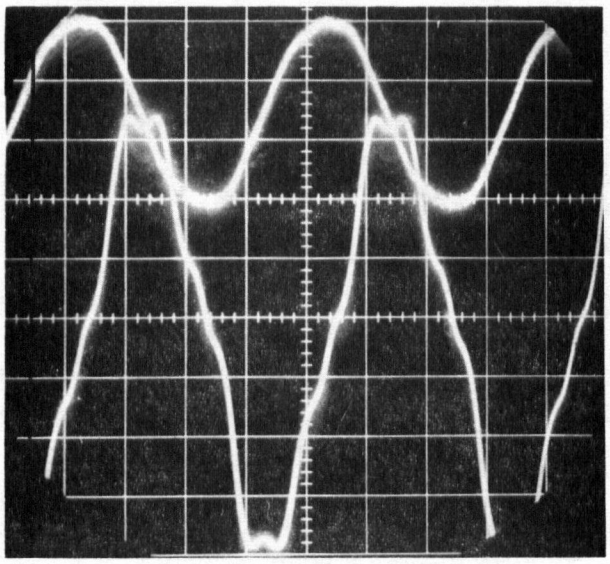

Strain gauge signal

Crystal signal

Non-sinusoidal Wave Form - 50 cps

TYPICAL OSCILLOSCOPE TRACES OF CRYSTAL AND CANTILEVER BEAM RESPONSE

Fig. 12

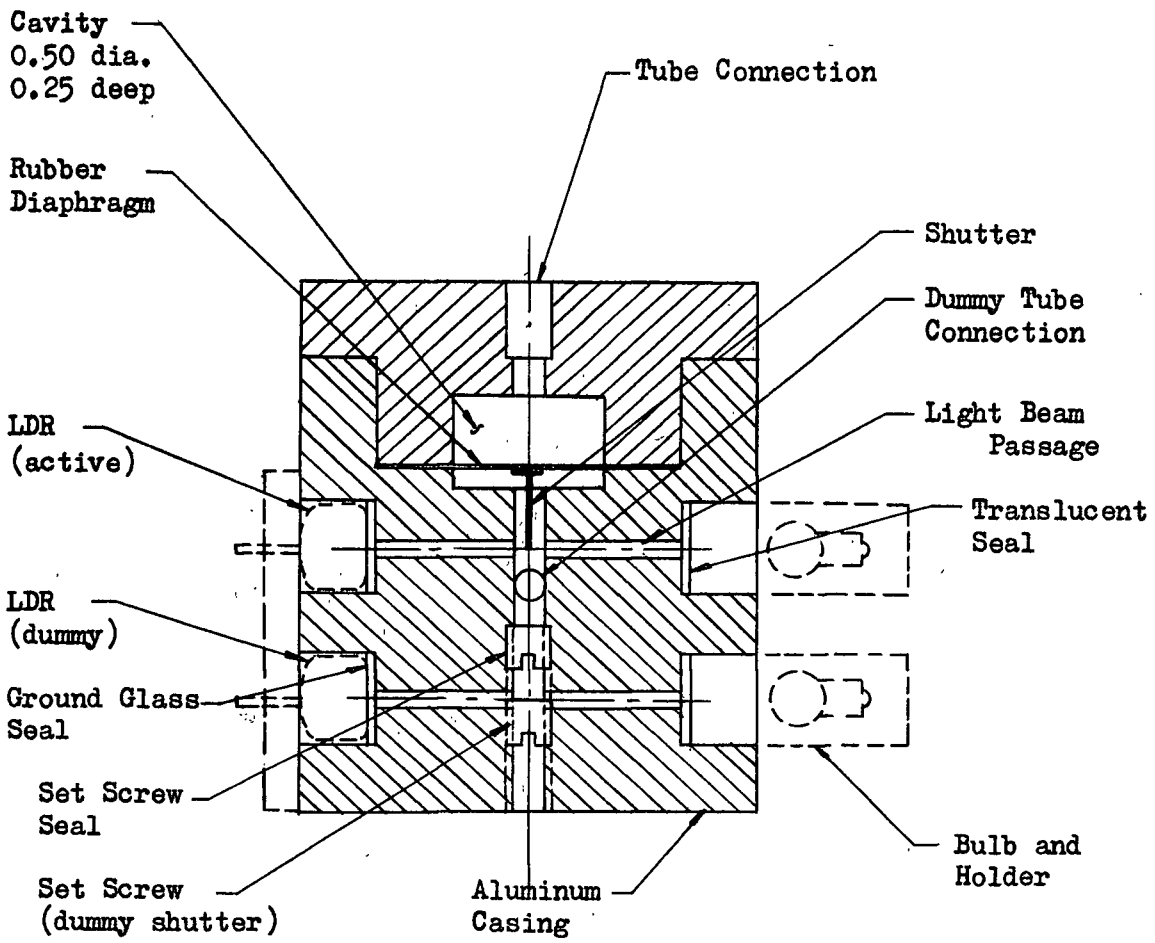

PRESSURE TRANSDUCER DETAILS

Fig. 13

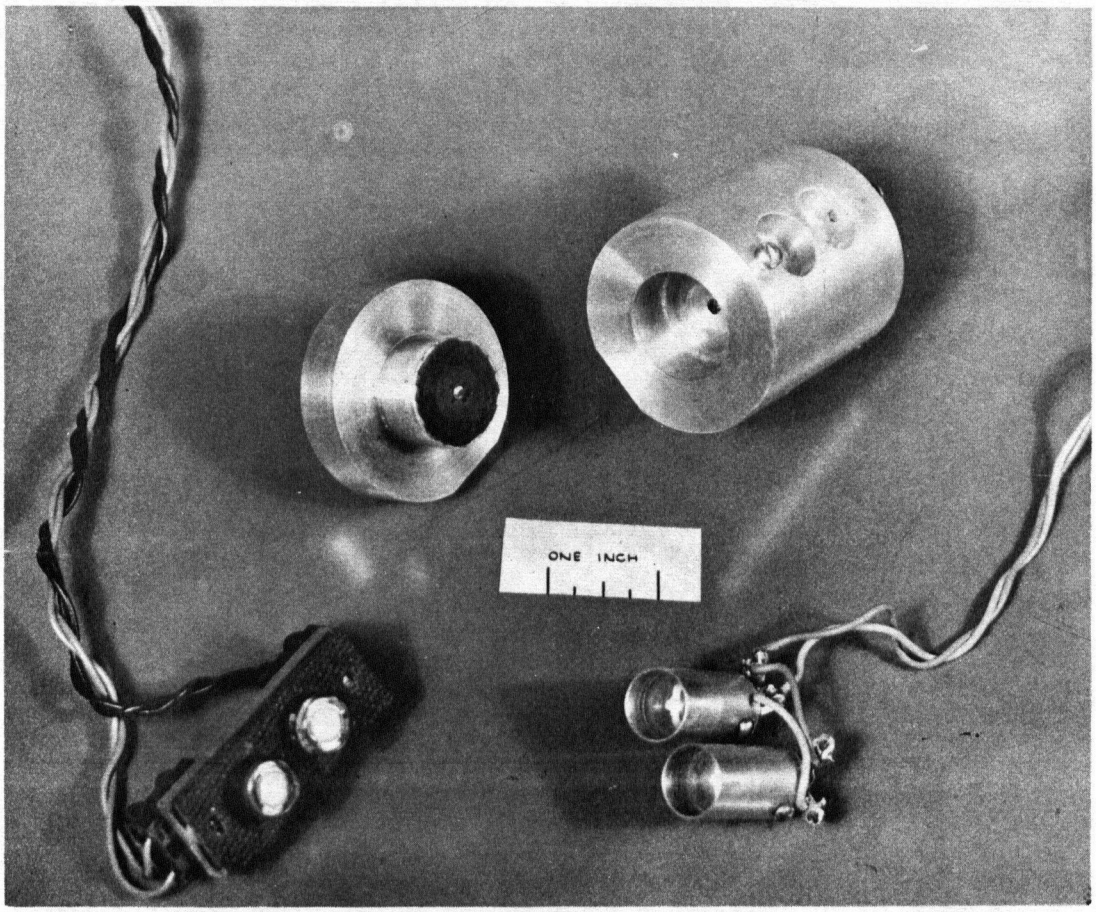

PRESSURE TRANSDUCER - DISASSEMBLY

Fig. 14

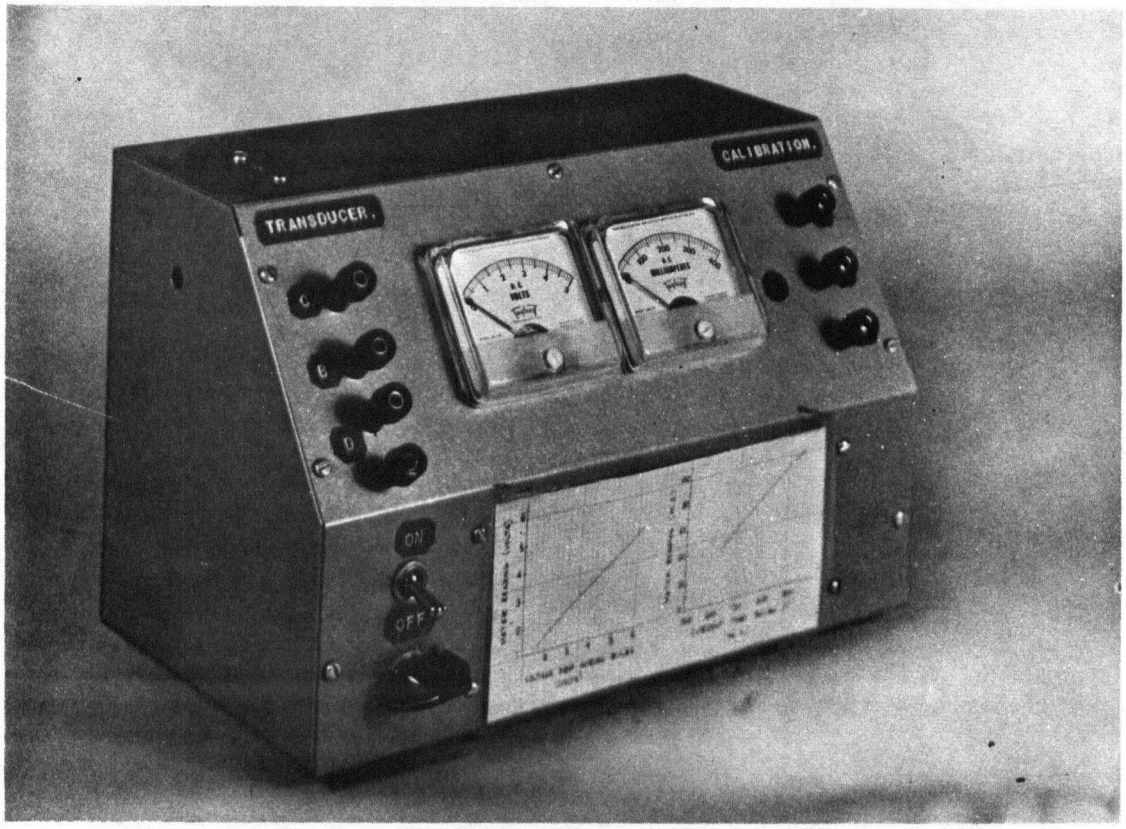

PRESSURE TRANSDUCER

Fig. 15

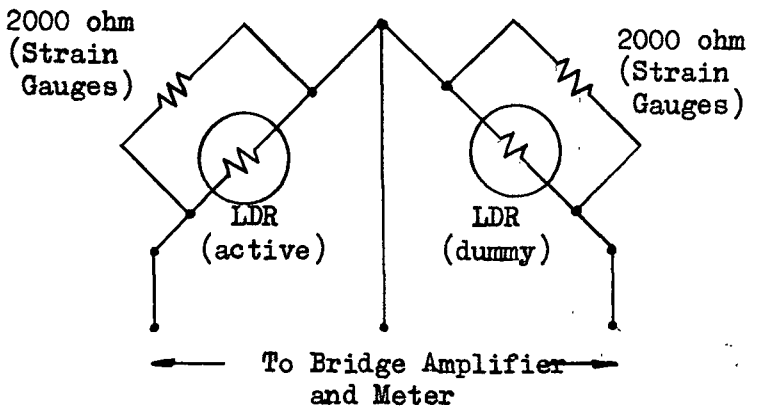

LDR - Light Dependent Resistance

(a) Bridge Circuit

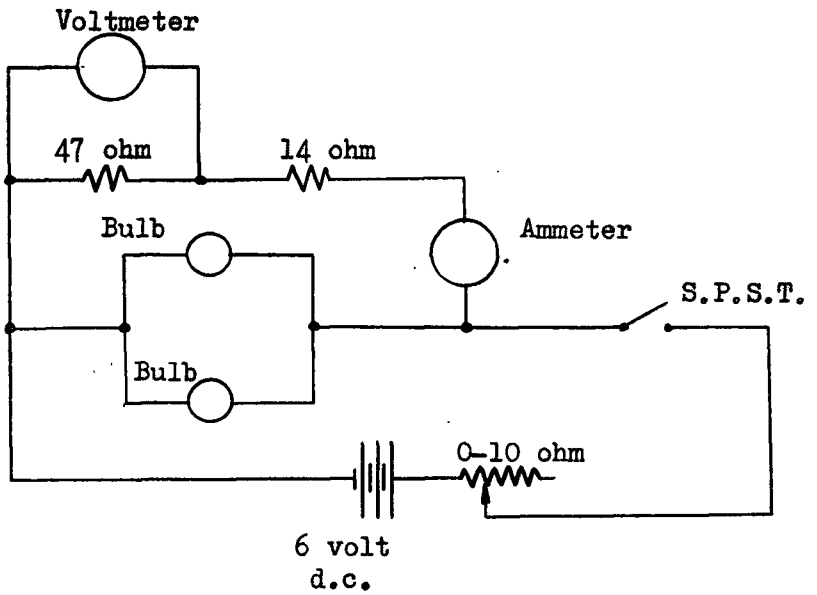

(b) Light Circuit

PRESSURE TRANSDUCER - CIRCUIT DIAGRAMS

Fig. 16

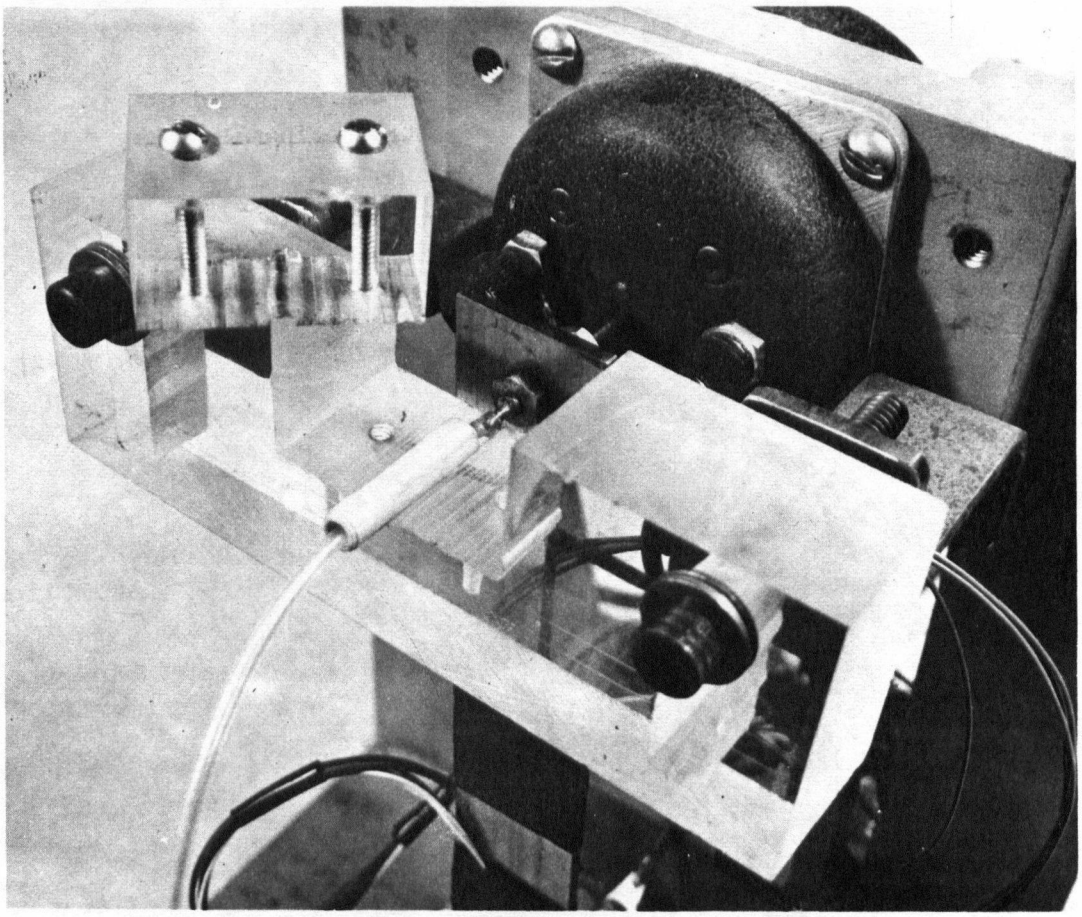

PISTON ARRANGEMENT AT UPPER END OF CANTILEVER BEAM
SHOWING TUBE AND TUBE CLAMP

Fig. 17

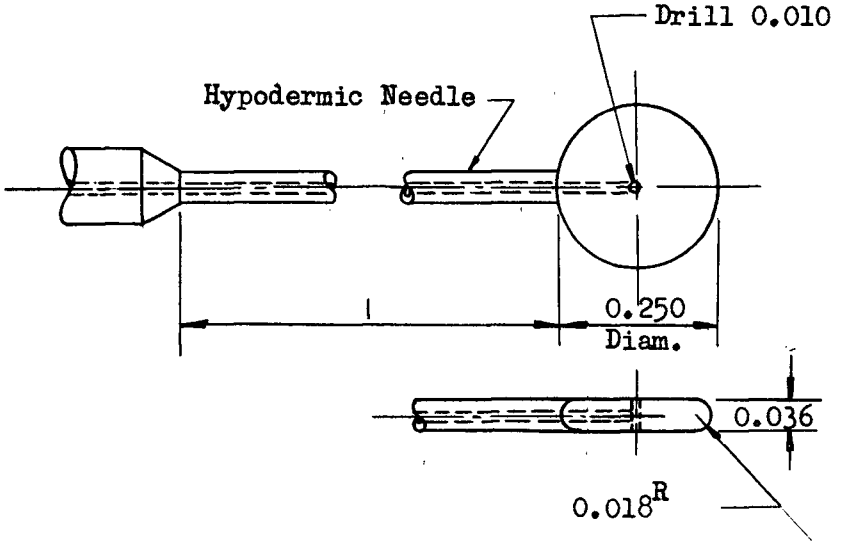

Disc Material: - Mild Steel

DISC PROBE

Fig. 18

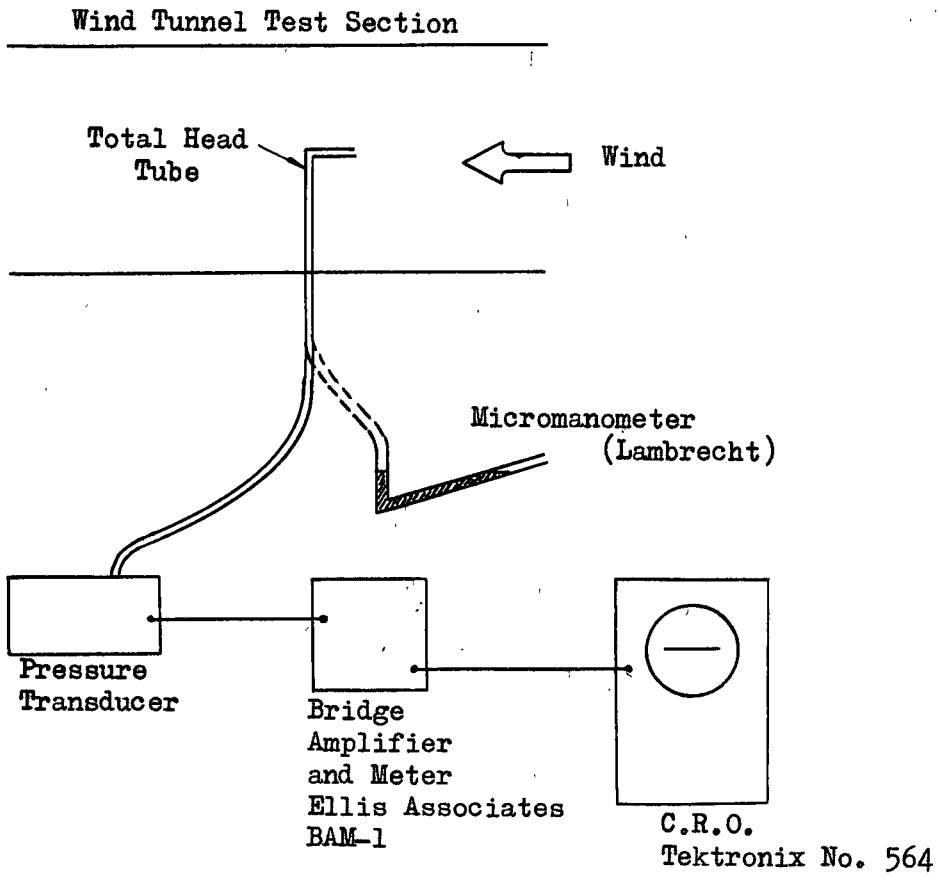

DIAGRAMMATIC LAYOUT OF STEADY PRESSURE CALIBRATION APPARATUS

Fig. 19

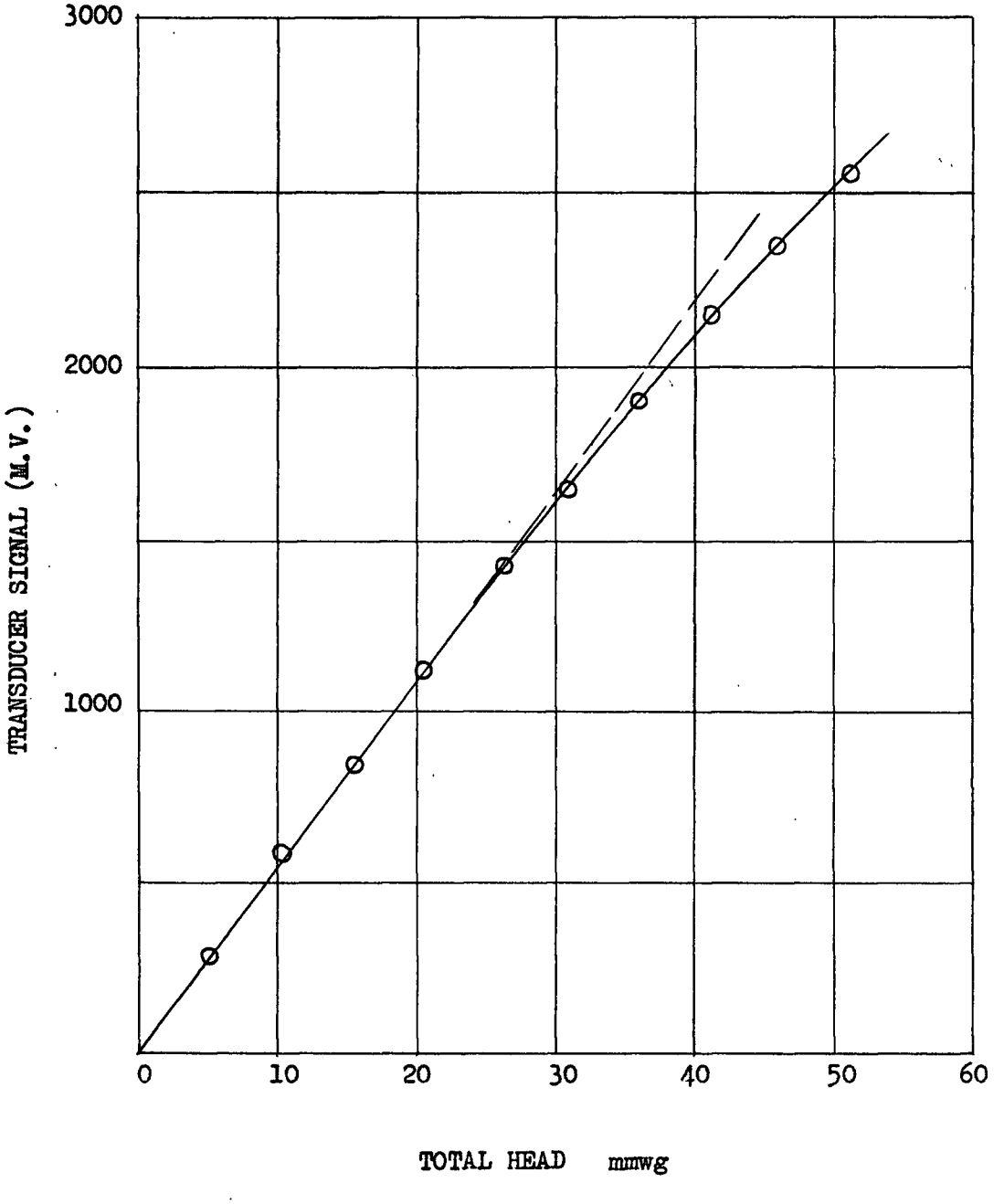

PRESSURE TRANSDUCER SIGNAL VS. TOTAL HEAD
STEADY PRESSURE

Fig. 20

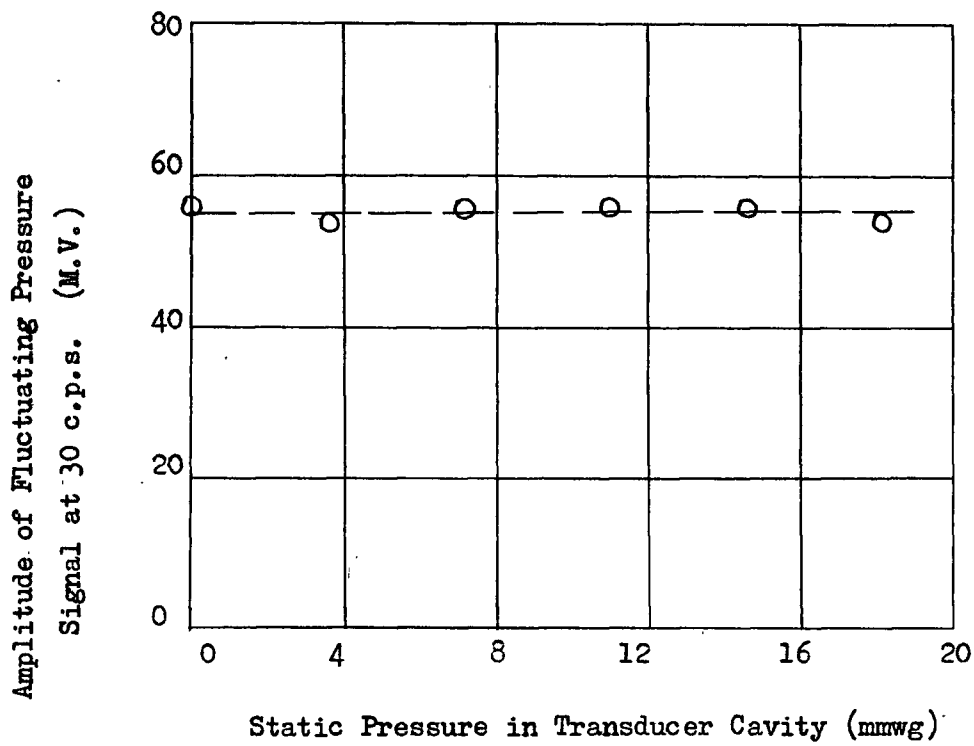

THE EFFECT OF A STATIC PRESSURE RISE IN THE TRANSDUCER CAVITY ON THE TRANSDUCER SENSITIVITY TO A FLUCTUATING PRESSURE

Fig. 21

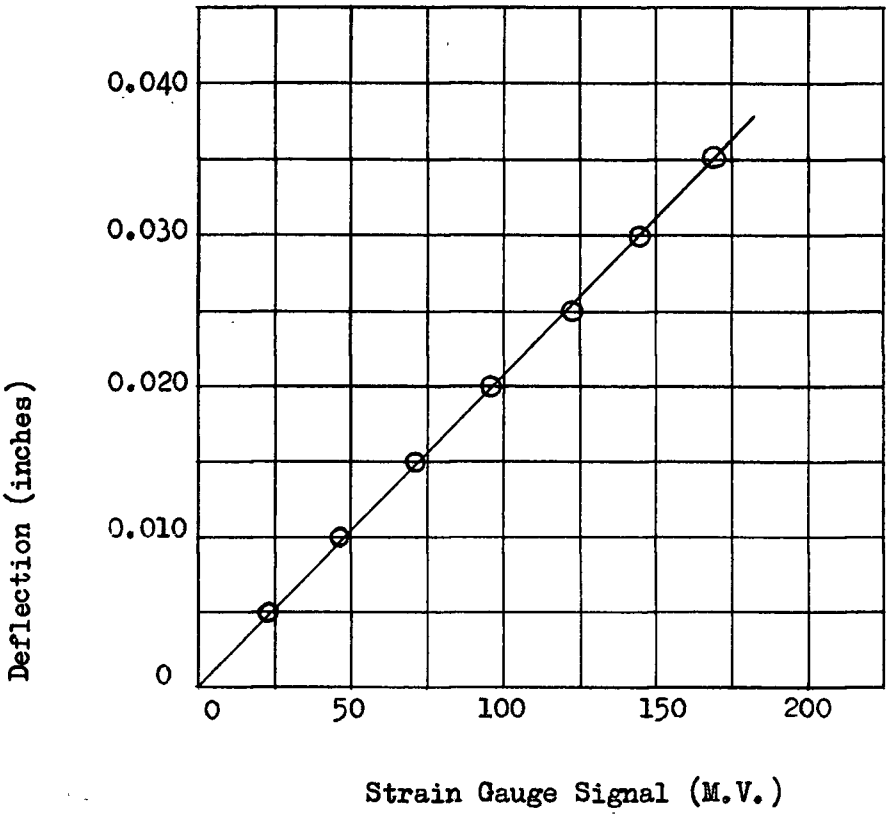

CANTILEVER BEAM DEFLECTION VS. STRAIN GAUGE SIGNAL

Fig. 22

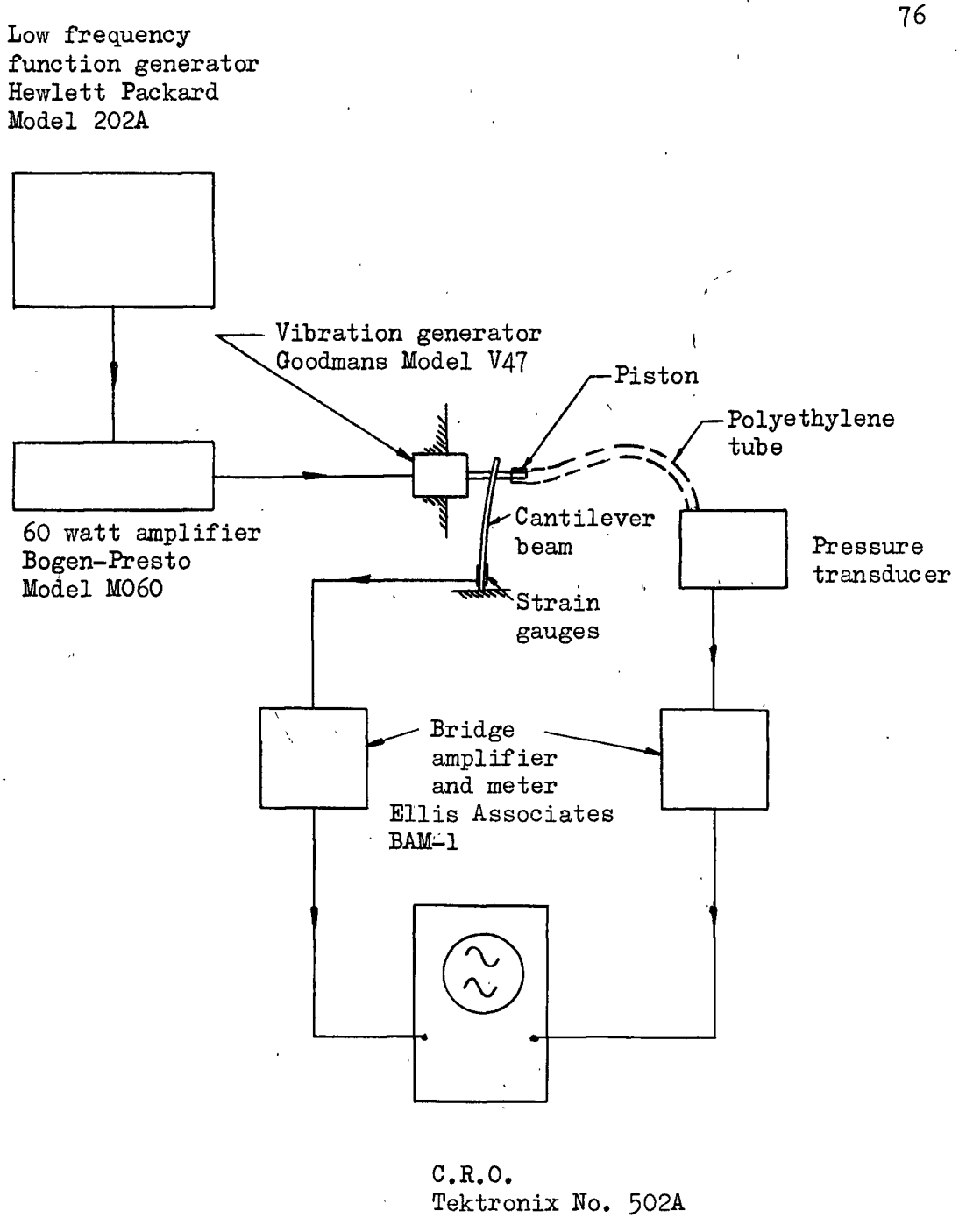

DIAGRAMMATIC LAYOUT OF PRESSURE
TRANSDUCER CALIBRATION APPARATUS

Fig. 23

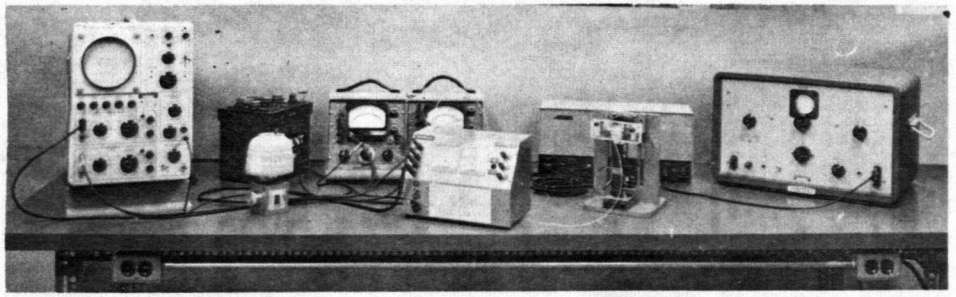

PRESSURE TRANSDUCER CALIBRATION APPARATUS

Fig. 24

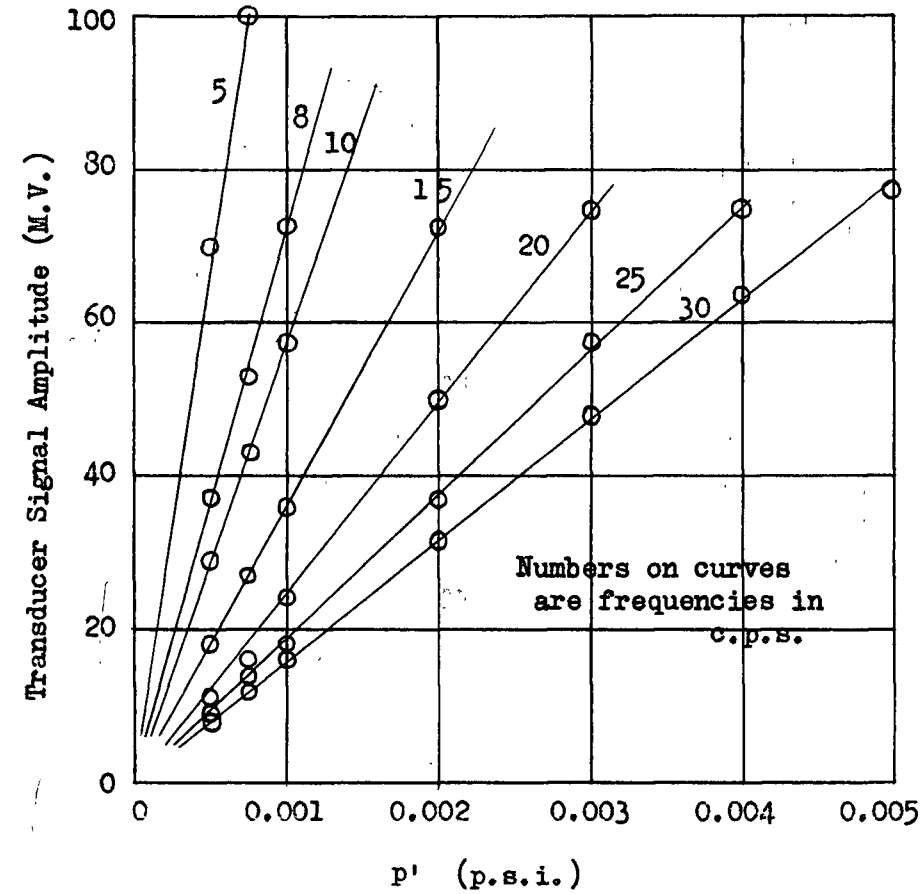

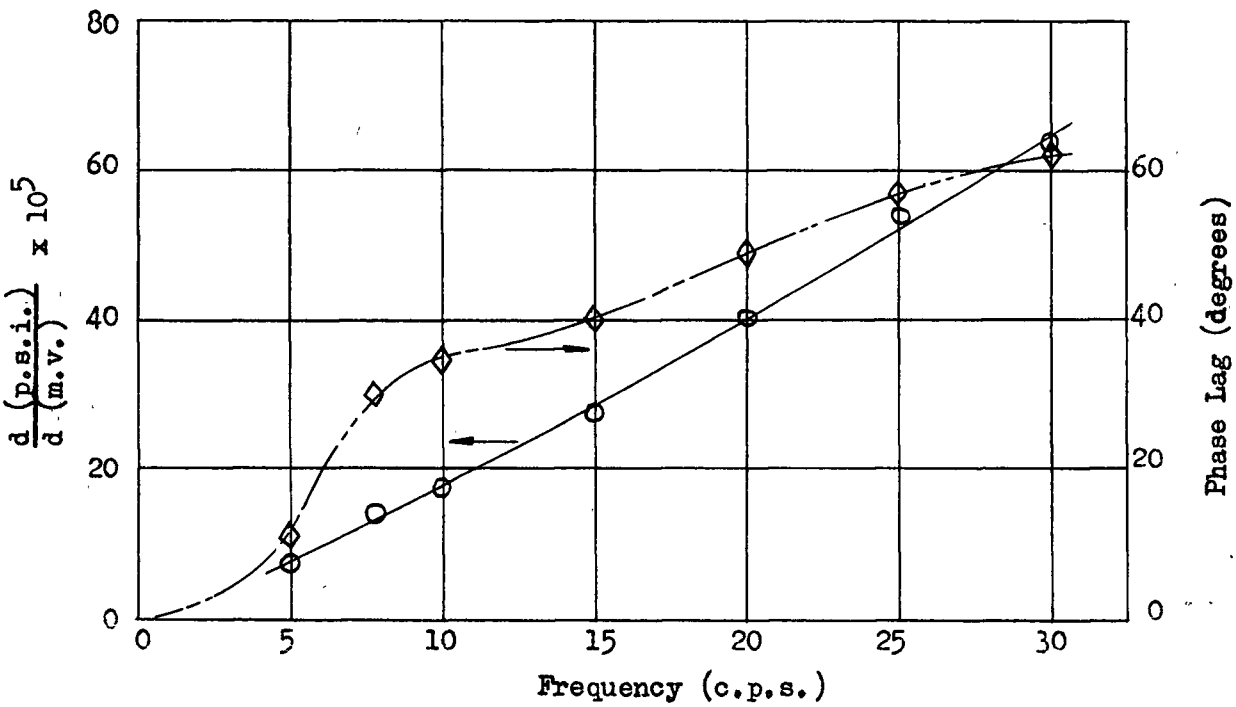

TRANSDUCER CALIBRATION DATA FOR USE WITH A TUBE 4.0 FT. LONG, 0.066 IN. INSIDE DIAMETER

Fig. 25

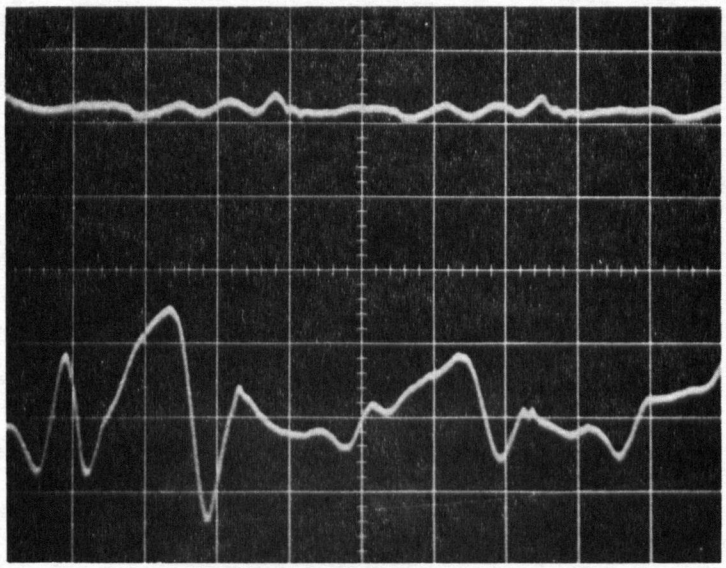

With dummy connected

Without dummy connected

PRESSURE TRANSDUCER SIGNAL DURING TUBE OSCILLATION
WITH AND WITHOUT A DUMMY TUBE CONNECTED

Fig. 26

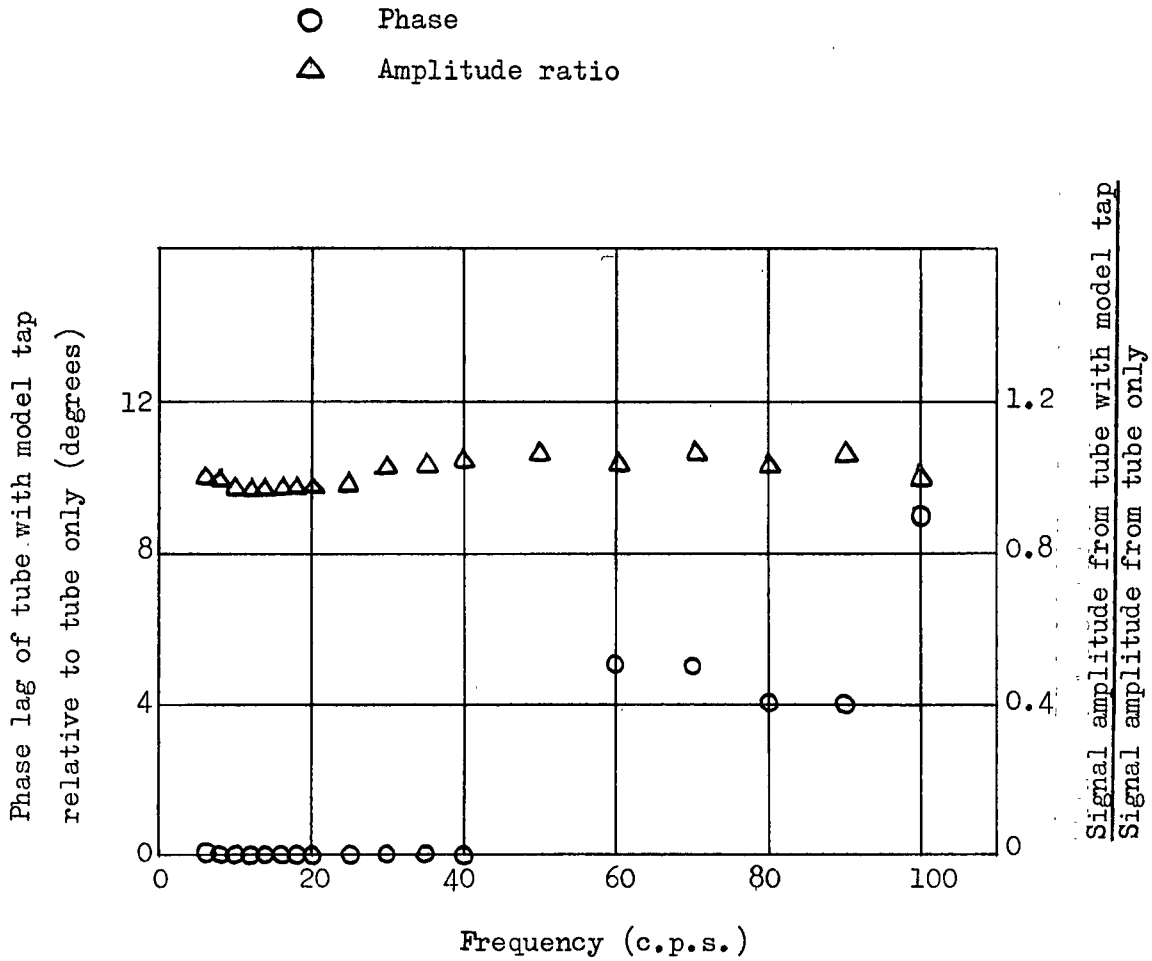

PHASE AND AMPLITUDE RATIO VS. FREQUENCY
MODEL TAP CONSTRICTION CALIBRATION

Fig. 27

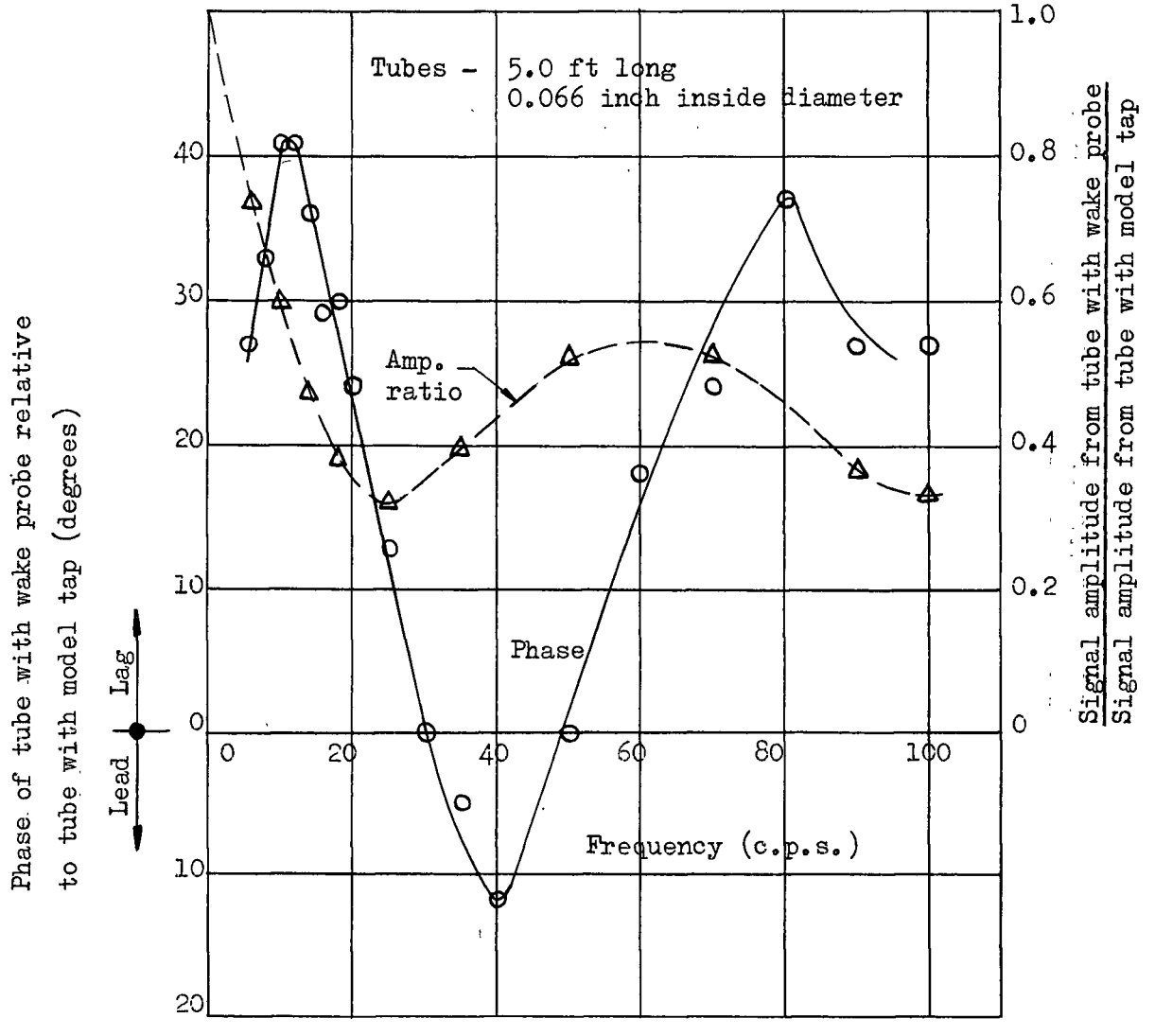

PHASE AND AMPLITUDE RATIO VS. FREQUENCY
DISC PROBE CALIBRATION

Fig. 28

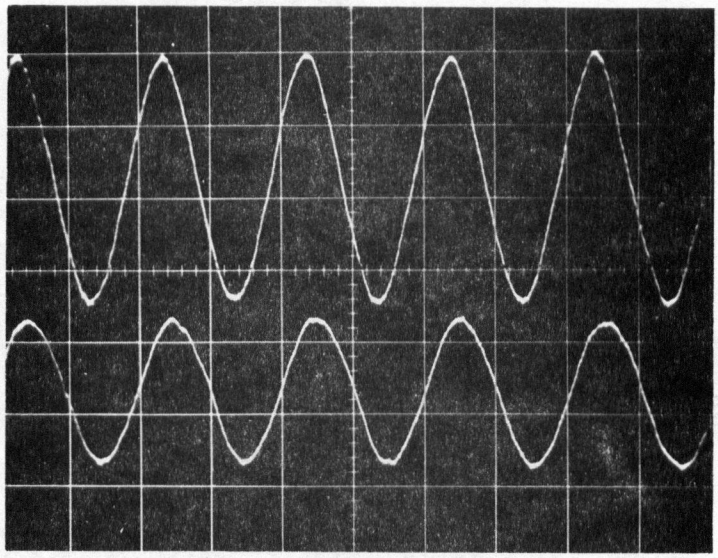

Tube only

Tube and disc probe

10 c.p.s.

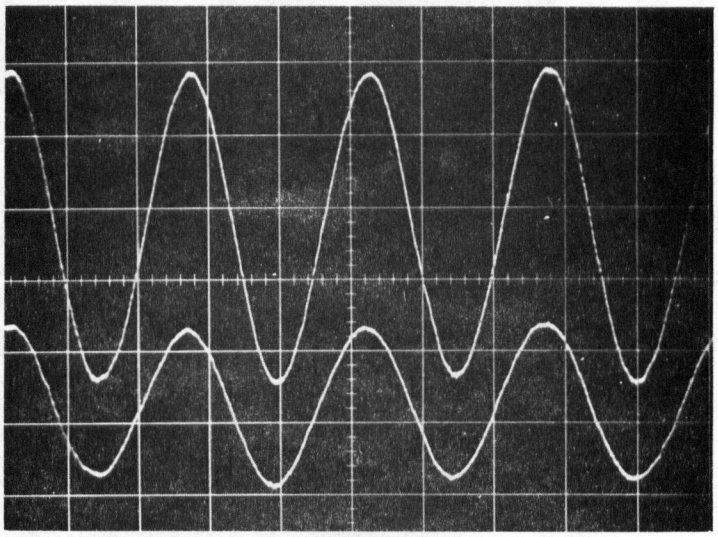

Tube only

Tube and disc probe

40 c.p.s.

TYPICAL OSCILLOSCOPE TRACES OF PRESSURE SIGNALS FROM DISC PROBE CALIBRATION

Fig. 29

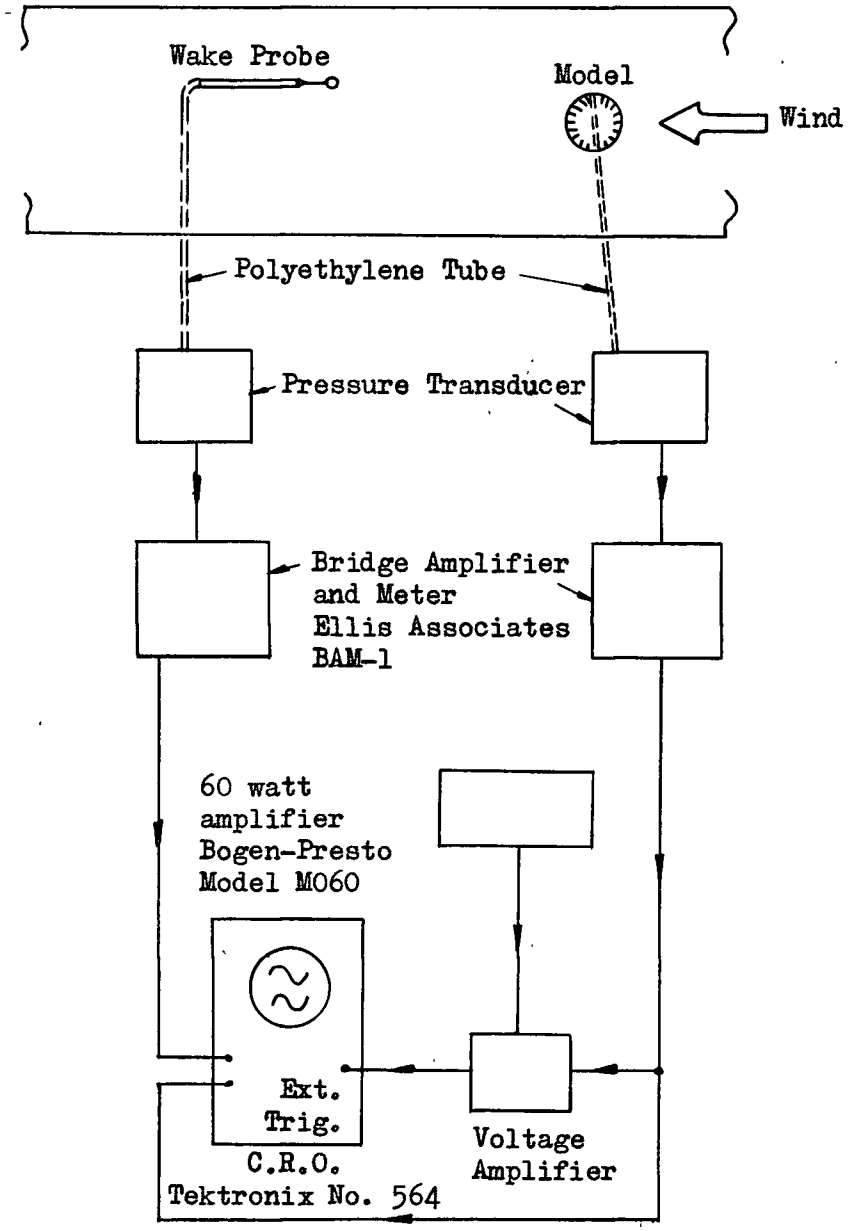

DIAGRAMMATIC LAYOUT OF WAKE
SURVEY APPARATUS

Fig. 30

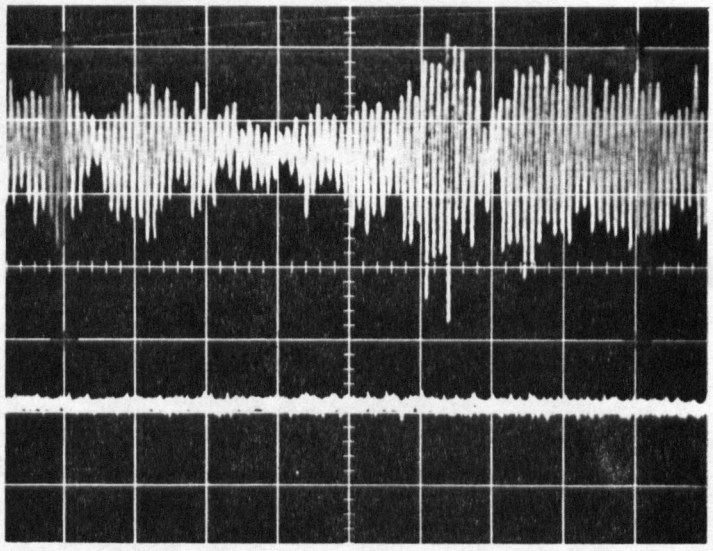

Time Base 1 sec/div

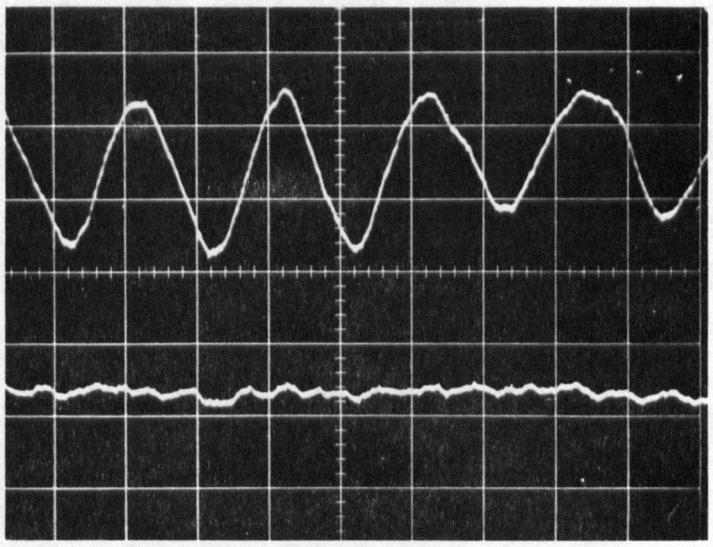

Time Base 50 ms/div

(a)

TYPICAL OSCILLOSCOPE TRACES OF FLUCTUATING

.... CYLINDER

Fig. 31

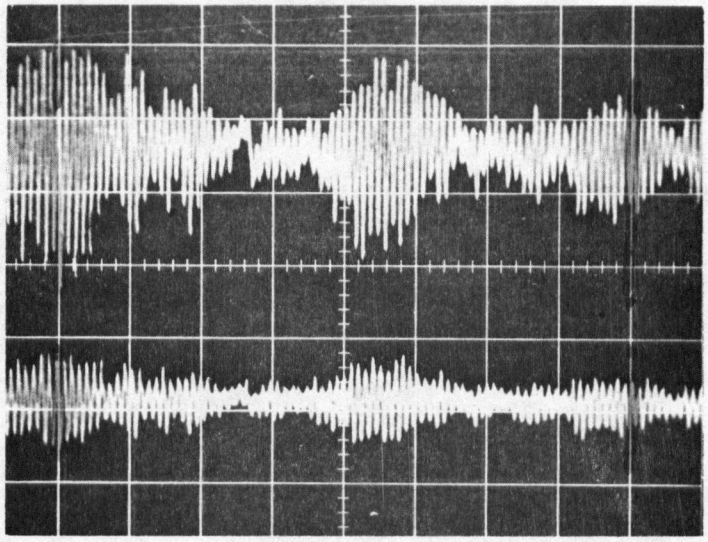

Time Base 1 sec/div

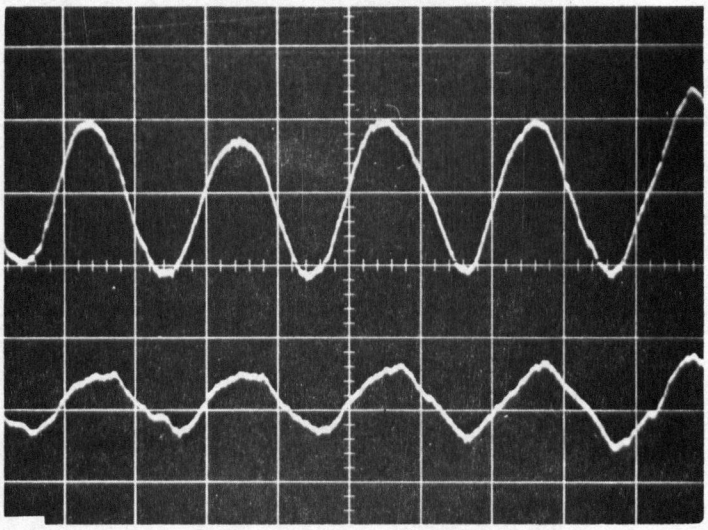

Time Base 50 ms/div

(b)

Fig. 31 (continued)

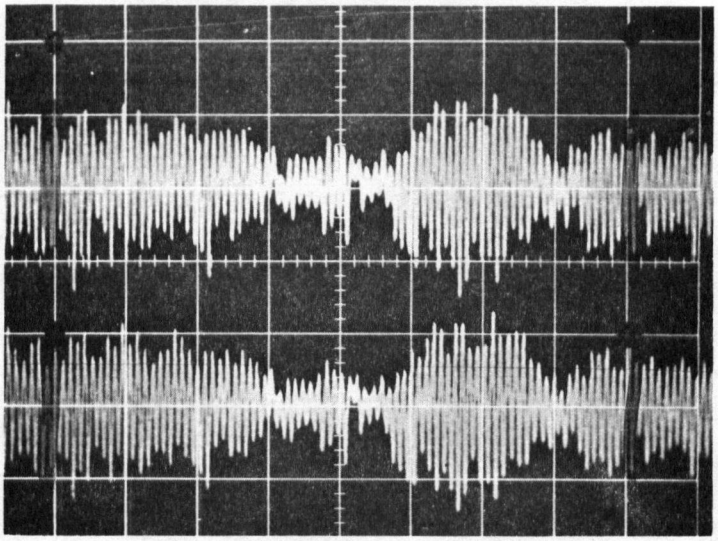

Time Base 1 sec/div

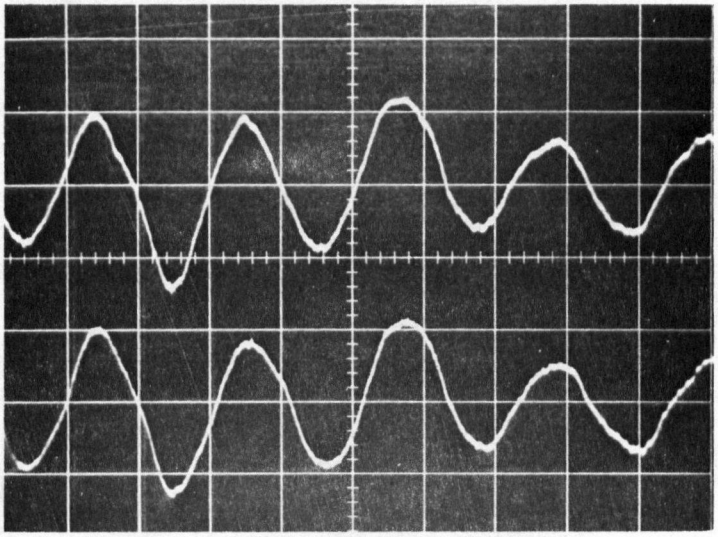

Time Base 50 ms/div

(c)

Fig. 31 (continued)

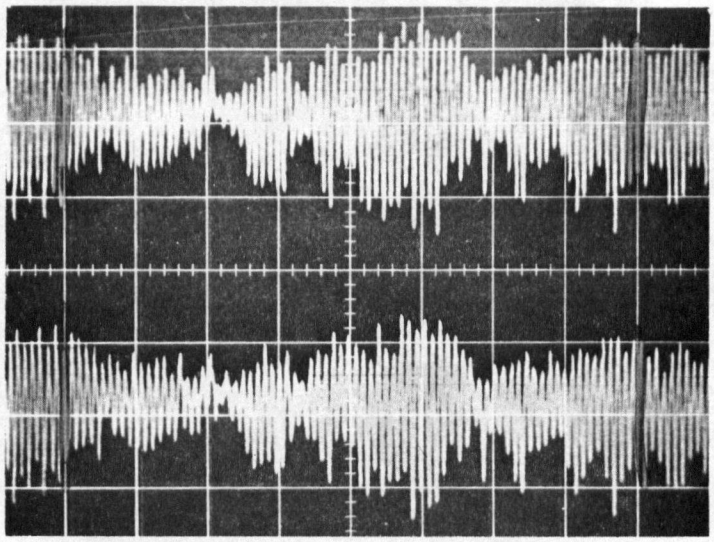

Time Base 1 sec/div

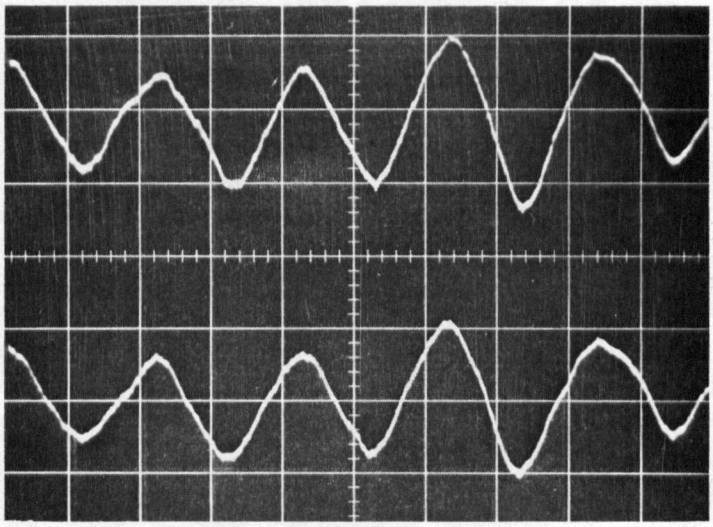

Time Base 50 ms/div

(d)

Fig. 31 (continued)

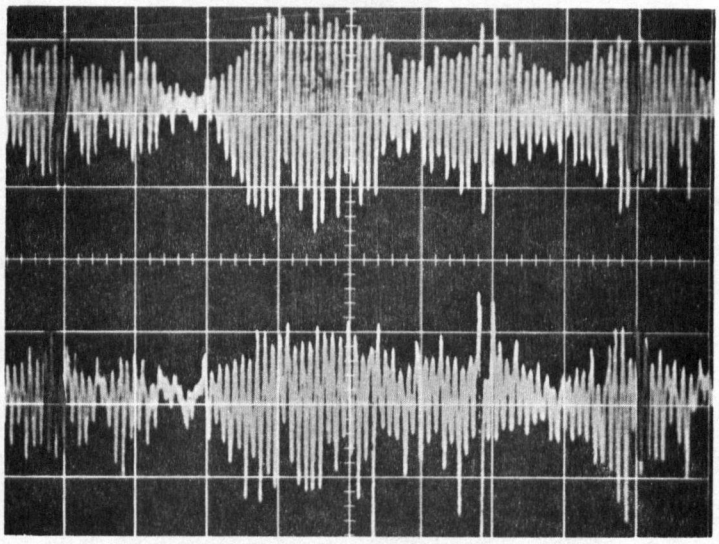

Time Base 1 sec/div

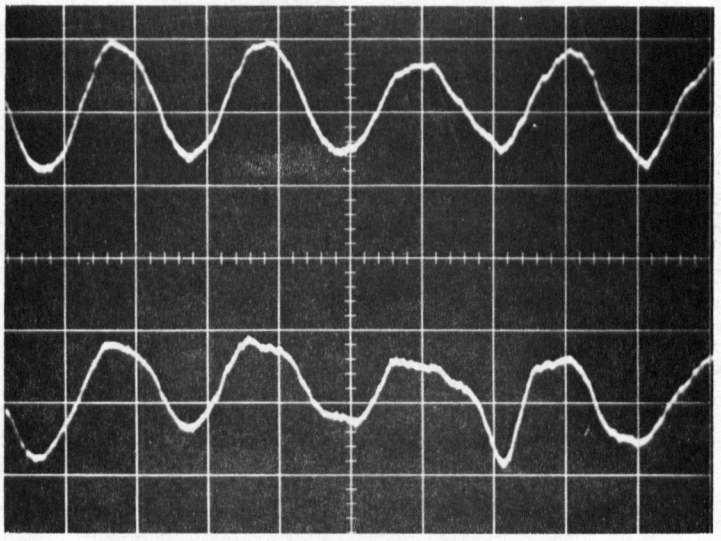

Time Base 50 ms/div

(e)

Fig. 31 (continued)

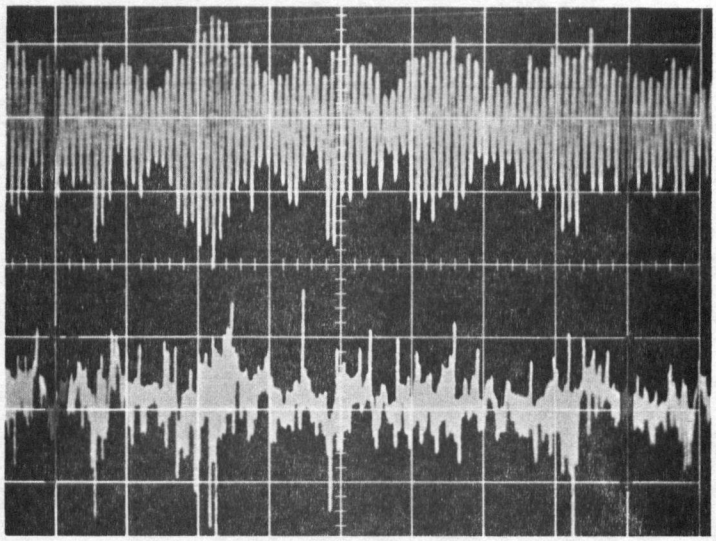

Time Base 1 sec/div

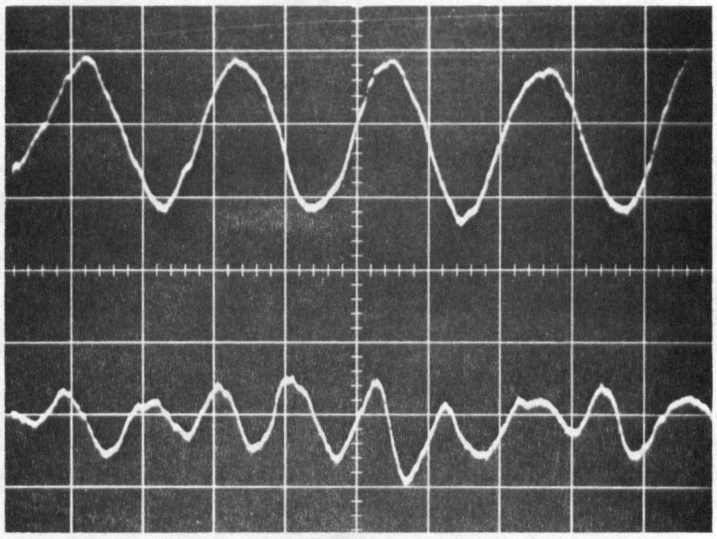

Time Base 50 ms/div

(f)

Fig. 31 (continued)

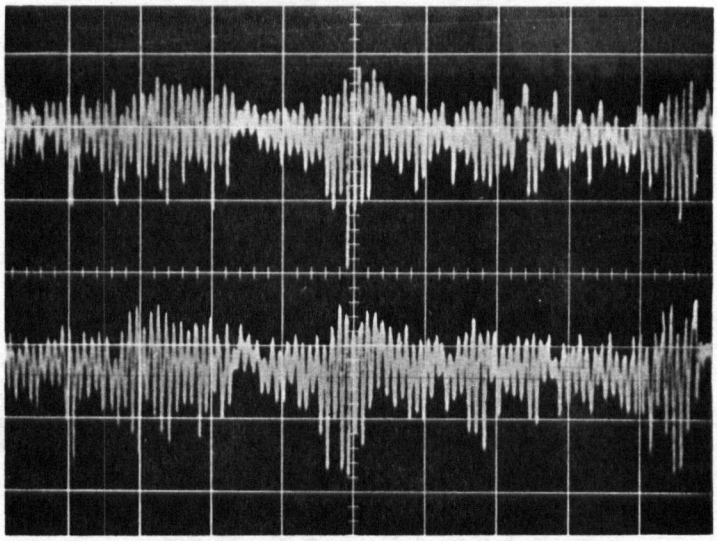

150°

-150°

Time Base 1 sec/div

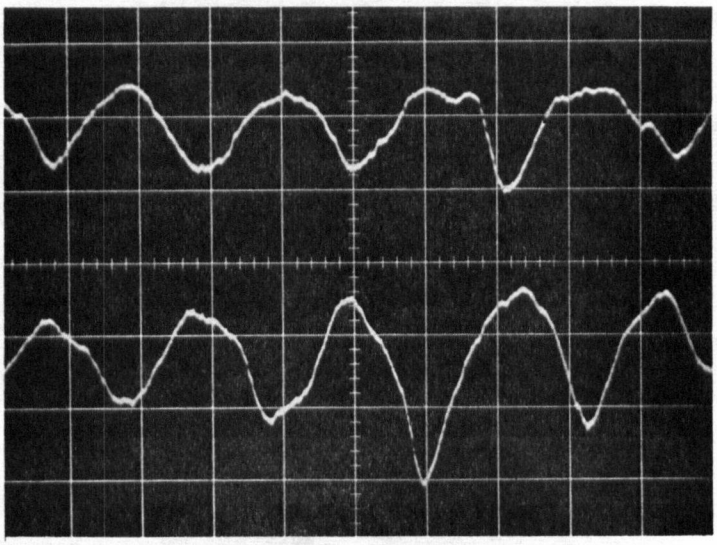

150°

-150°

Time Base 50 ms/div

(g)

Fig. 31 (continued)

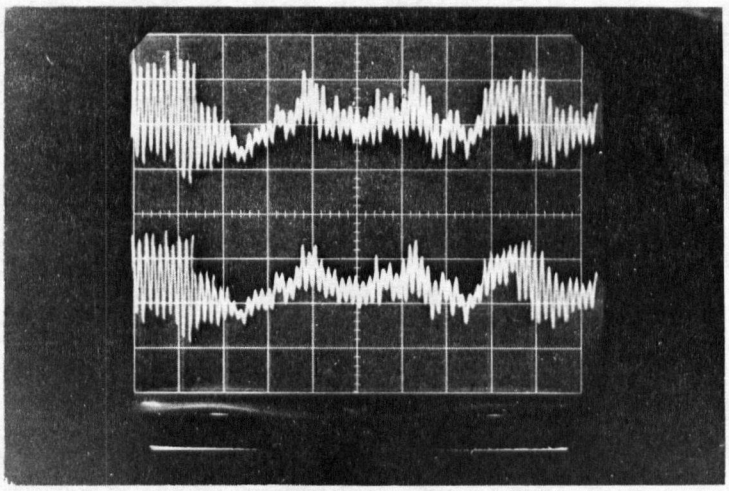

TYPICAL OSCILLOSCOPE TRACES OF FLUCTUATING PRESSURE FROM THE SURFACE OF A 3 INCH DIAMETER STATIONARY CIRCULAR CYLINDER

(h)

Fig. 31

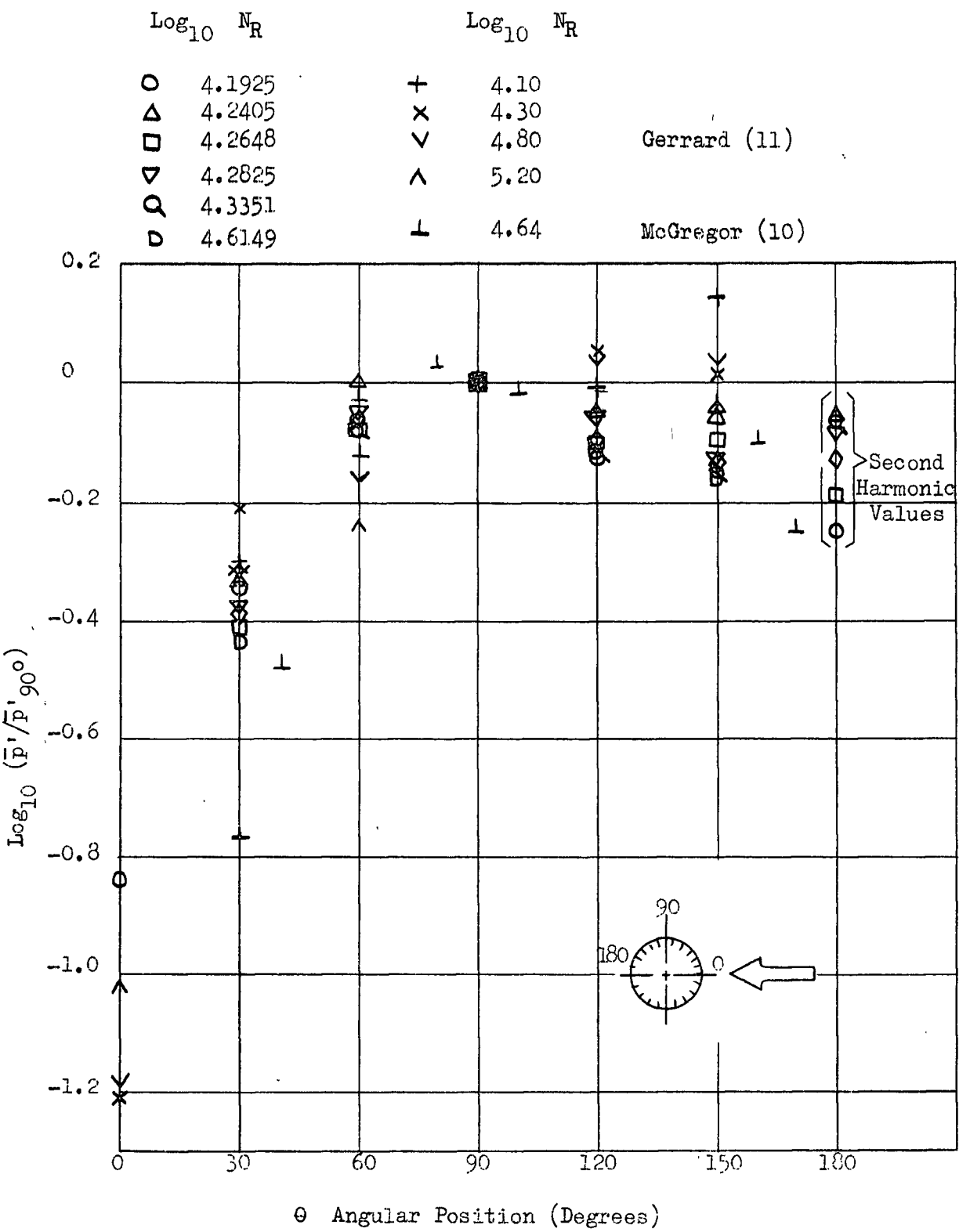

ANGULAR DISTRIBUTION OF FLUCTUATING PRESSURE AMPLITUDE AT THE FUNDAMENTAL FREQUENCY ON THE SURFACE OF A 3 INCH DIAMETER, STATIONARY, CIRCULAR CYLINDER

Fig. 32

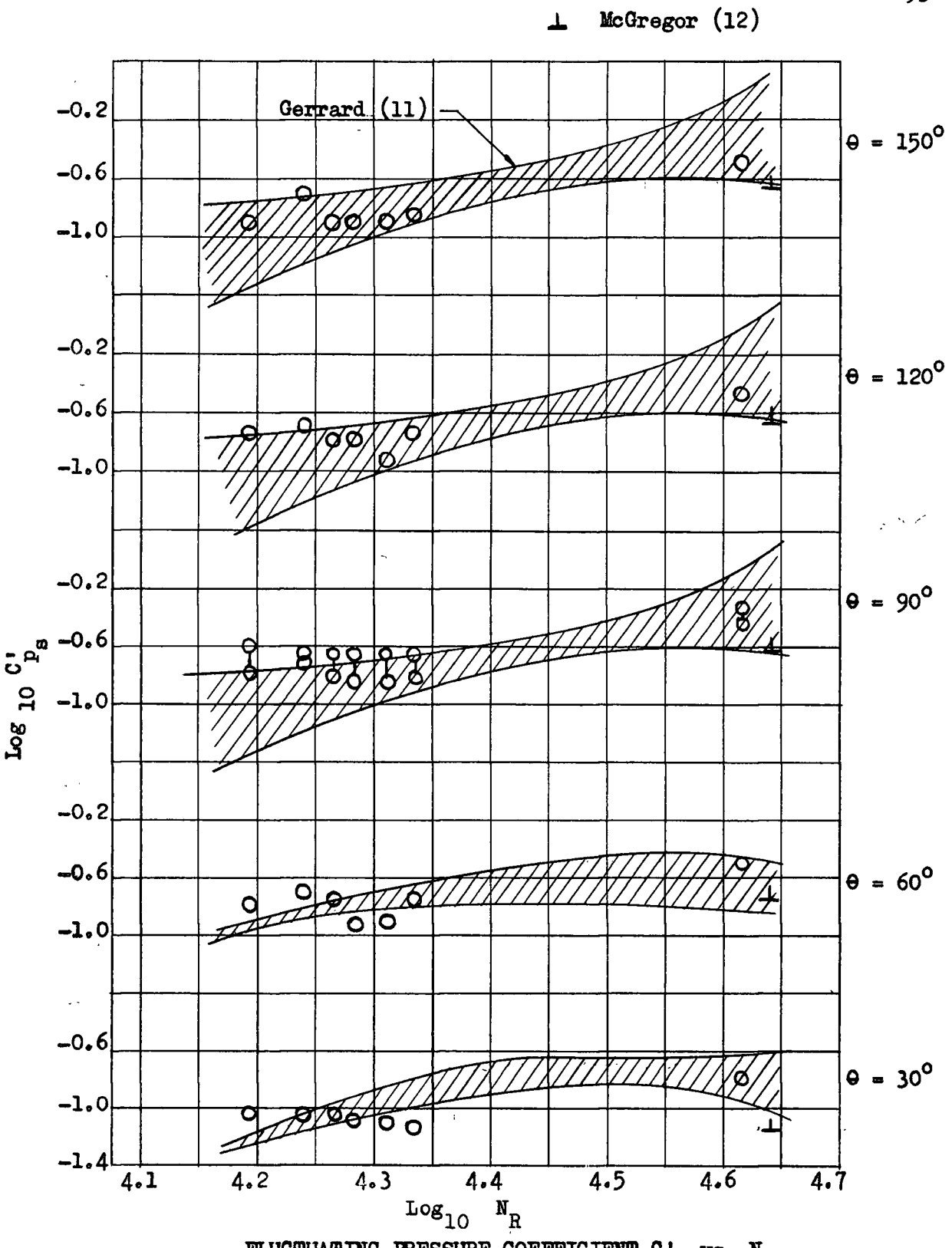

FLUCTUATING PRESSURE COEFFICIENT C'_{p_s} vs. N_R

Fig. 33

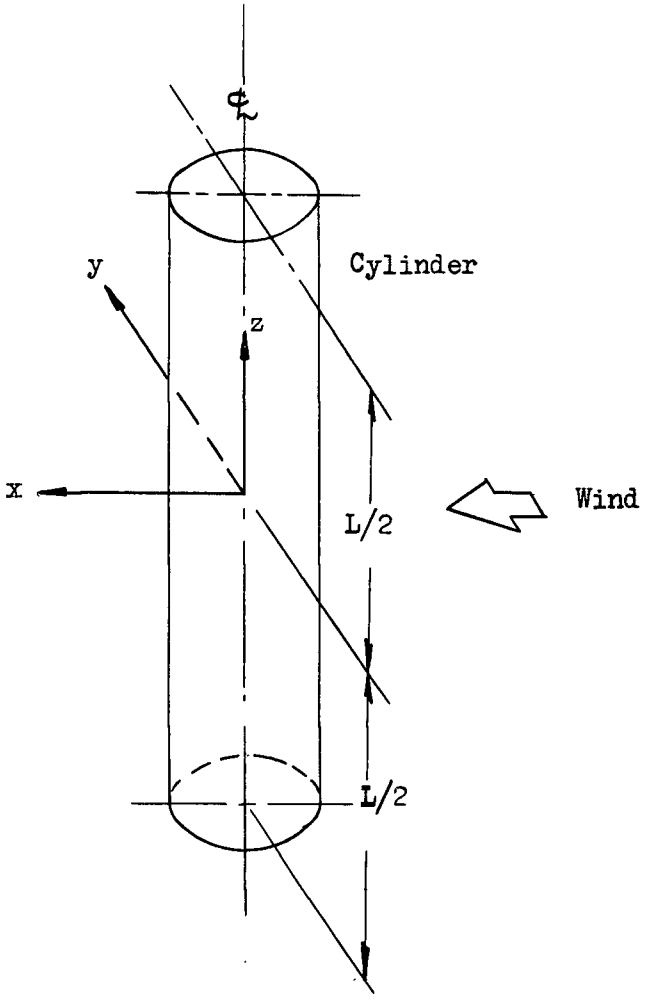

COORDINATE AXES FOR WAKE SURVEY

Fig. 34

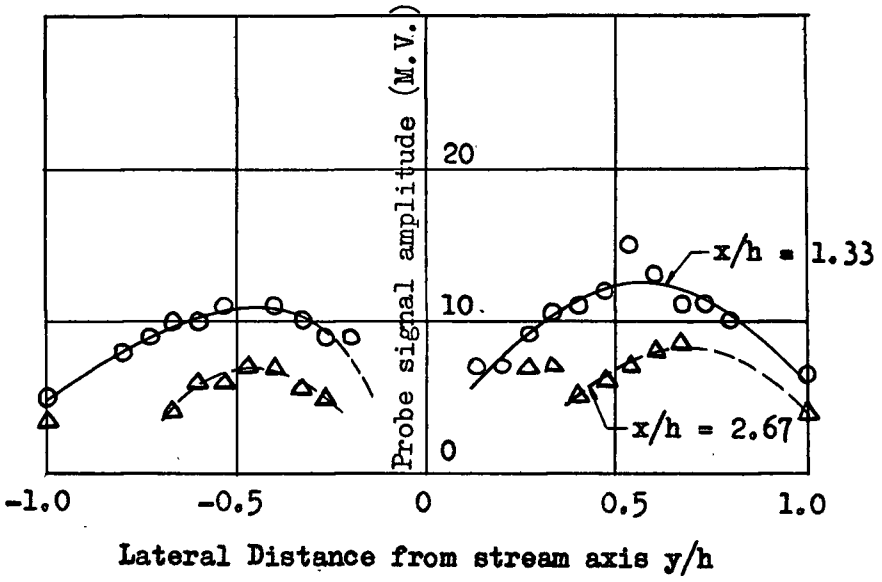

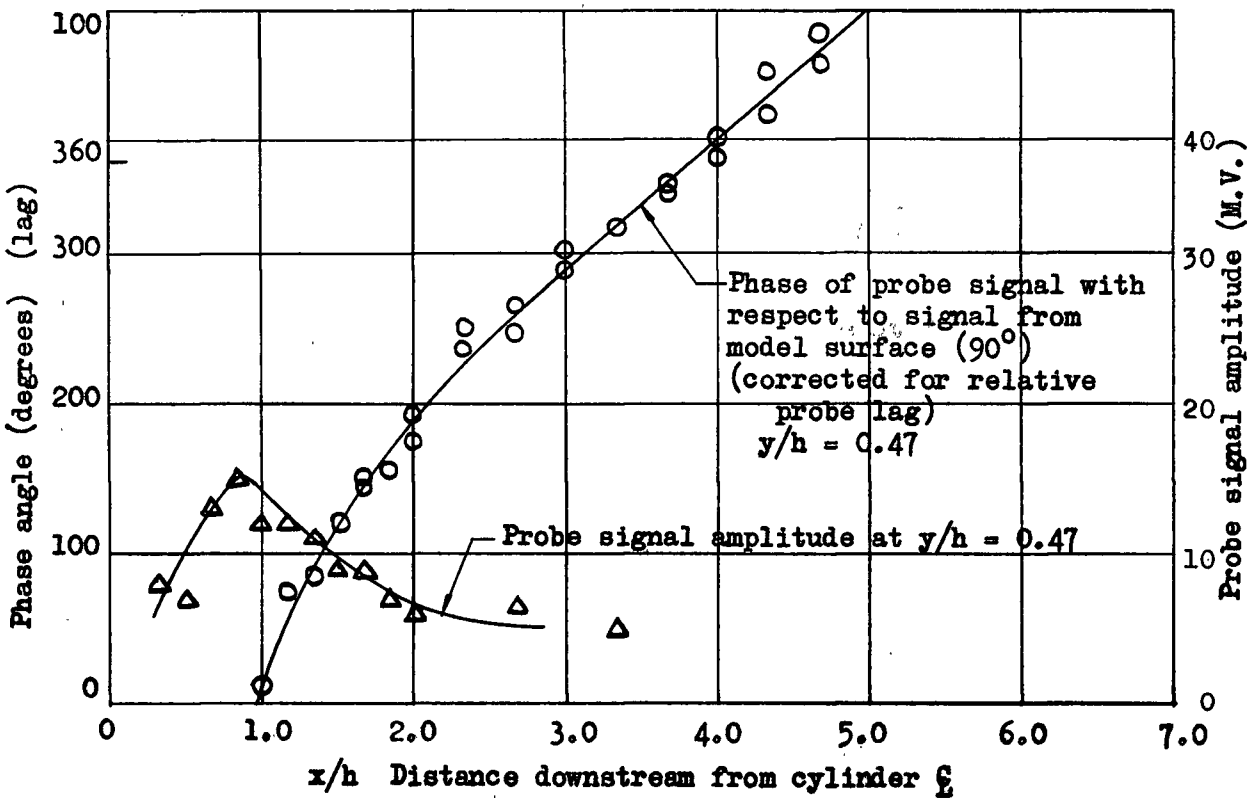

PHASE AND AMPLITUDE OF PROBE SIGNAL IN THE WAKE OF A 3 INCH DIAMETER, STATIONARY CIRCULAR CYLINDER

V = 13.80 f.p.s., f = 10.52 c.p.s., S = 0.191

Fig. 35

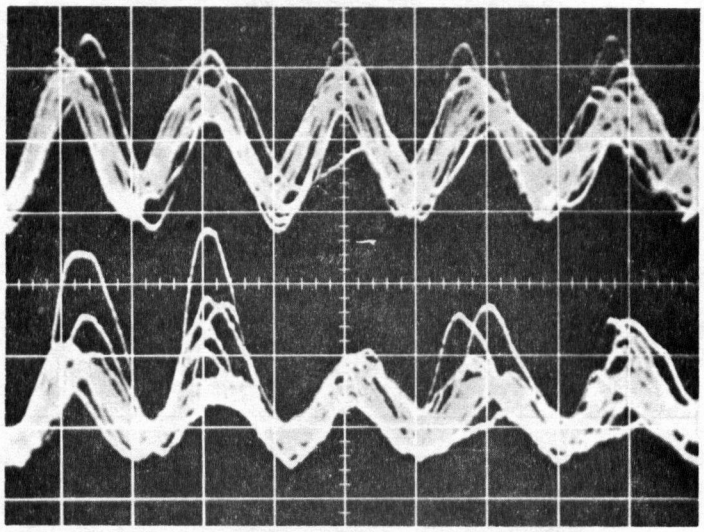

(a) After signal build-up

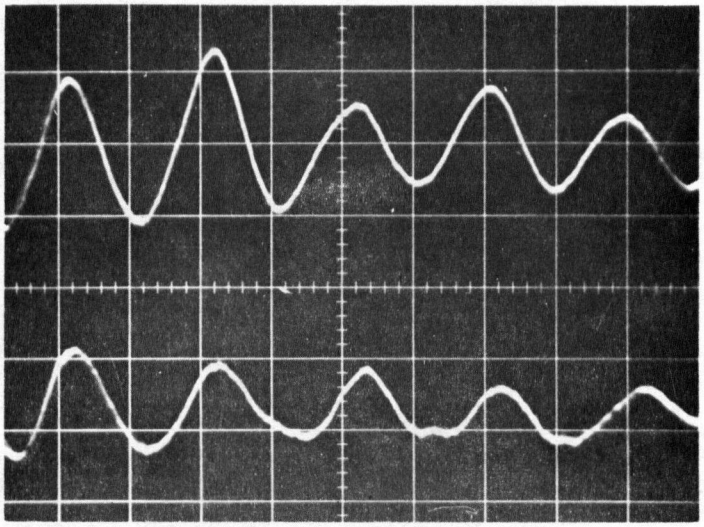

(b) Single sweep

x = 1.5 in., y = 1.4 in., z = 0

TYPICAL OSCILLOSCOPE TRACES ... STATIONARY CIRCULAR CYLINDER

Fig. 36 (continued)

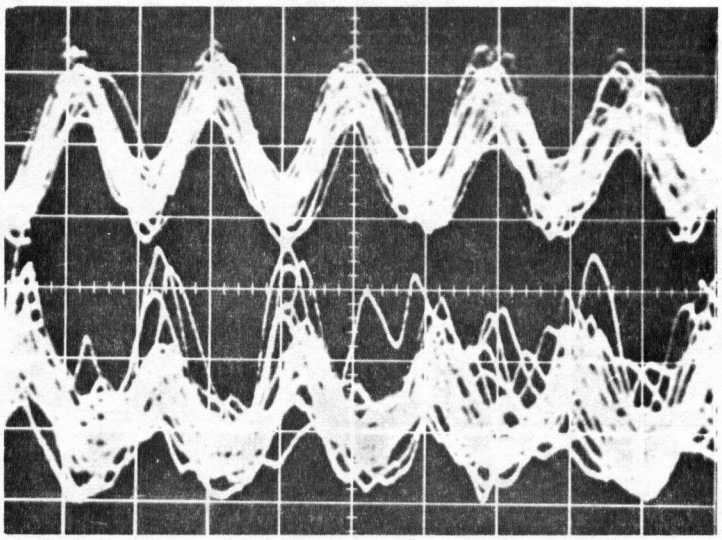

90° Surface pressure signal

Wake probe signal

(c) After signal build-up

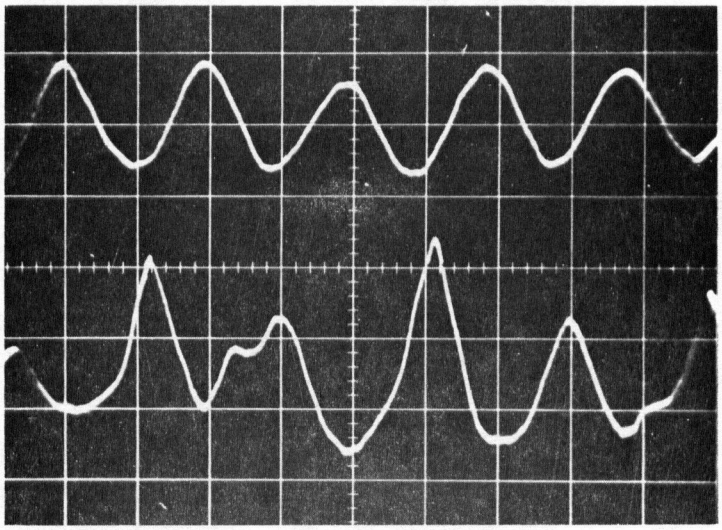

90° Surface pressure signal

Wake probe signal

(d) Single sweep

x = 6.0 in., y = 1.4 in., z = 0

TYPICAL OSCILLOSCOPE TRACES OF SURFACE PRESSURE AND WAKE PROBE SIGNAL FOR A 3 INCH DIAMETER, STATIONARY CIRCULAR CYLINDER

Fig. 36

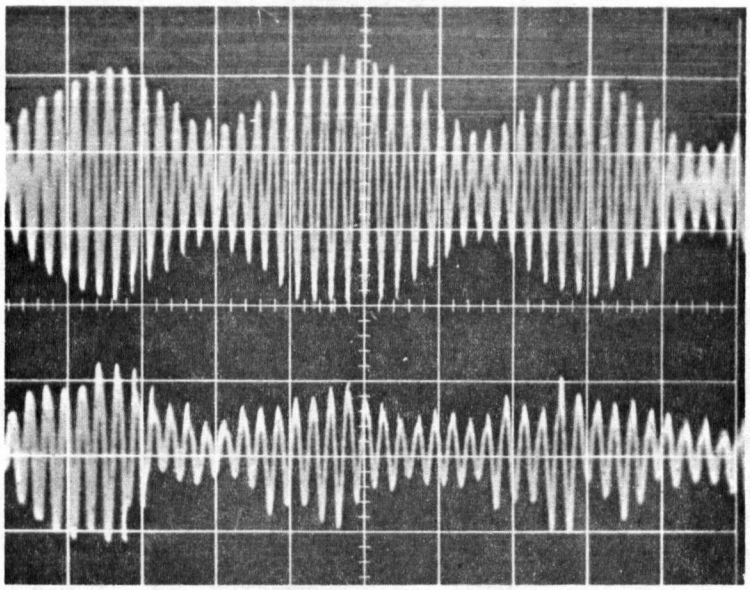

Cylinder oscillation

90° Pressure

(a) Wind speed 10.57 fps.
Amplifier sensitivity 5 mv/div Top trace
20 mv/dic Bottom trace
Time base 0.5 sec/div

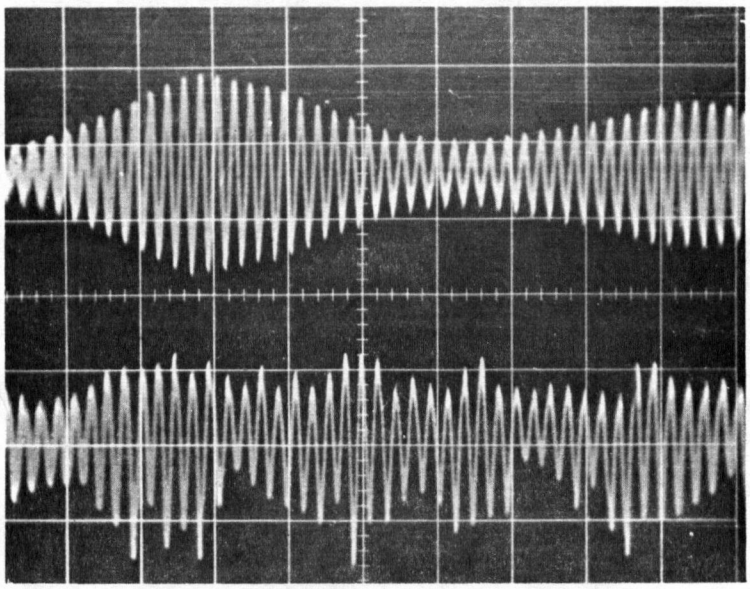

Cylinder oscillation

90° Pressure

(b) Wind speed 11.09 fps.
Amplifier sensitivity 10 mv/div Top trace
20 mv/div Bottom trace
Time base 0.5 sec/div.

TYPICAL OSCILLOSCOPE TRACES ... VORTEX-EXCITED OSCILLATION

Fig. 37 (continued)

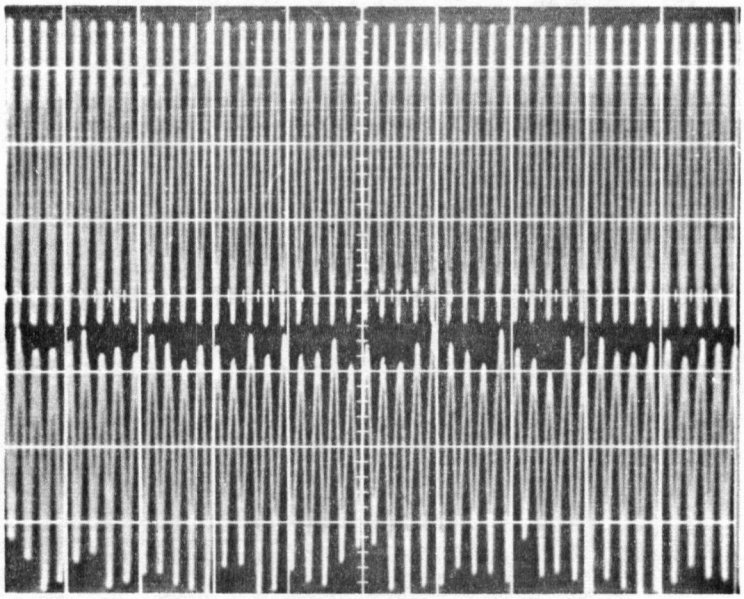

Cylinder oscillation

90° Pressure

Time base 0.5 sec/div

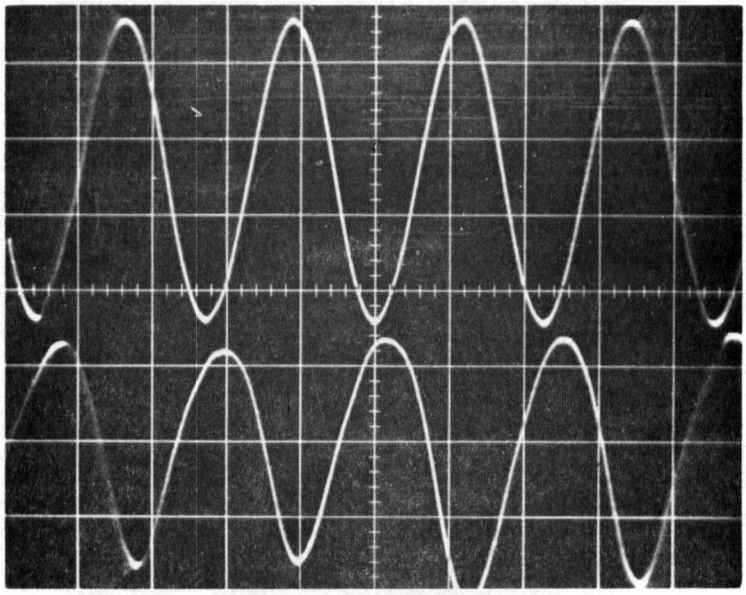

Cylinder oscillation

90° Pressure

(c) Time base 50 ms/div

Wind speed 13.61 fps.
Amplifier sensitivity 50 mv/div

TYPICAL OSCILLOSCOPE TRACES ... VORTEX-EXCITED OSCILLATION
Fig. 37 (continued)

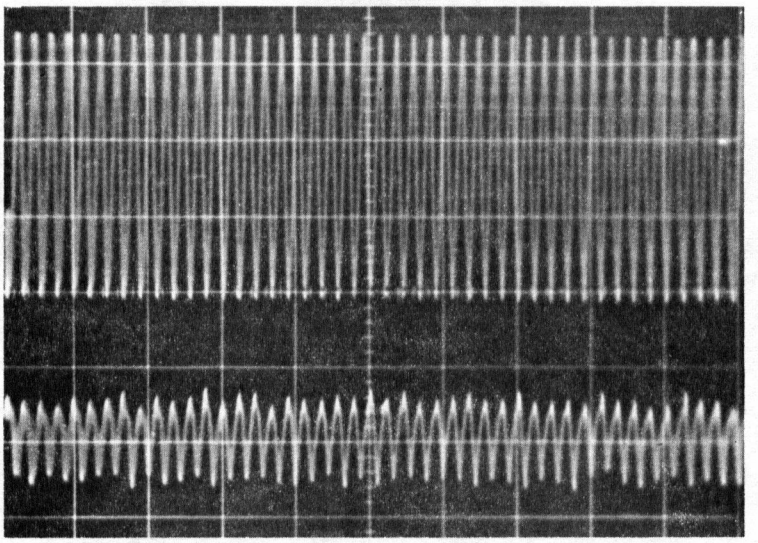

Cylinder oscillation

90° Pressure

Time base 0.5 sec/div

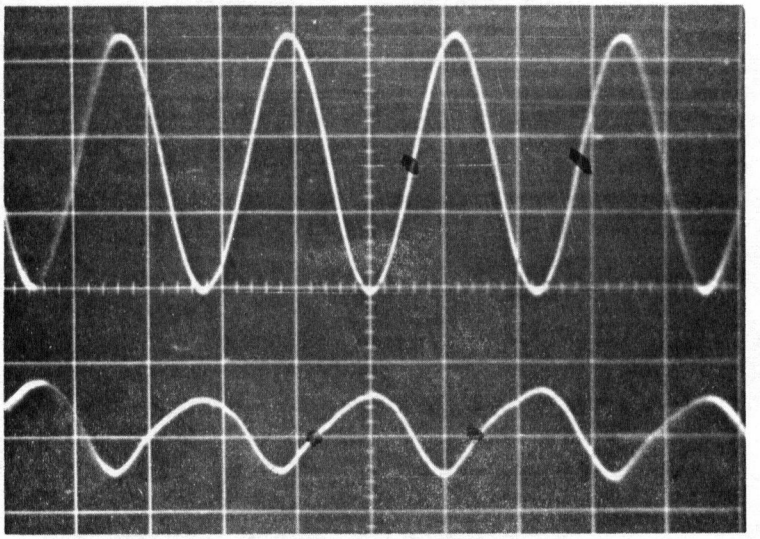

Cylinder oscillation

90° Pressure

(d) Time base 50 ms/div

Wind speed 14.02 fps
Amplifier sensitivity 50 mv/div

TYPICAL OSCILLOSCOPE TRACES ... VORTEX-EXCITED OSCILLATION

Fig. 37 (continued)

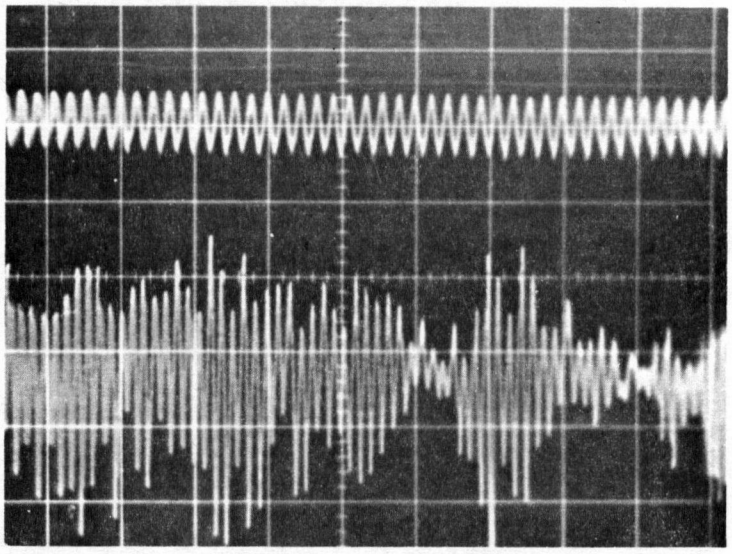

Cylinder oscillation

90° Pressure

Time base 0.5 sec/div
Amplifier sensitivity cylinder oscillation 50 mv/div
90° pressure 20 mv/div

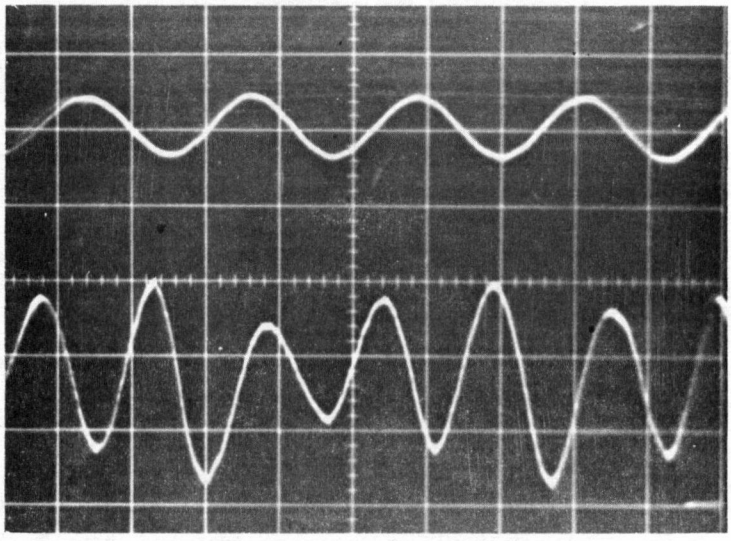

Cylinder oscillation

90° Pressure

(e) Time base 50 ms/div
Amplifier sensitivity: cylinder oscillation 50 mv/div
90° pressure 20 mv/div.

TYPICAL OSCILLOSCOPE TRACES OF CYLINDER OSCILLATION AND 90° SURFACE PRESSURE FOR 3 INCH DIAMETER CIRCULAR CYLINDER EXHIBITING VORTEX-EXCITED OSCILLATION

Fig. 37

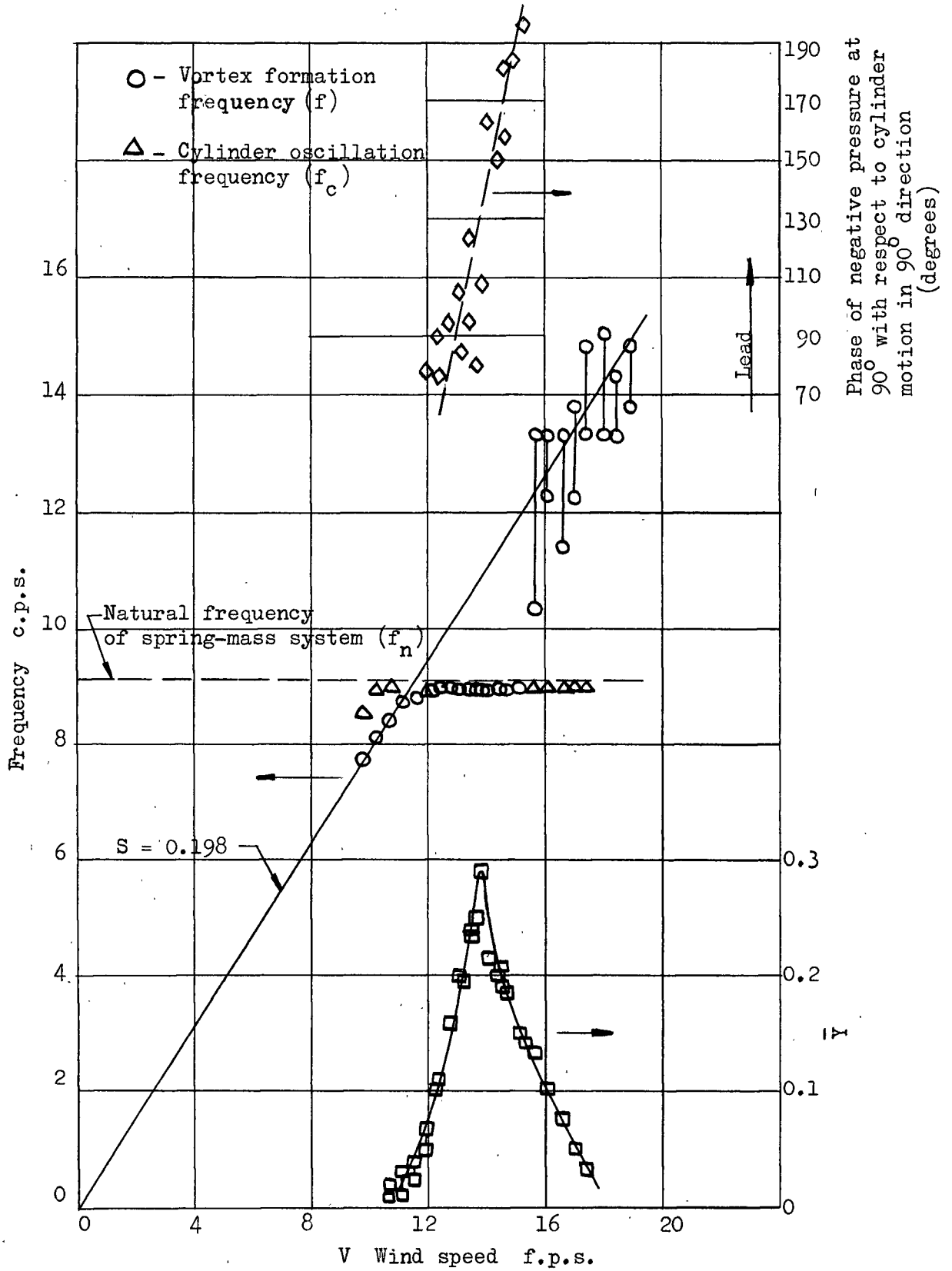

CYLINDER OSCILLATION AMPLITUDE AND FREQUENCY, FLUCTUATING PRESSURE FREQUENCY AND PHASE VS. WIND SPEED

Fig. 38

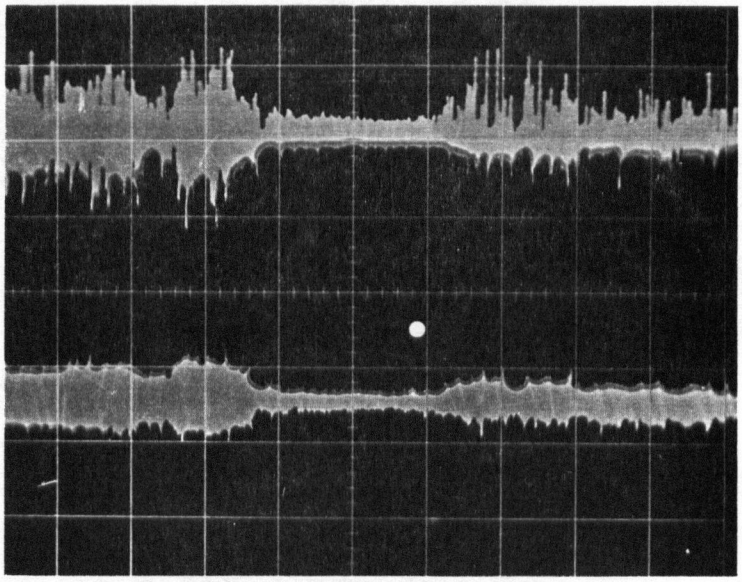

(a)

Fluctuating pressure signals-wind increased through resonant range while cylinder oscillated.

TYPICAL OSCILLOSCOPE TRACES OF FLUCTUATING PRESSURE ... VORTEX-EXCITED OSCILLATION

Fig. 39 (continued)

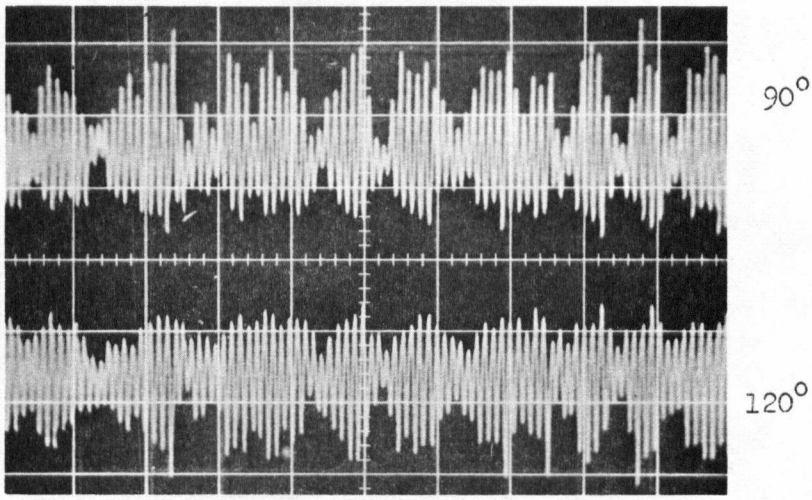

Time base 1 sec/div

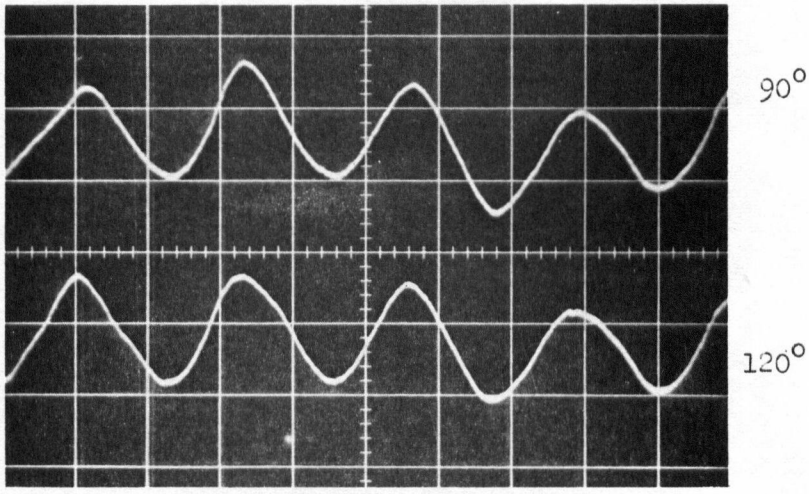

(b) Time base 50 ms/div

Amplifier sensitivity 50 mv/div
Wind speed 11.80 fps.

TYPICAL OSCILLOSCOPE TRACES OF FLUCTUATING PRESSURE ... VORTEX-EXCITED OSCILLATION
Fig. 39 (continued)

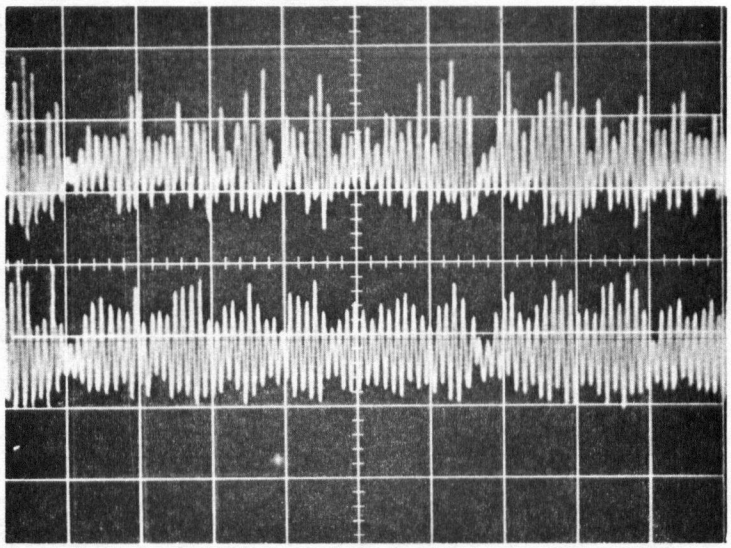

Time base 1 sec/div

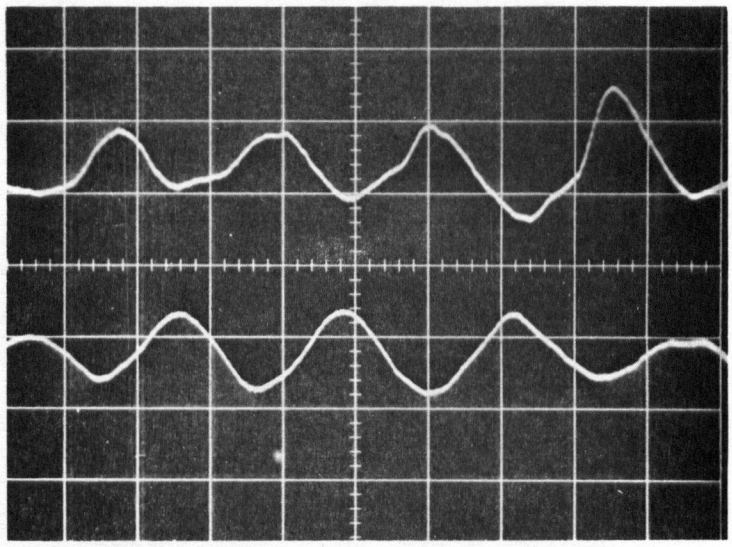

(b continued) Time base 50 ms/div

Amplifier sensitivity 50 mv/div
Wind speed 11.80 fps.

TYPICAL OSCILLOSCOPE TRACES OF FLUCTUATING PRESSURE ... VORTEX-EXCITED OSCILLATION
Fig. 39 (continued)

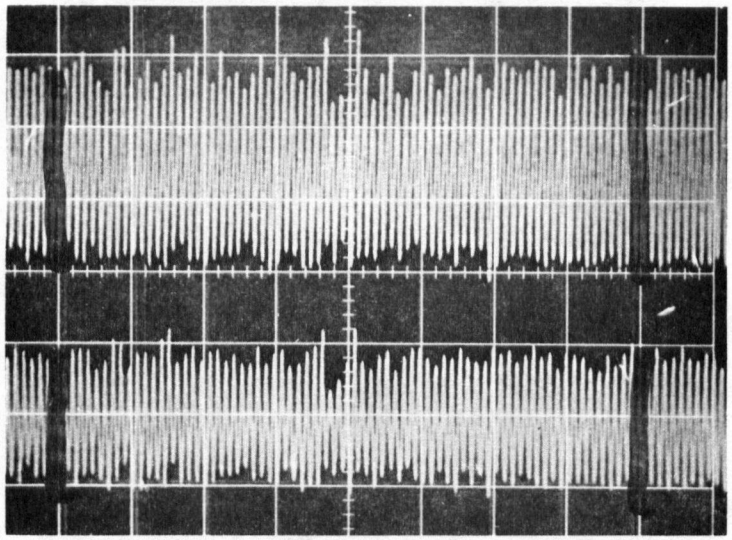

Time base 1 sec/div

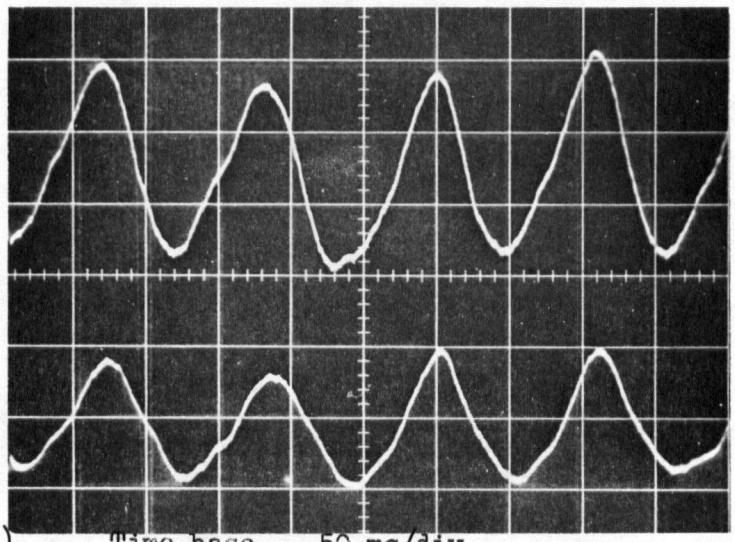

(c) Time base 50 ms/div

Amplifier sensitivity 20 mv/div
Wind speed 13.35 fps.

TYPICAL OSCILLOSCOPE TRACES OF FLUCTUATING PRESSURE ... VORTEX-EXCITED OSCILLATION

Fig. 39 (continued)

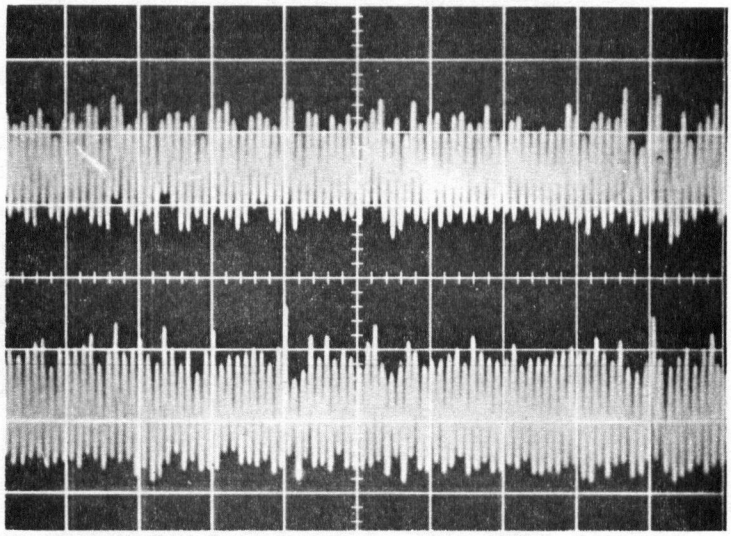

150°

-120°

Time base 1 sec/div

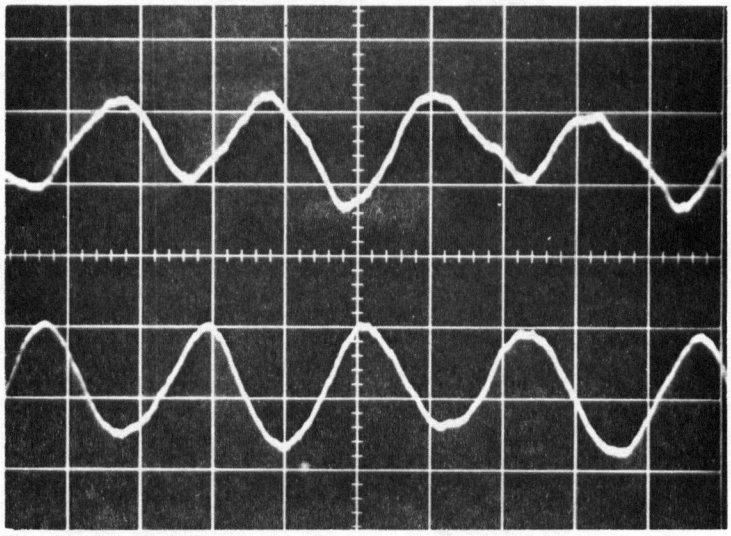

150°

-120°

(c continued) Time base 50 ms/div

Amplifier sentivity 20 mv/div
Wind speed 13.35 fps.

TYPICAL OSCILLOSCOPE TRACES OF FLUCTUATING PRESSURE ... VORTEX-EXCITED OSCILLATION

Fig. 39 (continued)

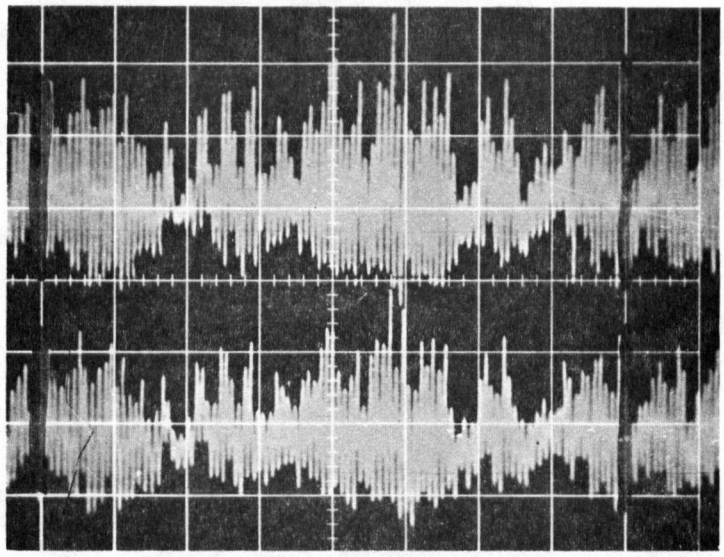

90°

120°

Time base 1 sec/div

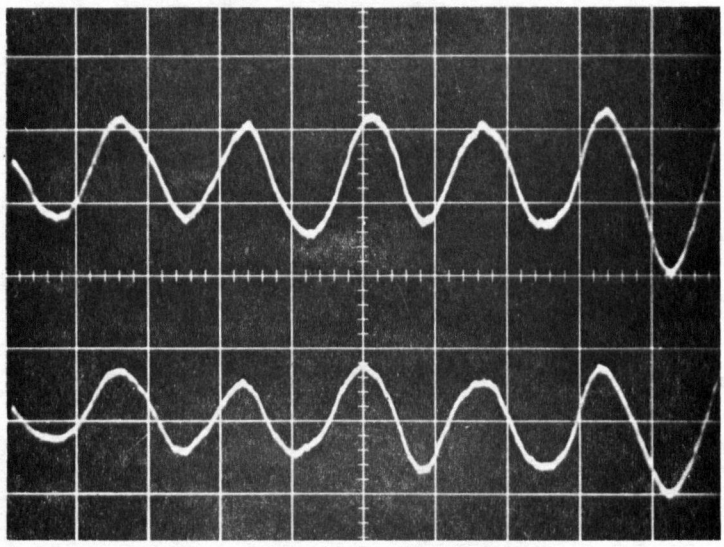

90°

120°

(d) Time base 50 ms/div
Amplifier sensitivity 20 mv/div
Wind speed 14.73 fps.

TYPICAL OSCILLOSCOPE TRACES OF FLUCTUATING PRESSURE ... VORTEX-EXCITED OSCILLATION
Fig. 39 (continued)

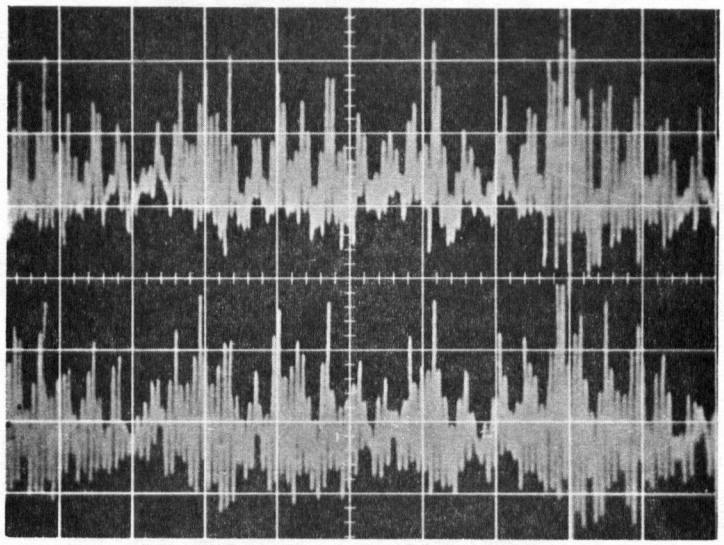

150°

-120°

Time base 1 sec/div

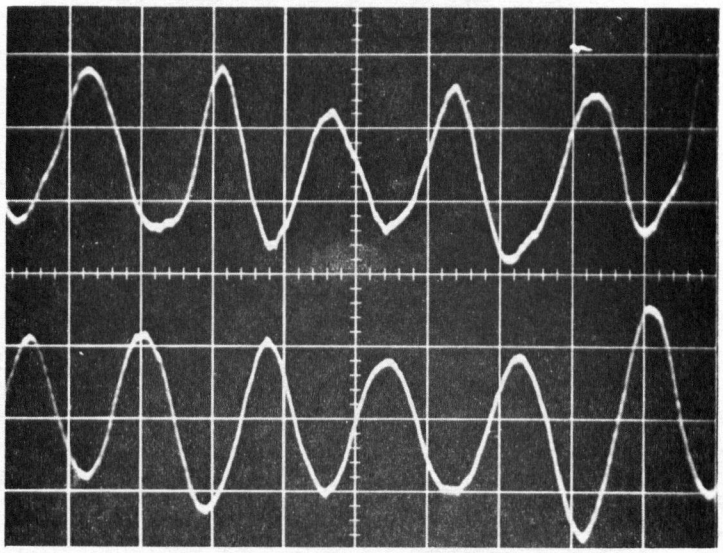

150°

-120°

(d continued) Time base 50 ms/div
Amplifier sensitivity 20 mv/div
Wind speed 14.73 fps

TYPICAL OSCILLOSCOPE TRACES OF FLUCTUATING PRESSURE ON THE SURFACE OF A 3 INCH DIAMETER, CIRCULAR CYLINDER EXHIBITING VORTEX-EXCITED OSCILLATION

Fig. 39

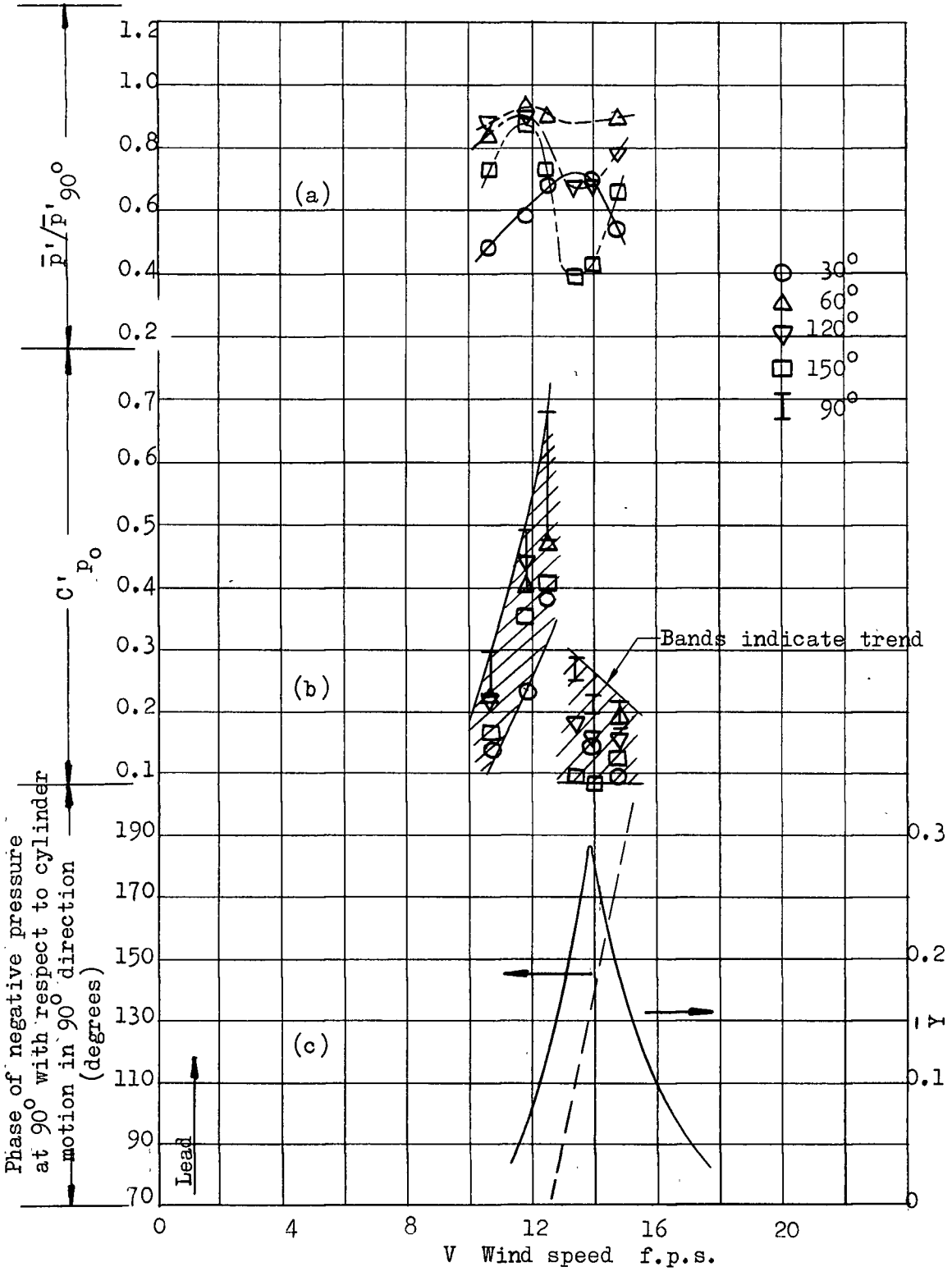

C'_{p_o} AND ANGULAR DISTRIBUTION OF FLUCTUATING PRESSURE ON THE SURFACE OF A 3 INCH DIAMETER CIRCULAR CYLINDER EXHIBITING VORTEX-EXCITED OSCILLATION

Fig. 40

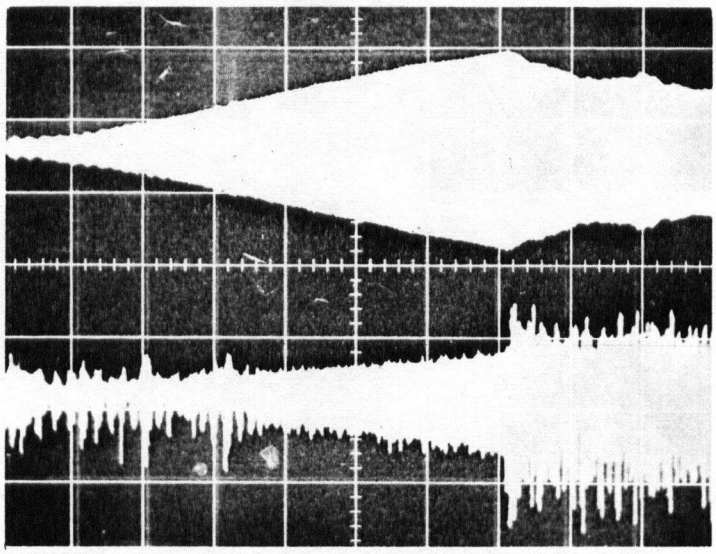

OSCILLOSCOPE TRACE OF CYLINDER OSCILLATION AMPLITUDE AND 90° FLUCTUATING PRESSURE DURING TRANSIENT BUILD-UP OF CYLINDER DISPLACEMENT. WIND SPEED 12.4 f.p.s.

Fig. 41

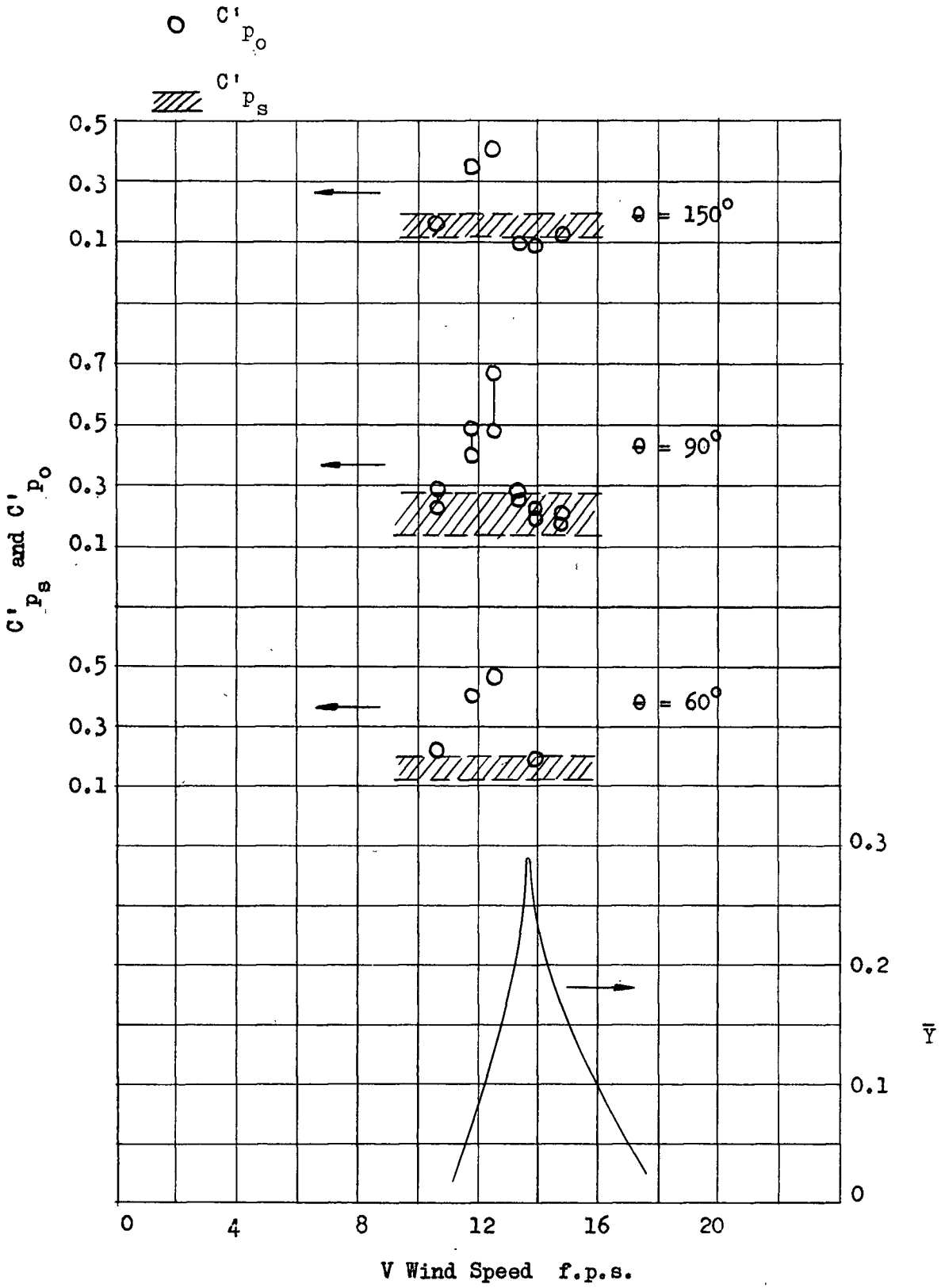

C'_{p_s} AND C'_{p_o} VS. WIND SPEED

Fig. 42

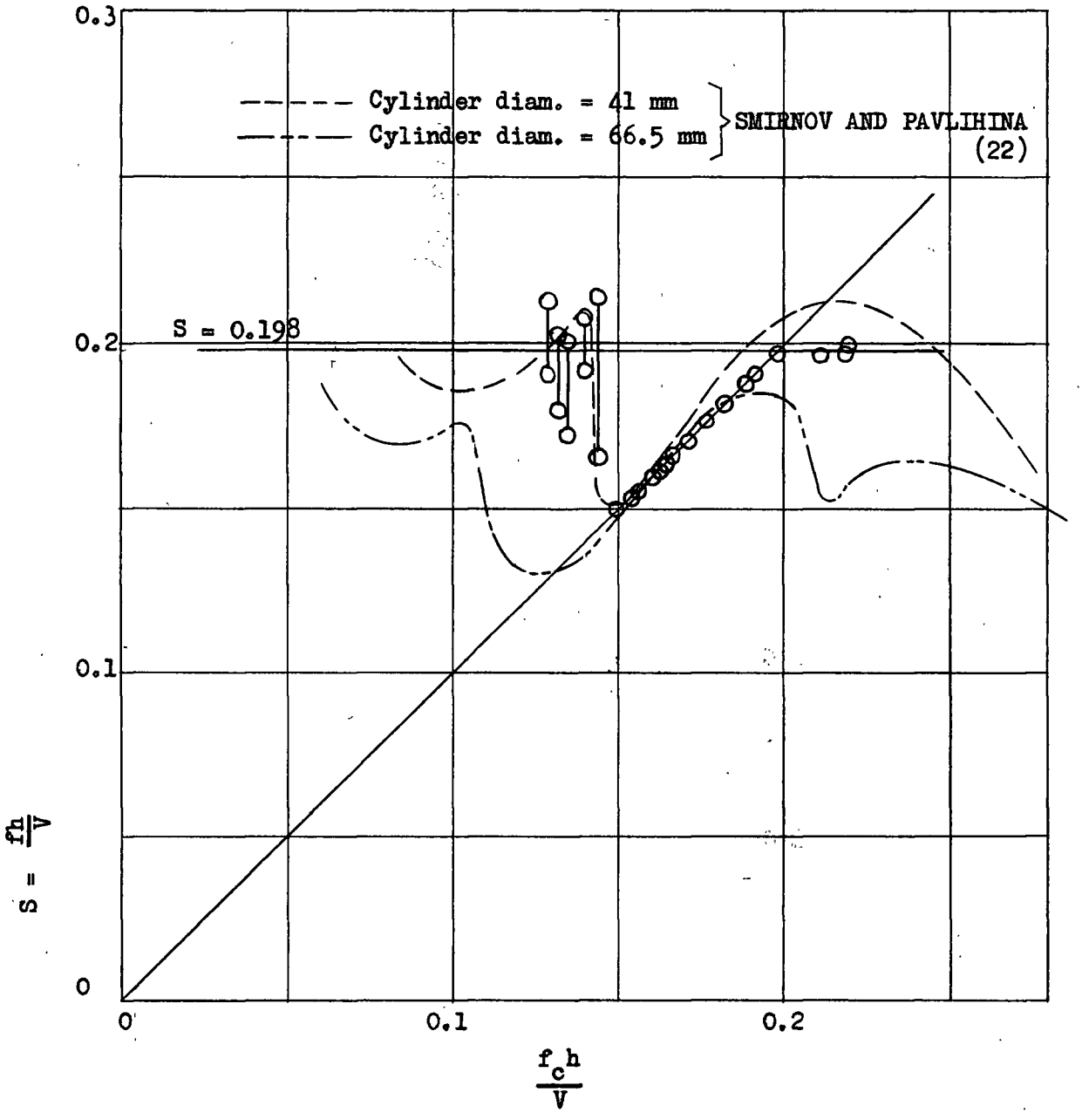

COMPARISON OF 'CAPTURE' DATA WITH REF. (22)

Fig. 43

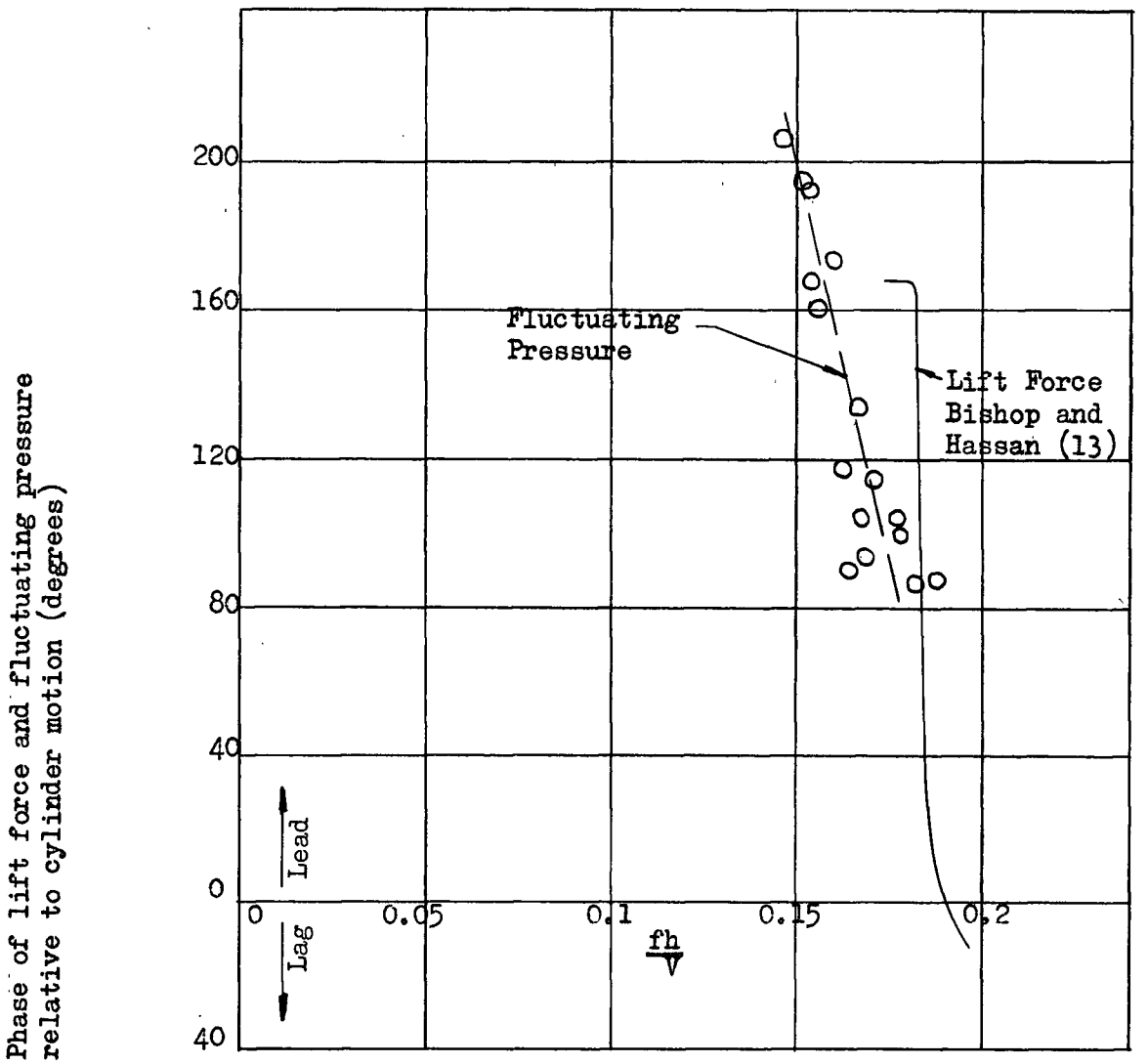

COMPARISON OF PHASE DATA WITH REF. (23)

Fig. 44

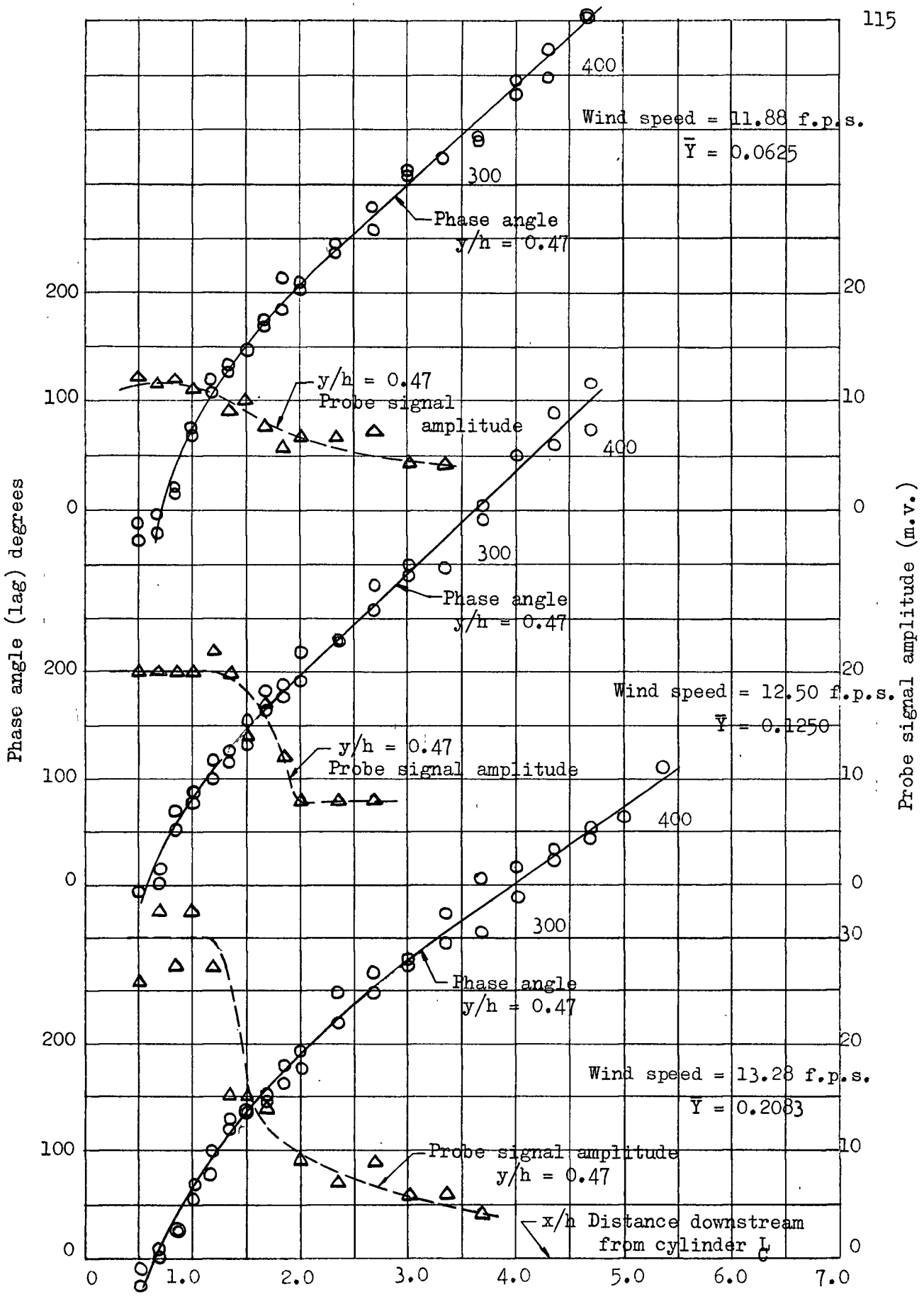

PHASE AND AMPLITUDE OF PROBE SIGNAL IN THE WAKE OF A 3 INCH DIAMETER CIRCULAR CYLINDER EXHIBITING VORTEX-EXCITED OSCILLATION (LONGITUDINAL TRAVERSE)

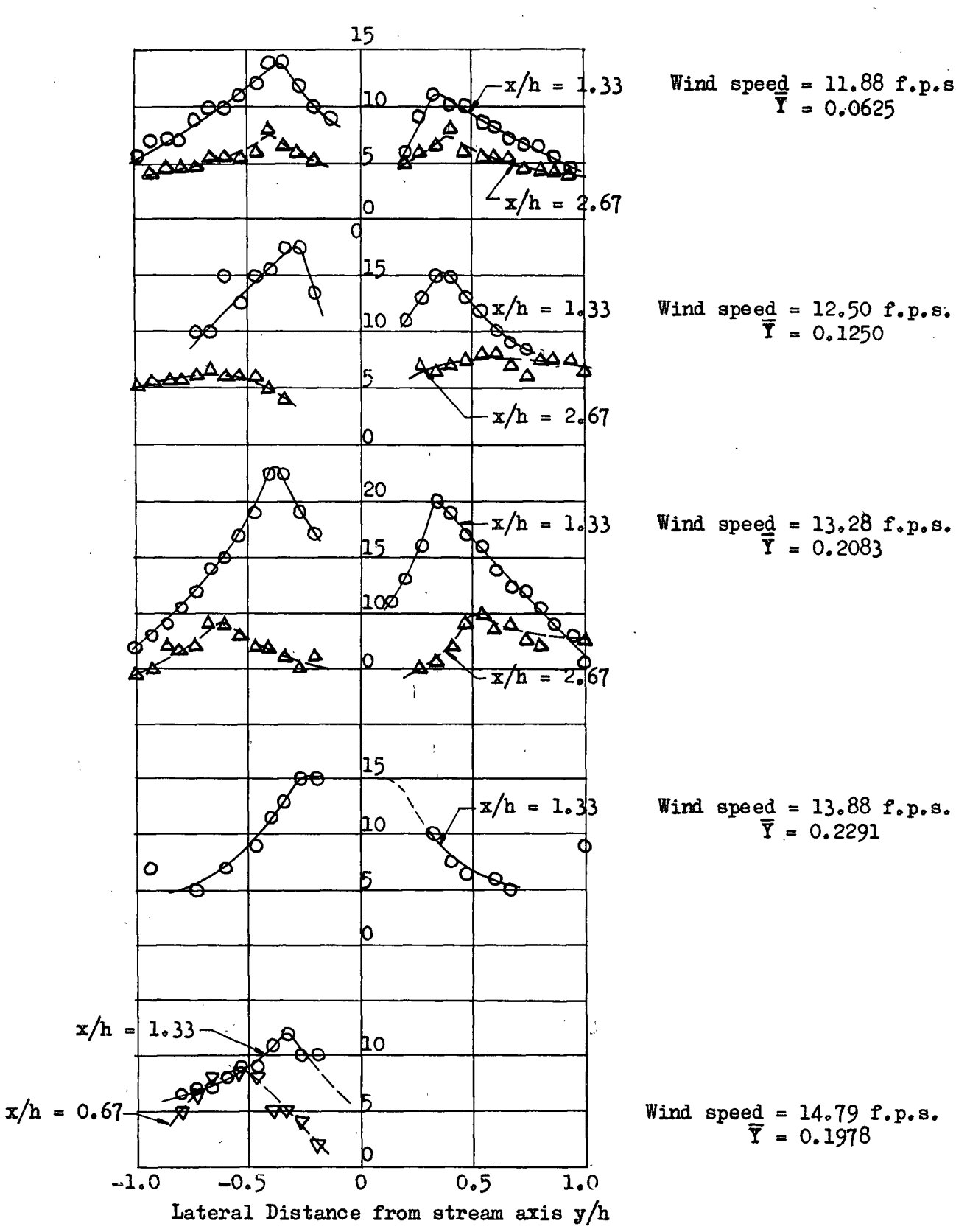

AMPLITUDE OF PROBE SIGNAL IN THE WAKE OF A 3 INCH DIAMETER CIRCULAR CYLINDER EXHIBITING VORTEX-EXCITED OSCILLATION (LATERAL TRAVERSE)

Fig. 46

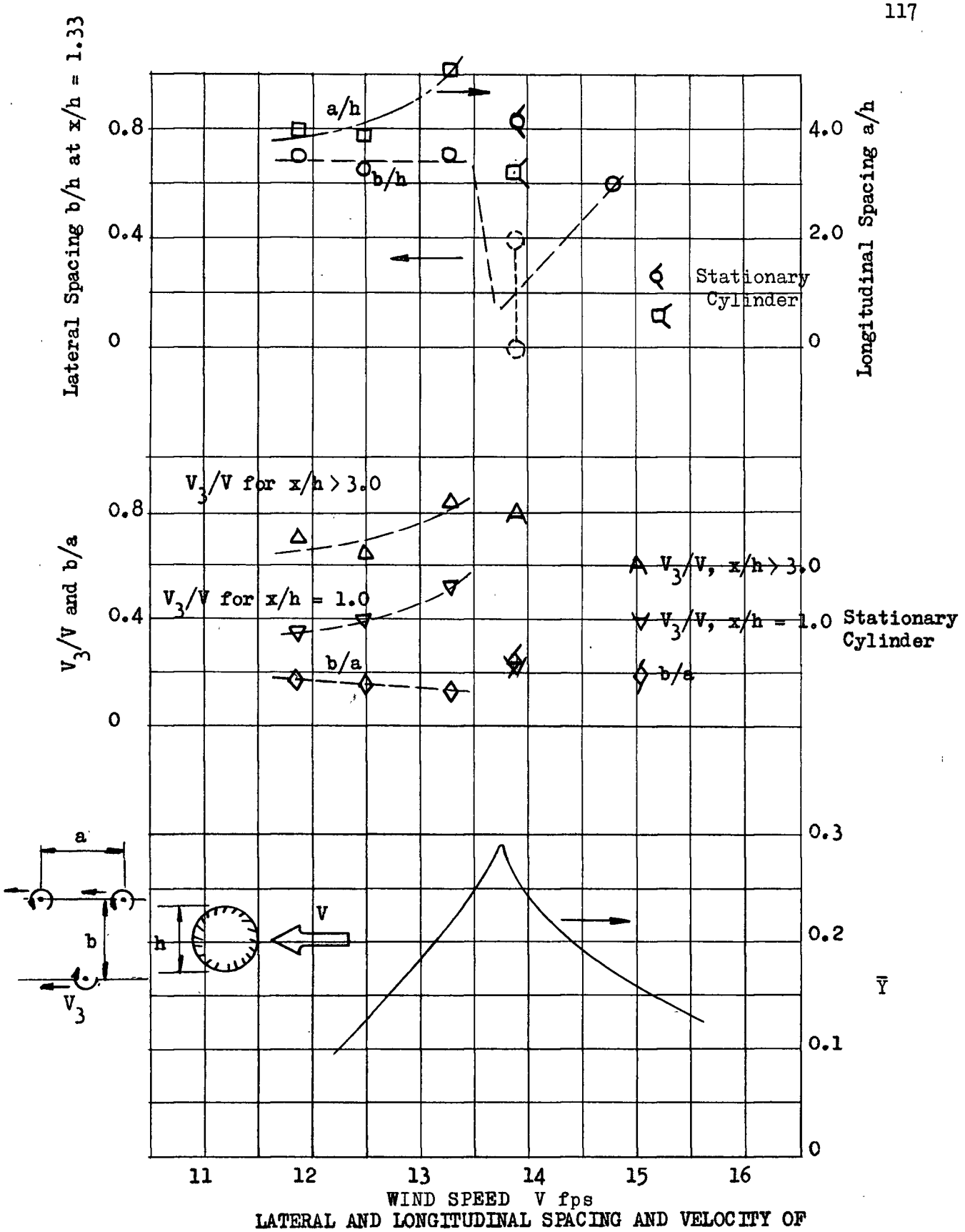

LATERAL AND LONGITUDINAL SPACING AND VELOCITY OF VORTICES IN THE WAKE OF A 3 INCH DIAMETER CIRCULAR CYLINDER EXHIBITING VORTEX-EXCITED OSCILLATION

Fig. 47